Enzymatic hydrolysis with cholesterol esterase in the presence of surfactant improves efficiency for sample preparation of side-chain oxysterols in biosamples

Maria Therese Sande

Thesis for the Master's degree in chemistry
60 credits

Department of Chemistry
Faculty of Mathematics and Natural Sciences

UNIVERSITY OF OSLO

May 29th, 2019

Enzymatic hydrolysis with cholesterol esterase in the presence of surfactant improves efficiency for sample preparation of side-chain oxysterols in biosamples

Maria Therese Sande

Department of Chemistry

Faculty of Mathematics and Natural Sciences

University of Oslo

May 2019

2019

Enzymatic hydrolysis with cholesterol esterase in the presence of surfactant improves efficiency for sample preparation of side-chain oxysterols in biosamples

Maria Therese Sande

http://www.duo.uio.no/

Print: Reprosentralen, Universitetet i Oslo

Abstract

Side-chain oxysterols are associated with breast cancer (BC), and more efficient methods for their quantification in biological samples are needed. Our present liquid chromatography-mass spectrometry (LC-MS) method for determination of oxysterols in biological samples requires hydrolysis and derivatization prior to the LC-MS and the sample preparation time is > 1 day. To shorten the sample preparation time and sample handling for determination of oxysterols, alternative (published) techniques to the present Girard T method and the present alkaline hydrolysis with KOH were explored. The techniques were derivatization to picolinyl esters and thiyl radical-based charge tagging, and enzymatic hydrolysis with cholesterol esterase (ChE).

Derivatization to picolinyl esters resulted in poor yield and arbitrary formation of picolinate derivatives, even after several modifications of the procedure. The thiyl radical-based charge tagging did not provide a detectable signal for cholesterol, 24S-hydroxycholesterol (24S-OHC) or 25-hydroxycholesterol (25-OHC). Hence, the derivatization procedures investigated were, by our hands, difficult to reproduce and derivatization with Girard T was maintained.

Using human plasma (5 µL) as sample matrix for enzymatic hydrolysis (1 hour), higher yields were obtained for 24S-OHC, 25-OHC, and 27-hydroxycholesterol (27-OHC), compared to alkaline hydrolysis (3 hours). The surfactant Triton X-100 (TX-100) was a critical component for obtaining high yield. The method linearity was good (R^2 = 0.99 for all oxysterols) in the presence of TX-100 in human plasma.

Thus, the sample preparation time for detection of side-chain oxysterols in human plasma was shortened with 2 hours by using enzymatic hydrolysis with ChE in the presence of TX-100. Enzymatic hydrolysis also provided higher yields for 24S-, 25-, and 27-OHC compared to alkaline hydrolysis. Consequently, enzymatic hydrolysis should be considered a more efficient hydrolysis method than alkaline hydrolysis for measurements of oxysterols in biological samples. The method should also be applicable for tumors from BC patients and thus should be beneficial for the oxysterol community.

Preface

The work of this thesis was carried out at the Department of Chemistry at the University of Oslo in the period of August 2017 – May 2019.

First and foremost, I wish to thank my supervisors; professor Steven Ray Wilson for his motivational words and enthusiasm regarding my work, professor Elsa Lundanes, whose door was always open for discussion, and Dr. Hanne Røberg-Larsen for her continual guidance and advice. I would also like to express my gratitude to Steven and Hanne for including me in the European Network for Oxysterol Research.

Furthermore, I would like to thank Marita Clausen for lending me chemicals and equipment, and Inge Mikalsen for technical support, particularly when the pump malfunctioned.

Thank you to the entire group of Bioanalytical Chemistry for providing the best environment anyone could ask for. I gratefully acknowledge the helpful advice from Ingvild Comfort Hvinden about derivatization of sterols and the pleasant collaboration I had with Maria Schüller. Also, thank you to Stian Solheim for answering my questions regarding his sample preparation procedure, and thank you to Erik Konradsen and Sverre Løyland for helping me understand reaction mechanisms.

Moreover, I owe a special thanks to Esma Ben Hassine, Christine Olsen, and PhD candidate Frøydis Sved Skottvoll for their support. In addition, I am very grateful to Astrid Hermansen and Ago Mrsa for their care and our friendship throughout my education.

This degree would not have been achievable without my friends and my family. A special thanks to my brother Espen for encouraging me to pursue a Master's degree and for proofreading of this thesis.

At last, I wish to thank my loving parents for always being there.

While being aware that abbreviations should be kept out of titles, the term "hydroxycholesterol" will be abbreviated "OHC" in some of the titles in this thesis.

Maria Therese Sande

Oslo, May 2019

Table of contents

1 Abbreviations

%RSD	Relative standard deviation in percentage
22R-OHC	22R-Hydroxycholesterol
22S-OHC	22S-Hydroxycholesterol
24S-OHC	24S-Hydroxycholesterol
25-OHC	25-Hydroxycholesterol
27-OHC	27-Hydroxycholesterol
AC	Alternating current
ACN	Acetonitrile
AFFL	Automatic filtration and filter flush
ApoB	Apolipoprotein B
BC	Breast cancer
CH25H	Cholesterol-25-hydroxylase
ChE	Cholesterol esterase
ChX	Cholesterol oxidase
CID	Collision induced dissociation
cLOD	Concentration limit of detection
cLOQ	Concentration limit of quantification
CYP27A1	Cholesterol-27-hydroxylase
CYP450	Cytochrome P450
CYP46A1	Cholesterol-24-hydroxylase
CYP7B1	25-Hydroxycholesterol-7α-hydroxylase
Da	Dalton
DC	Direct current
DMAP	4-Dimethylaminopyridine
DMF	Dimethylformamide
DMPA	2,2-Dimethoxy-2-phenylacetophenone
ER	Estrogen receptor
ESI	Electrospray ionization
FA	Formic acid
GC	Gas chromatography
HESI-II	Heated electrospray ionization interface
HMG-CoA	3-Hydroxy-3-methyl-glutaryl-coenzyme A
ID	Inner diameter
IPA	Isopropanol/2-propanol
IS	Internal standard
IUPAC	International Union of Pure and Applied Chemistry
LC	Liquid chromatography
LC-ESI-MS	Liquid chromatography-electrospray ionization-mass spectrometry
LC-MS	Liquid chromatography-mass spectrometry

LDL	Low-density lipoprotein
LIPID MAPS	LIPID Metabolites and Pathways Strategy
LLE	Liquid-liquid extraction
LXR	Liver X receptor
m/z	Mass-to-charge ratio
MeOH	Methanol
MNBA	2-Methyl-6-nitrobenzoic anhydride
MP	Mobile phase
MRM	Multiple reaction monitoring
MS	Mass spectrometry/mass spectrometer
MS/MS	Tandem mass spectrometry
NPLC	Normal-phase liquid chromatography
OHC	Hydroxycholesterol
R^2	Correlation coefficient
RF	Radio frequency
ROS	Reactive oxygen species
RPLC	Reversed-phase liquid chromatography
Rs	Resolution
SNR	Signal-to-noise ratio
SP	Stationary phase
SPE	Solid phase extraction
SPH	SuperPhenylHexyl
SRM	Selected reaction monitoring
SST	Stainless steel
TGA	Thioglycolic acid
THF	Tetrahydrofuran
TIC	Total ion current
TLC	Thin layer chromatography
TQ	Triple quadrupole
t_R	Retention time
TX-100	Triton X-100
UN	Units

2 Introduction

2.1 Cancer

Cancer is a term used to describe a dangerous group of diseases, which is mainly characterized by uncontrollable and abnormal cell growth [1 (p. 2)]. Cancer occurs when DNA damage causes the cell's mechanism of reproduction inhibition to fail and cancer cells will grow and divide (proliferate) beyond what is normal [2 (p. 1092)]. The proliferation will give rise to a tumor, which is an accumulation of cancer cells.

If the cancer cells spread and invade other tissues/organs (metastasis), the tumor is said to be malignant and is considered especially dangerous because it is hard to eliminate. Some tumors are not invasive (benign tumors), and surgical removal of the tumor will usually be a sufficient cure. The malignant type of cancer is therefore considered "true cancer", as metastasis is generally the reason for patient death.

2.1.1 Breast cancer

BC is the second most common cancer worldwide, the most frequent malignancy in women, and hence one of the most studied types of cancer [3, 4]. In 2012, approximately 1.7 million women worldwide were diagnosed with the disease, which resulted in over 520 000 deaths, ranking BC 5th as the cause of death among cancers [3]. In Norway, there were over 3500 new cases in 2017, however, female BC only accounted for about 6% of the deaths from cancer that year [5]. The low death occurrence is mostly a result of early detection and systemic therapies, *e.g.* hormone therapy.

There are several different types of BC, and they are usually categorized based on different molecular expressions of receptors, *e.g.* the estrogen receptor (ER) and the progesterone receptor. About 70% of all BCs are ER-positive [6, 7]. In this type, the cancer cells grow in response to the hormone estrogen because the cells have receptors selective for this hormone. Hence, if estrogen binds to the receptors, cell proliferation is promoted. However, hormone receptor-positive tumors are sensitive to targeted hormone therapy, which is the least toxic form of treatment for BC [8].

If the cancer cells lack receptors for estrogen, they are categorized as ER-negative. Thus, the cells usually do not stop growing when treated with hormones that can block estrogen from binding (*e.g.* tamoxifen), because they do not need estrogen to grow. Due to the lack of the ER, treatments are mainly based on surgery, chemotherapy, and radiation. The prognosis is, therefore, poorer than for ER-positive BC, and those with ER-negative tumors are usually diagnosed at a younger age and have higher mortality [9].

With the interest of developing better treatment for both ER-positive and ER-negative BC, it is important to achieve a greater understanding of the function of the cancer cells, and especially their metabolism.

2.1.2 The metabolism of cancer cells

Being fundamentally a disorder of cell growth and proliferation, cancer cells require nutrients as cellular building blocks, *e.g.* nucleic acids, proteins, and lipids. Therefore, cancer cells have the ability to adapt their metabolism in a way that allows them to accumulate metabolites as sources of energy, and thereby support tumor initiation and progression. Alteration of metabolism is important for cancer cells and has become a recognizable characteristic of cancer [10-12].

A well-known example is *the Warburg effect* (also known as aerobic glycolysis) discovered in 1927. Otto Warburg observed an increase in the uptake of glucose in cancer cells, probably with the purpose of building biomass [13, 14]. No other pathway has received more attention than the Warburg effect in cancer biology and principles involving glycolytic regulation has been extensively reviewed [15]. However, in the past few years, lipid metabolic abnormalities in tumors have become increasingly recognized [16-18].

2.2 Lipids

The term “lipid” is used to describe a diverse group of biomolecules that are generally soluble in nonpolar solvents, and are one of four types of molecules that comprise the human body (along with nucleic acids, proteins, and carbohydrates) [19]. Lipids are crucial components of the cell membrane; they regulate membrane proteins, participate in signaling pathways and serve as energy storage sources [20]. In the cell membrane, lipids constitute about 50% of the mass, forming the lipid bilayer, which is a polar membrane that provides the basic fluid

structure of the cell membrane [2 (p. 566)]. In other words, lipids are along with proteins the building blocks of the cell, and the lipid bilayer regulates the transportation of biomolecules and prevents them from diffusing into areas they should not be. An illustration of the lipid bilayer is shown in **Figure 1**.

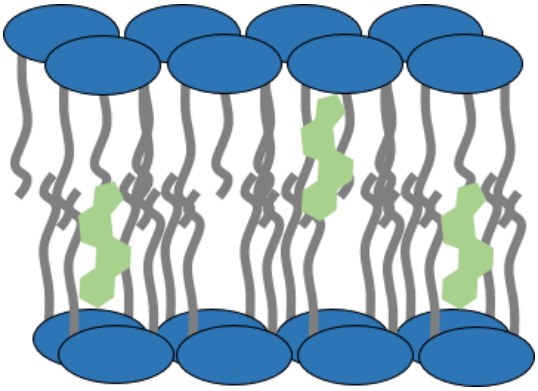

Figure 1. The lipid bilayer in the cell membrane, which mainly consists of phospholipids (blue) and cholesterol (green). Adapted from [2 (p. 569)].

Because lipids comprise an extremely heterogeneous collection of molecules, both structural and functional, the classification of the compounds diverge, and several different classification systems have been used over the years. The Lipid Library and Cyberlipid Center characterize lipids as either "simple" or "complex"; the simple lipids yield at most two types of products after hydrolysis (*e.g.* acylglycerols: fatty acids and glycerol), while the complex yield three or more products (*e.g.* glycerophospholipids: fatty acids, glycerol, and a headgroup). Further, in 2005, the International Lipid Classification and Nomenclature Committee and LIPID Metabolites and Pathways Strategy (LIPID MAPS) developed a comprehensive lipid classification system. In this system, lipids have been divided into eight different categories: fatty acyls, glycerolipids, glycerophospholipids, sphingolipids, saccharolipids, polyketides, prenol lipids, and sterol lipids [21, 22].

Lipids have diverse molecular composition, various cellular functions and their structure change constantly with physiological and environmental conditions. Therefore, the study of these biomolecules has been hampered by analytical limitations, *i.e.* precise structure elucidation due to the presence of chiral centers, the position of functional groups and double bond locations [23]. Consequently, lipids have remained in the shadow of the study of metabolites (metabolomics), proteins (proteomics) and genes (genomics). However, analysis of

lipids and factors that interact with lipids emerged in the early 2000s as lipidomics and has advanced in recent years, largely due to the development of mass spectrometry (MS, explained in detail in **Section 2.5**) [24-27]. Particularly the lipid cholesterol and its metabolites oxysterols have gained major attention for their role in several biological functions in the body, including their effect on cancer development [28].

2.2.1 Cholesterol

Cholesterol is classified as a 27-carbon sterol lipid, which consists of a rigid steroid structure, a polar hydroxyl group, and a non-polar hydrocarbon chain, as illustrated in **Figure 2**. Cholesterol makes up approximately 30% of the cell membrane, rendering it the most prominent lipid in eukaryotic cells and a necessary component for modulating the lipid bilayer and maintaining cellular homeostasis [2 (p. 571), 29, 30]. In addition, cholesterol is a precursor for bile acids, steroid hormones and vitamin D, which are all important for controlling *e.g.* the metabolism and immune functions [31, 32].

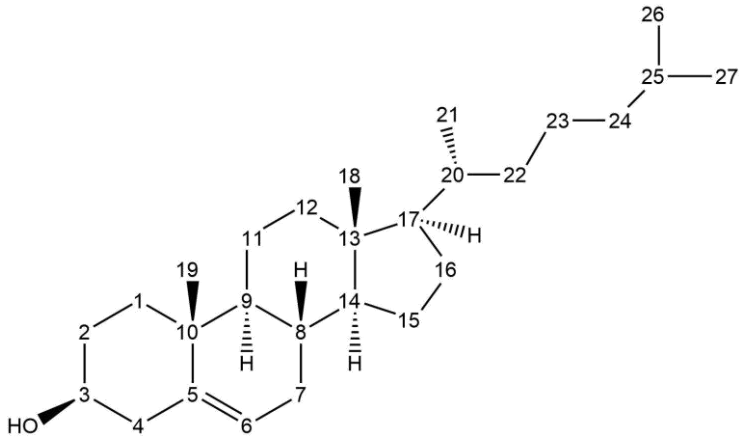

Figure 2. The structure of cholesterol with numbered carbon atoms, according to The International Union of Pure and Applied Chemistry (IUPAC) [33].

Cholesterol is primarily synthesized in the liver by the enzyme 3-hydroxy-3-methyl-glutaryl-coenzyme A (HMG-CoA) reductase or obtained from the diet and is stored as cholesterol esters together with fatty acids in low-density lipoproteins (LDL, shown in **Figure 3**) [34]. Lipoproteins are proteins whose function is to transport hydrophobic lipids through the more hydrophilic extracellular body fluid, *e.g.* water and blood plasma [35]. Several studies have

shown that ER-negative breast cancer cells have a higher uptake of LDL and that LDL *de facto* increase proliferation [36, 37].

The connection between cancer progression and LDL is presumably that cancer cells are in constant need of lipids for membrane construction, especially cholesterol. Many types of cancer cells synthesize cholesterol and fatty acids *de novo* through the upregulation of glycolysis [38]. However, increasing the uptake of LDL (which supplies both cholesterol and fatty acids) may be accomplished under conditions where oxidative metabolism is compromised, and direct uptake of LDL is more energetically favorable than oxidative metabolism, as *e.g.* HMG-CoA is not required.

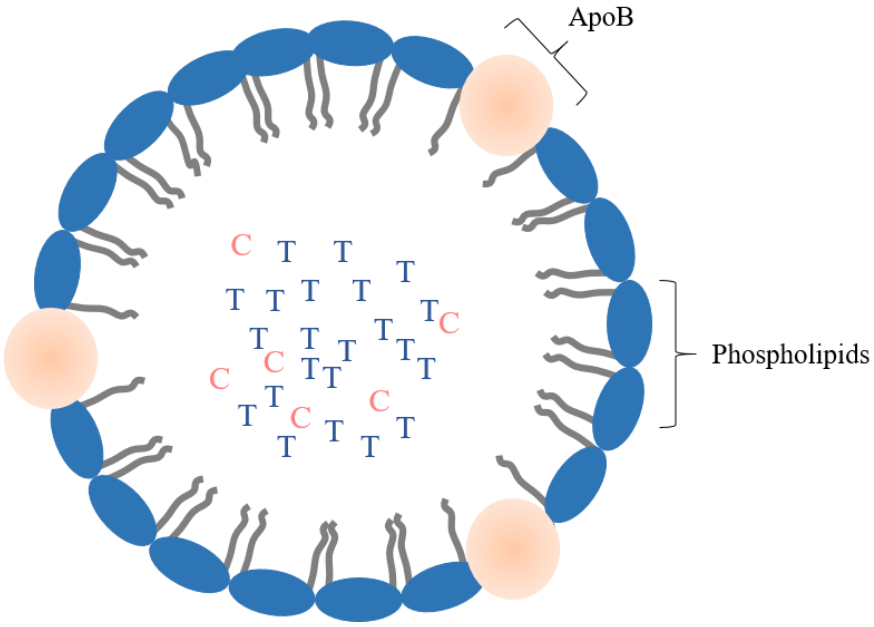

Figure 3. The structure of an LDL. The outer hydrophilic core is made of phospholipids and apolipoprotein B (ApoB), and the inner hydrophobic core consists of esterified cholesterol (C) and triglycerides (T). Adapted from [39].

2.2.2 Oxysterols

Oxysterols (hydroxycholesterol, OHC) are neutral, oxygenated 27-carbon metabolites, derived from the oxidation of cholesterol and are transported either as free or bound (*e.g.* as oxysterol esters) form in LDL [40, 41]. They consist of the same steroid structure, albeit with an additional hydroxyl group located either on the side-chain or on the steroid ring. Side-chain oxysterols are usually formed enzymatically, while oxysterols with the hydroxyl group on the

steroid ring are formed non-enzymatically [42]. The non-enzymatic formation has also been referred to as “autoxidation”, and may occur both *in vivo* and *ex vivo* (**Textbox 1**).

With the hydroxyl group placed on the ring structure, the oxysterols behave similarly to cholesterol [43, 44]. They are therefore not assessed in this thesis. The side-chain oxysterols investigated in this thesis are shown in **Figure 4**, along with cholesterol and known enzymes. The systematic IUPAC names for these oxysterols are shown in **Table 1**. However, for simplification, the trivial names will be used from now.

Textbox 1. Autoxidation of cholesterol.

Autoxidation

Non-enzymatic oxidation of cholesterol (or autoxidation) *ex vivo* was first reported in 1941, where cholesterol appeared to oxidize with only oxygen present [45]. However, “autoxidation” is potentially a misleading term, as an initial autoxidation process requires factors like reactive oxygen species (ROS) or trace metals. Nevertheless, biological systems are complex and cholesterol can consequently be oxidized *in vivo* by ROS [46, 47]. The term “autoxidation” is, therefore, a legitimate term, and will thus be used further to describe non-enzymatic oxidation of cholesterol, both endogenously and during sample preparation.

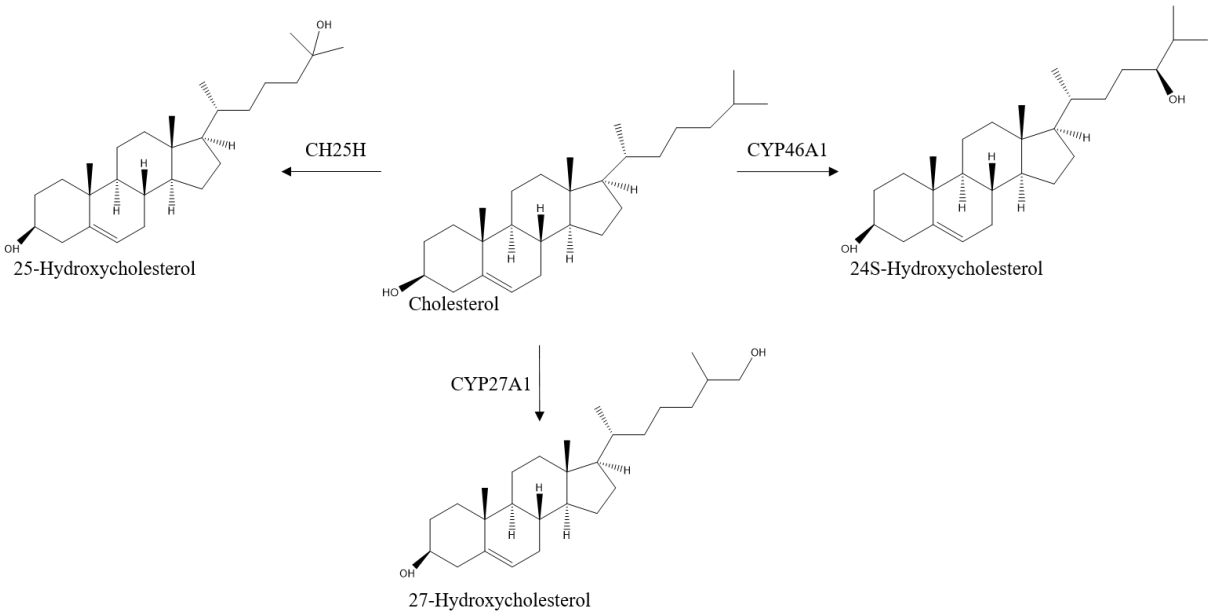

Figure 4. Structures of 24S-OHC, 25-OHC, and 27-OHC with corresponding enzymes along with their precursor, cholesterol.

Table 1. Trivial names and systematic IUPAC names for 25-, 24S-, and 27-OHC [33].

Trivial name	**Systematic IUPAC name**
25-Hydroxycholesterol	Cholest-5-ene-3β,25-diol
24S-Hydroxycholesterol	Cholest-5-ene-3β,24S-diol
27-Hydroxycholesterol	Cholest-5-ene-3β,27-diol

The enzymatic formation of side-chain oxysterols is catalyzed by cytochrome P450 (CYP450) enzymes [48, 49]. The enzyme cholesterol-27-hydroxylase (CYP27A1) is present in macrophages and tissue and is responsible for the formation of 27-OHC [46, 50, 51]. 24S-OHC is converted from cholesterol by the enzyme cholesterol-24-hydroxylase (CYP46A1), which mostly exists in neurons in the brain [46, 52, 53]. Formation of 25-OHC is catalyzed by the enzyme cholesterol-25-hydroxylase (CH25H), an enzyme that is not *de facto* a part of the CYP450 family [46, 53].

Several important biological roles are connected to oxysterols, *e.g.* atherosclerosis, apoptosis, inflammation, immunosuppression, and development of gallstones [42, 54, 55], as well as being potential targets for Parkinson's and Alzheimer's disease [56]. In addition, oxysterols operate

as cholesterol metabolism mediators [57] and as signaling molecules, *e.g.* in the Hedgehog signaling pathway [58], on the Liver X receptors (LXRs) [59] and on the ER [60, 61]. Oxysterols can also pass cell membranes due to their more hydrophilic properties, and thereby modulate the activity of membrane proteins and change the permeability of the lipid bilayer [62-65]. The biological roles related to oxysterols will not be elaborated further in this thesis, as the focus will be on their role in cancer development.

2.3 The role of oxysterols in cancer

Oxysterols have shown to affect cancer progression in several ways, especially on BC through the activation of ER. Recent studies have shown that 27-OHC accumulates in the ER-positive BC tumor tissue, and regulates the transcriptional activity by binding to the ER, which will stimulate tumor growth [61, 66-68]. The amount of 27-OHC in BC tissue and tumors has been reported as 2.3-fold greater compared to controls, and the variations in the amount of serum 27-OHC relative to cholesterol are 40% in control samples, versus 18% in samples from patients with ER-positive BC [67]. These findings imply that the synthesis of 27-OHC from cholesterol is altered in ER-positive BC. Presumably, the accumulation of 27-OHC in ER-positive BC tumors does not arise from increased activity of CYP27A1, but rather due to the diminished expression of the 27-OHC metabolizing enzyme 25-hydroxycholesterol-7α-hydroxylase (CYP7B1), which transforms 27-OHC to 27-cholestenoic acid. Hence, 27-OHC is a locally modulated ligand for the ER [67]. In addition, 27-OHC is a potential blocker for tamoxifen, which is a hormone used for the treatment of ER-positive BC [69].

Several studies have demonstrated that the LXRs are able to inhibit cell proliferation for *e.g.* ovarian and prostate cancer, as well as glioblastoma and BC, and are therefore considered potential therapeutic targets for cancer [70, 71]. The LXRs are hormone receptors that are considered targets for *e.g.* 24S-, 25-, and 27-OHC *in vivo*, and they control cholesterol metabolism with activation by the above-mentioned oxysterols [71-73]. By being lipid sensitive receptors, their anti-proliferative role may be connected to a reduction of cholesterol levels by blocking the uptake of LDL [74]. However, the binding of the oxysterols on the LXRs has shown to stimulate tumor formation, either by the promotion of tumor growth or by modulation of the anti-tumor immune response [71, 75]. The role of the oxysterols in conjunction with the LXRs and cancer has not been fully understood, and more efficient techniques for determination of oxysterols must be developed.

2.4 Determination of oxysterols

There are several challenges related to the quantification of oxysterols. Firstly, oxysterols in plasma membranes and lipoproteins are only present in trace concentrations (ng/mL range) compared to cholesterol, which is present with a great excess (103 to 106-fold) [40, 50]. Determination of oxysterols will, therefore, be in competition with a high concentration of cholesterol. In addition, the formation of several oxysterols (*e.g.* 7β-OHC [45]) by autoxidation of cholesterol during sample preparation make their determination challenging as the autoxidation, even at a small extent, can give elevated concentrations of analytes and lead to misleading results [50, 76]. The most accurate method for monitoring the autoxidation is by adding isotope labeled cholesterol to the sample (*e.g.* 25-, 26-, 27-$^{13}C_3$ cholesterol or $^{2}H_6$ cholesterol) [40, 77]. The isotope-labeled cholesterol will not prevent the autoxidation, but if autoxidation occurs for cholesterol, it will also occur for the isotope-labeled cholesterol and can be monitored by MS.

When investigating the role of oxysterols in biological samples (*e.g.* tumors and blood plasma), only small sample amounts are available. Griffiths *et al*. have previously reported measurements of oxysterols using 50 – 200 μL plasma [78]. In this study, 5 μL plasma will be used. Therefore, a sufficient sensitivity is necessary; the low concentrations of the oxysterols in a small sample can be enriched by large-volume injection (explained in detail in **Section 2.6.3**).

Several methods for identification and quantification of oxysterols have been reported, including separation techniques such as thin layer chromatography (TLC) [79], gas chromatography (GC) [77] and liquid chromatography (LC, further explained in **Section 2.6**) [80-83]. Nevertheless, TLC is not suited for the complex mixtures of oxysterols found in biological samples [57]. The traditional method for oxysterol determination has been GC-MS with derivatization to make the oxysterols volatile and thermally stable [78, 84, 85]. However, the sample preparation is laborious and time-consuming [86, 87], and the sensitivity is not as good as in LC coupled to electrospray ionization MS (LC-ESI-MS) [50]. In addition, the hard ionization techniques often used in GC-MS (*e.g.* electron ionization) operates traditionally at 70 eV, which yields extensive fragmentation of biological molecules and the mass spectra can thereby be hard to interpret.

Due to the aforementioned drawbacks of GC-MS, the popularity of LC-MS determination of oxysterols has evolved over the past years [50, 78, 88]. Perhaps the most known method in the scientific community is a comprehensive and high throughput method developed by McDonald and co-workers [89, 90]. However, the requirements for the LC separation are high, as many oxysterols are isomers and tend to give similar mass spectra (explained in **Section 2.6.1**). Furthermore, oxysterols are neutral compounds and ionize poorly with ESI (explained in **Section 2.5.1**). In order to enhance ionization efficiency, a derivatization procedure is necessary. Furthermore, the oxysterol esters must be hydrolyzed prior to LC-MS for a total oxysterol measurement. The sample preparation requirements for determination of oxysterols with LC-ESI-MS can, therefore, be tedious, although less laborious and time-consuming than for the GC-MS methods. A possible shortening of the sample preparation steps (for LC-MS determination of oxysterols) addressed in the next subsections will be pursued in this thesis.

2.4.1 Hydrolysis of oxysterol esters

Because oxysterols occur either as free or esterified, they are quantified by determining the free concentration or the total concentration (*i.e.* free and bound). In order to perform a total oxysterol quantification, the oxysterol esters must be transformed to free oxysterols, as shown in **Figure 5**. Traditionally, alkaline hydrolysis (also called saponification) has been carried out for this purpose [77, 81, 91, 92]. However, this hydrolysis suffers from major drawbacks, *e.g.* degradation of triglycerides and phospholipids, generation of undesirable products due to thermal degradation of 7-ketocholesterol and cholesterol, because of the basic environment and high temperatures [89, 93-95]. These issues reduce sample integrity and produce high background noise, which complicates the analysis. Furthermore, the method of McDonald and co-workers suffers from incomplete hydrolysis of oxysterol esters in pathological samples [89]. The alkaline hydrolysis also requires more sample handling, as the alkaline compound must be removed by liquid-liquid extraction (LLE). In addition, the use of alkaline solutions and the chemical waste produced have a negative impact on the environment.

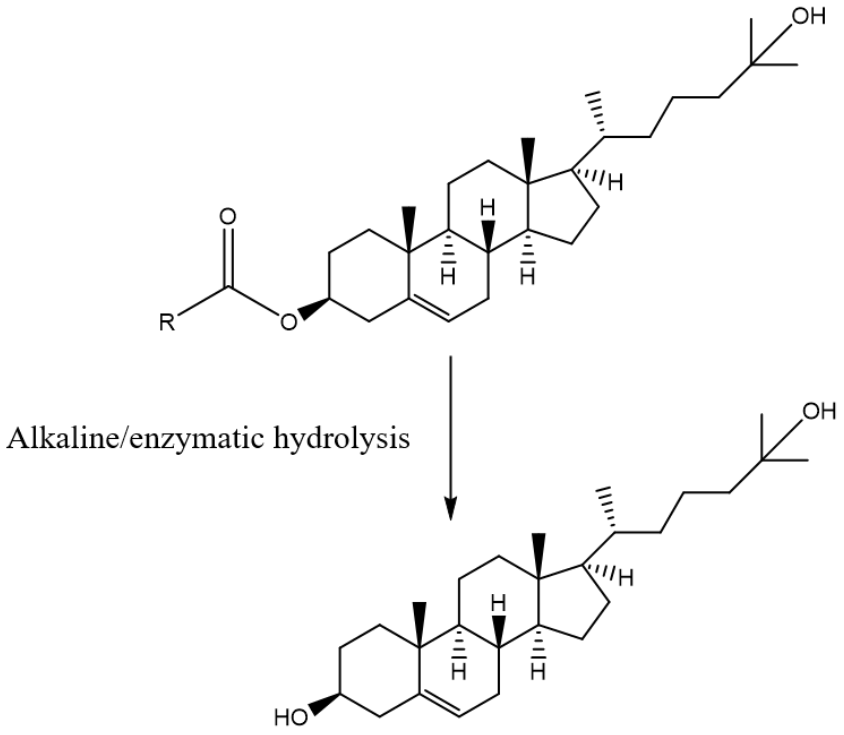

Figure 5. Hydrolysis of a 25-OHC ester to free 25-OHC.

Mendiara *et al*. have developed a method for hydrolysis of oxysterol esters using the enzyme cholesterol esterase (ChE) [96]. The issues with alkaline hydrolysis are supposedly solved when using ChE, as the sample preparation time and unknown compounds generated are reduced. Cleaner chromatography compared to alkaline hydrolysis is also reported. Thus, the enzymatic hydrolysis with ChE was to be thoroughly studied in this thesis.

2.4.2 Cholesterol esterase

ChE (also called the bile-salt activated lipase) is a glycoprotein in the esterase/lipase family and is one of two major enzymes contributing to lipolysis in the pancreatic secretion of mammals [97]. The enzyme has a broad substrate selectivity and is responsible for the hydrolysis of cholesterol esters, lipid-soluble vitamin esters, phospholipids and triglycerides [98, 99]. The catalytic activation of the enzyme against these substrates requires a bile salt (*e.g.* cholate) [100].

The amino acid sequence of ChE in different species has small variations, especially for the N-terminus catalytic domain, which consists of the first 1 - 530 amino acids in human ChE. The C-terminus consists of 531 - 722 amino acids in human ChE and is rich in proline, threonine,

and serine [99]. Several propositions for the crystallographic structure of ChE have been presented since 1990, and reveal a core of mixed β sheets (5 – 14 strands), flanked by α helices [101, 102]. **Figure 6** shows a ribbon structure of ChE from bovine, which is structurally similar to the one from humans, although with fewer amino acids.

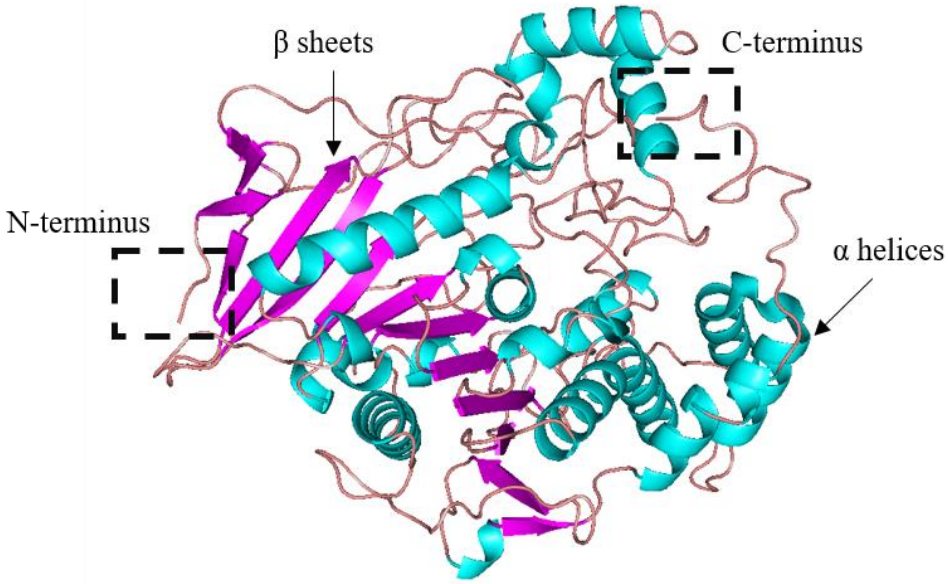

Figure 6. A ribbon structure of bovine ChE with α helices (cyan), β sheets (magenta) and coiled coil (beige). The image of the 1AKN [103] structure was created with PyMOL [104].

The active sites for ChE consist of the catalytic triad with Ser194, His435, and Asp320 [103]. A catalytic triad is a set of three coordinated amino acids, which is found in the active site of the enzyme. Even though the triad amino acids may be far apart in the primary structure, the coiling of the protein brings them together.

In the Ser-His-Asp triad, aspartate (Asp) functions as an acid residue, which hydrogen bonds and polarizes histidine (His) that functions as a base. The pKa of the imidazole nitrogen of histidine increases and the lone pair activates the nucleophile, serine (Ser). Following, the nucleophile attacks the carbonyl carbon in the ester bond in the oxysterol esters. The Ser-His-Asp system is shown in **Figure 7**. In order for ChE to reach the esterified sterols, the plasma LDL membrane must be solubilized, and the solubilization can be performed by using surfactants.

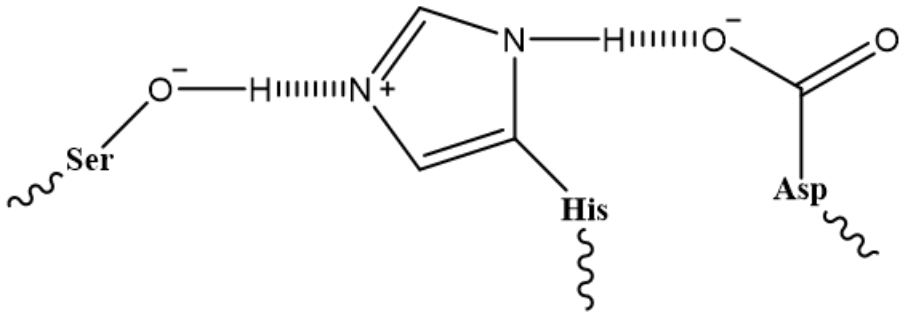

Figure 7. The structure of the Ser-His-Asp catalytic triad.

Surfactants

Surfactants are amphiphilic compounds that consist of a hydrophobic alkyl chain and a hydrophilic ionic or non-ionic head group [105 (p. 3)]. In aqueous solutions at specific surfactant concentrations and temperature, surfactants self-associate into clusters called micelles. Micelles are aggregates whose hydrophilic head are in contact with the surrounding water, with a hydrophobic tail pointed towards the center, forming a hydrophobic core (much like the lipid bilayer) [105]. The structure of a micelle is shown in **Figure 8**. When forming micelles, the surfactant is able to solubilize lipid membranes, *e.g.* the phospholipid-membrane in LDL [106].

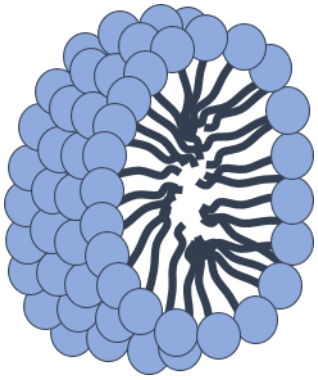

Figure 8. The structure and cross-section of a micelle. The hydrophilic head (blue) is facing the aqueous environment, while the hydrophobic tail (dark grey) is pointed towards the hydrophobic center. Adapted from [2 (p. 569)].

The interactions within surfactant-phospholipid systems have been extensively studied [107, 108]. The mechanism is presumably that the non-micellar detergent first partitions into the phospholipid bilayer and the incorporated detergents will co-exist with mixed phospholipid-

surfactant micelles saturated with phospholipids. Following, the phospholipids will solubilize by a final uptake into the surfactant micelles.

2.4.3 Derivatization of oxysterols

In order to increase the ESI ionization efficiency (and thereby improve the method sensitivity) of the neutrally charged oxysterols, a derivatization (or a charge tagging) must be carried out. Determination of oxysterols without derivatization has previously been performed (*e.g.* in the method by McDonald and co-workers), but determination without derivatization has proven to be challenging for *e.g.* nano-LC-MS systems [109].

2.4.4 Derivatization with Girard's reagent T

Possibly the most used derivatization procedure for oxysterols is derivatization with the Girard hydrazones, Girard T and Girard P, which have been used for decades in steroid analysis [110-113]. Oxysterols have a 3β-hydroxy-5-ene group which is prone to treatment with the enzyme cholesterol oxidase (ChX) [114]. By first oxidizing the 3β-hydroxy-5-ene group, the Girard T reagent can secondly be added to the 3-oxo-4-ene group and form the charge tagged oxysterol with a molecular weight of 514.4. The derivatization process is shown in **Figure 9**. Derivatization with Girard T will be used in this thesis, as it has by our hands, provided better performance regarding separation and detection than Girard P.

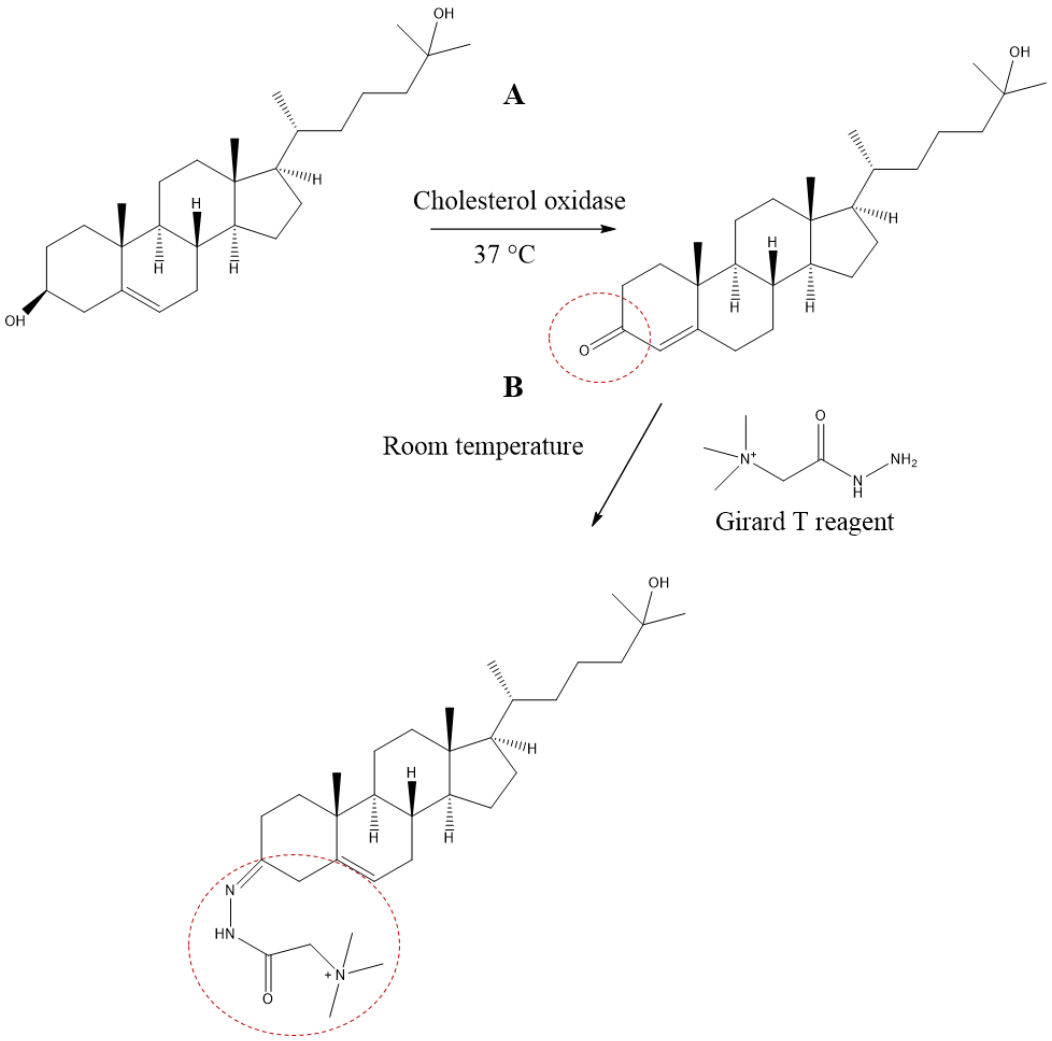

Figure 9. Derivatization of 25-OHC with the Girard T reagent. ChX oxidizes the 3β-hydroxy-5-ene group (**A**) by incubation at 37 °C for 1 hour. The Girard T reagent attacks the 3-oxo-4-ene group (**B**) by incubation at room temperature overnight and forms the charge tagged oxysterol. Adapted from [115].

An obvious drawback of the Girard T derivatization is the amount of time required; the oxidation step (**Figure 9A**) requires 1 hour, and the derivatization step (**Figure 9B**) is performed overnight. In addition, the extensive sample handling with ChX makes cholesterol more prone to autoxidation. A potential pitfall for the derivatization is that some oxysterols naturally possess a 3-oxo-4-ene group, and consequently, they can not be distinguished from the oxysterols oxidized by ChX (*e.g.* 7α-hydroxy-4-cholesten-3-one and 7α-OHC) [50, 116]. The problem can be solved by dividing the sample in two, and treating one fraction with ChX and one with no oxidation, in order to identify which oxysterols have been oxidized. Another drawback of the derivatization is that it is not stereospecific, *i.e.* cis and trans isomers are

introduced (**Figure 10**). This may lead to two separate peaks for a single compound when LC-MS is used [116, 117].

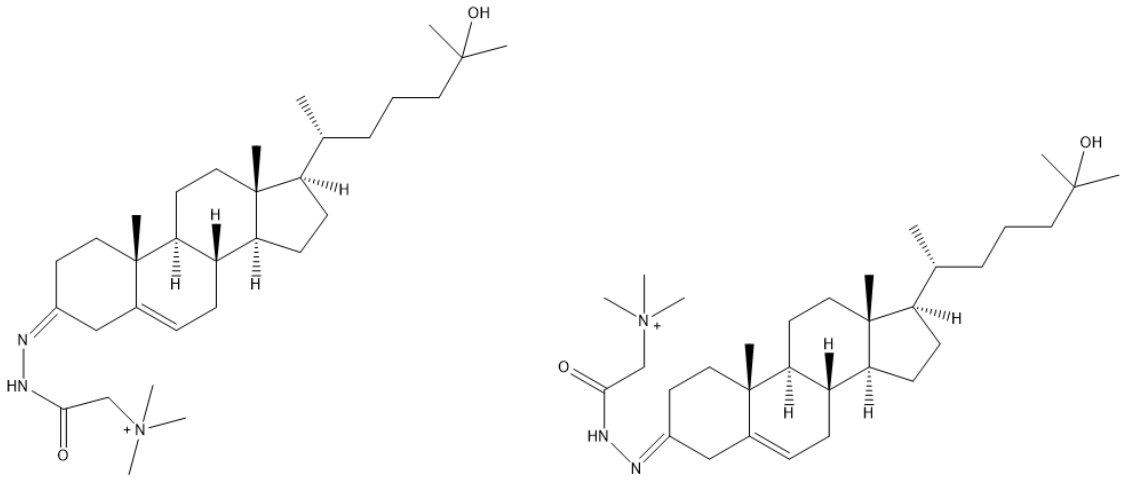

Figure 10. The cis and trans isomers formed for 25-OHC after derivatization with Girard T.

2.4.5 Derivatization with picolinic acid

Honda *et al*. have developed a rapid and sensitive LC-MS method exploiting charge tagging of oxysterols with picolinic acid, and hence transforming them into picolinyl esters in 1 hour [116, 118, 119]. The method was able to detect seven oxysterols at a level of 2 ng/mL with only 5 μL serum. The detailed derivatization reaction is not completely elucidated, but the picolinic acid is directly added to the 3β-hydroxy-5-ene group with the help of several reagents (discussed further in **Section 4.1.1**). The simplified derivatization process is shown in **Figure 11**. Oxysterols tend to give both mono- and dipicolinate derivatives after derivatization, as well as sodium adducts ($[M + Na]^+$) during MS, where the sodium gives rise to the positive charge.

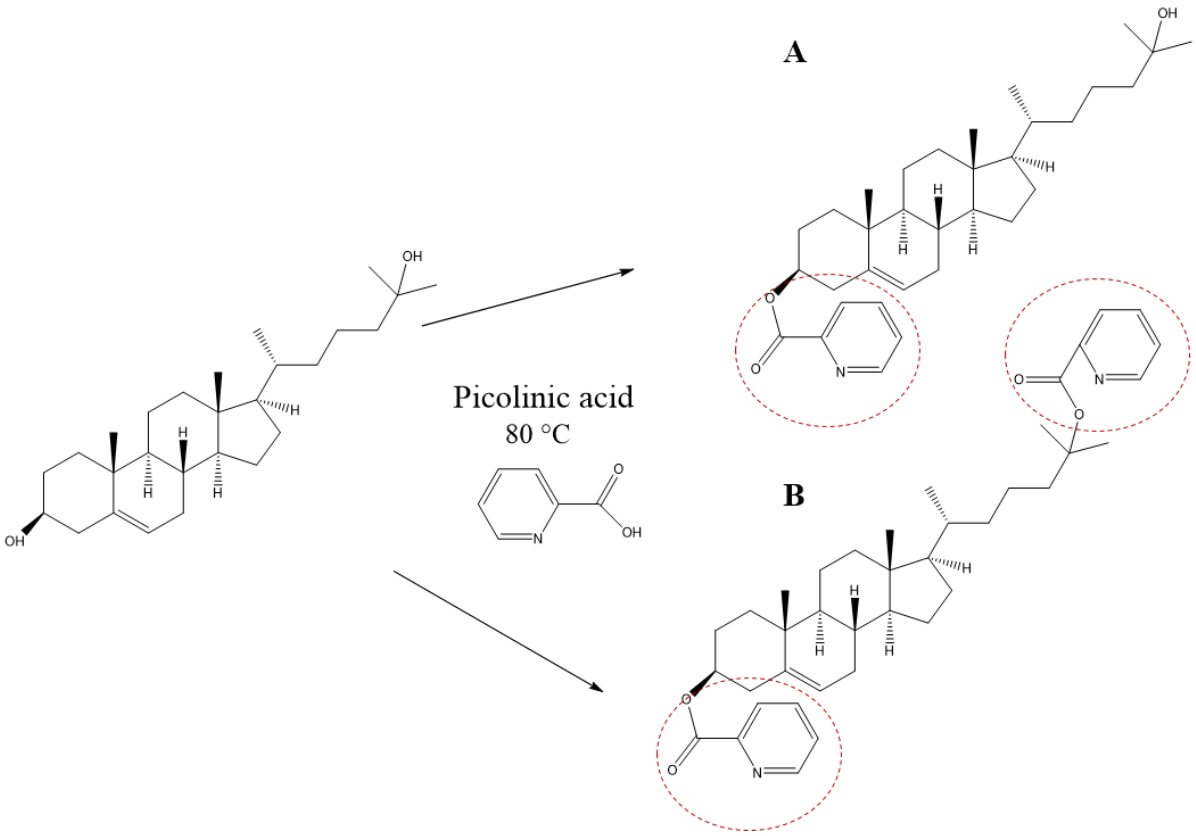

Figure 11. Derivatization of 25-OHC with picolinic acid by incubation at 80 °C for 1 hour, forming 25-OHC-monopicolinate (**A**) and 25-OHC-dipicolinate (**B**).

2.4.6 Thiyl radical-based charge tagging

Adhikari *et al*. performed a fast (< 1 min) charge tagging of cholesterol with thioglycolic acid (TGA) through a thiol-ene radical click chemistry reaction (thiyl radical-based charge tagging), by irradiation with UV-light [120]. Click chemistry is a term used to describe a group of "perfect" reactions that focuses on carbon-heteroatom bond formation [121]. The reactions are fast, give high yields and have a wide scope, as well as not being sensitive to water or oxygen. In addition, the TGA-tagged oxysterols will appear in negative ESI mode, which in general has a lower background noise than the positive mode. Therefore, a thiol-ene click chemistry derivatization of oxysterols is preferred compared to charge tagging with picolinic acid or with the Girard T reagent.

The thiyl radical-based charge tagging reaction can be divided into three steps and is shown in **Figure 12**. First, a thiyl radical is generated by irradiating the sample with UV-light in the presence of a photoinitiator (**Figure 12A**). Second, the radical attacks the C_5-C_6 double bond and forms an intermediate with a lone electron pair, while TGA is regenerated (**Figure 12B**).

The intermediate then reacts with the thiyl radicals present, and the final charge tagged oxysterol is formed (**Figure 12C**). The reaction is discussed in detail in **Section 4.1.2**.

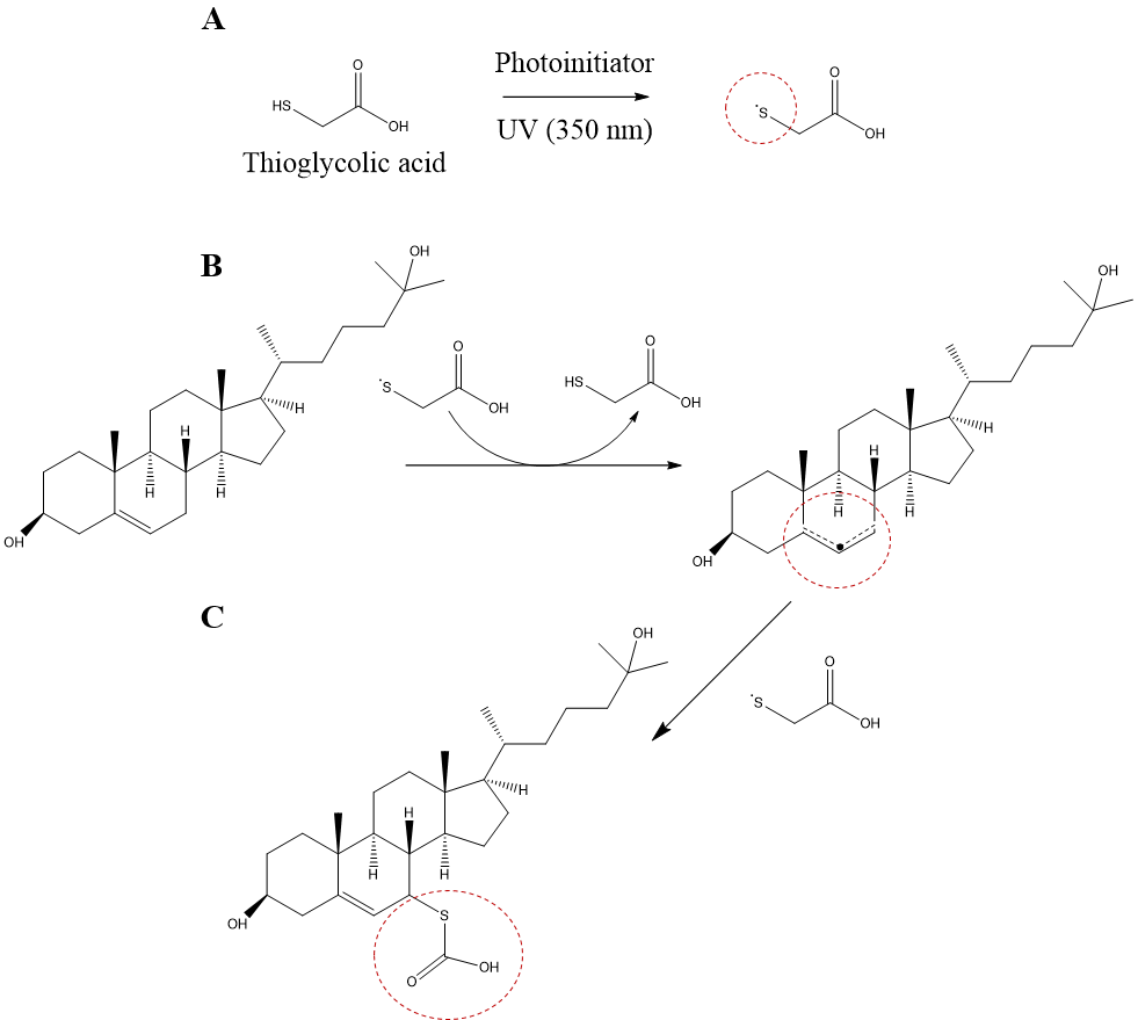

Figure 12. Thiyl radical-based charge tagging of 25-OHC. TGA is exposed to UV-light, and forms a thiyl radical in the presence of a photoinitiator (**A**). The thiyl radical attacks the C_5-C_6 double bond, which results in an oxysterol intermediate with a lone pair (**B**), while TGA is regenerated. The thiyl radical reacts with the lone pair, and TGA-tagged 25-OHC is formed (**C**).

2.5 Mass spectrometry

MS is a tool used to identify masses of molecular ions (precursor ions), or their fragments (product ions). Mass spectrometers operate at high vacuum; hence, the compounds of interest must be in a gaseous state. In addition, the MS uses electric and/or magnetic fields to manipulate the compounds of interest, therefore the analytes must be ionized. Following ionization, the ions are separated according to their mass-to-charge ratio (*m/z*). The major components of the MS are the sample introduction system, with the ion source where the solvent is vaporized and the ions are produced, the mass analyzer where the ions are separated, and the detection system.

2.5.1 Ion source: electrospray ionization

The challenge in coupling the LC to the MS is that the chromatograph operates with liquids, while the MS operates under high vacuum. Therefore, a device is needed between the chromatograph and the MS, where the transition from liquid to gas phase as well as ionization of neutral molecules occurs – this device is called an interface. There are many types of interfaces, and choosing a suitable one depends on the properties of the analytes, *e.g.* polarity and size, as well as the sample matrix.

MS is often operated as a mass sensitive detector, *i.e.* the signal is proportional to the mass flow (number of molecules per unit time). However, by using the ESI interface, the MS can be operated as a concentration sensitive detector. ESI is a soft ionization technique (meaning little fragmentation) and is not only extremely useful for large, non-volatile, chargeable molecules, but also for *e.g.* small, polar compounds and ionic metal complexes [122, 123]. The actual ionization does seldom occur in the ESI process, but *de facto* in the solvent due to pH adjustment, prior to injection [124, 125].

In ESI, the analytes are dissolved in an electrically conductive liquid and flow through a narrow steel capillary (an emitter). A positive or negative voltage (2-5 kV) is applied at the end, and the ions with the charge opposite to that of the applied voltage are removed; this yields a solution with a surplus of one type of charge. Due to the ions being charged when they enter the capillary and the repulsive forces that will occur between the charged capillary and the ions, the voltage will create an accumulation of ions at the outlet, named a Taylor cone [126].

Further, the ions will eventually explode into a fine mist of micrometer-sized electrically charged droplets. There are several theories of what happens next, but presumably, due to repulsive forces between the charges inside the droplets, they will explode into smaller droplets, resulting in gas phase ions. The ions will be attracted to the MS inlet, which acts as a counter electrode. **Figure 13** illustrates the ESI mechanism.

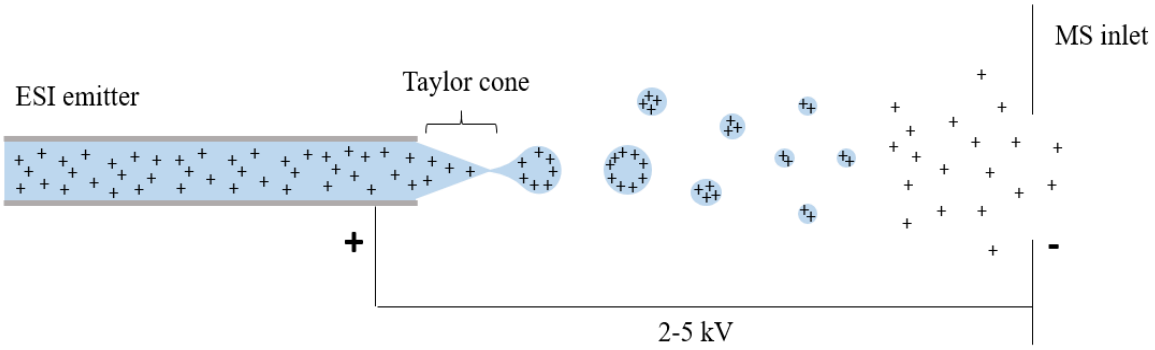

Figure 13. Illustration of the ESI mechanism. Adapted from [127].

2.5.2 Mass analyzer: the quadrupole

Once the gas phase ions have been formed, they must be separated according to their *m/z*; the separation is performed by the mass analyzer. There are several different mass analyzers with different modes of operation available. Examples of mass analyzers are time-of-flight, ion trap, orbitrap and the quadrupole [128]. In this study, a triple quadrupole (TQ) was used – a scanning mass analyzer, as the electric field applied can be varied continuously in order to obtain mass spectra.

The quadrupole consists of four metal rods that are placed parallel to each other in a square, with the opposite pairs connected electrically. The pairs of opposite rods are each held at the same potential; one pair has a potential composed of a positive direct current (DC), and the other pair has a negative DC. A radio frequency (RF) alternating current (AC) is superimposed on both of the pairs, which results in the rods constantly oscillating between positive and negative polarities. The quadrupole can be operated as a mass filter, as the ions will begin to oscillate when they enter the field produced by the DC and the RF potentials. An illustration of the quadrupole is shown in **Figure 14**. Only ions with a specific *m/z* value will have a stable trajectory (the green line), while all other ions with different *m/z* values develop unstable oscillation and are therefore lost by collision with the rods (the blue line).

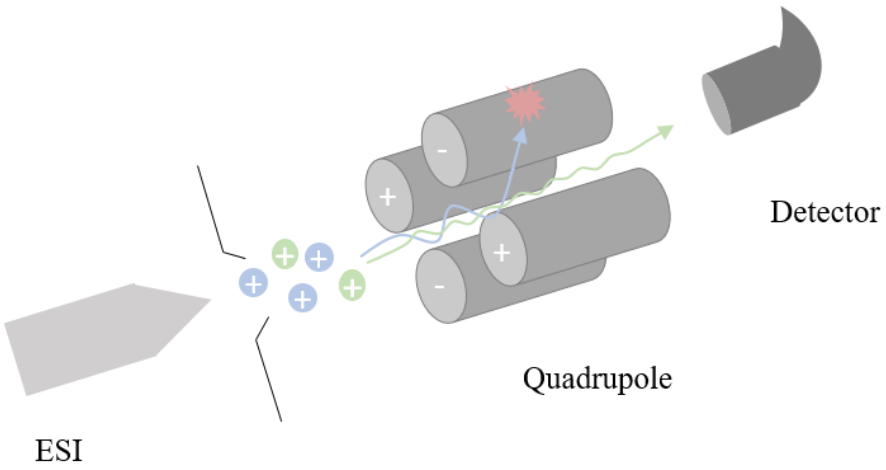

Figure 14. An illustration of the quadrupole. The quadrupole consists of four metal rods placed parallel to each other, with each pair connected electrically by a DC and an RF potential. Ions with selected m/z are will have a stable trajectory through the quadrupole (green line), while all the other ions will collide with the rods and be lost (blue line). Adapted from [129 (p. 72)].

In order to enable scanning of a mass range and hence obtain mass spectra comprised of different *m/z* values with high resolution, the quadrupole must be operated along a scan line. At the scan line, the DC and RF voltages are varied progressively while their ratio is kept constant, and hence the quadrupole is operated in mass selective stability mode. **Figure 15** shows the stability diagram of ions with three different *m/z*: m1, m2, and m3. The ions are stable inside the triangle, and the higher the slope of the operating line (blue), the higher the resolution of the instrument. A consequence of higher resolution is, however, a loss of sensitivity.

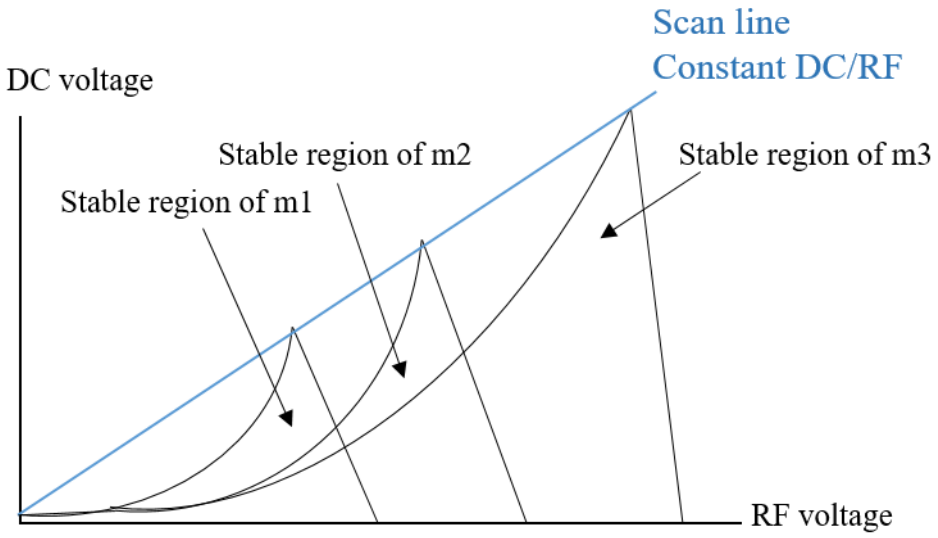

Figure 15. The stability diagram of the quadrupole operated in mass selective stability mode. The DC and RF potentials are varied while their ratio is kept constant at a scan line. A high-resolution sequential scanning of ions with different *m/z* can only be performed when the MS is operated along the scan line. Adapted from [130 (p. 37)].

2.5.3 Tandem mass spectrometry

Tandem mass spectrometry (MS/MS) is an important technique in most analytical applications of MS and involves multiple steps of MS selection with fragmentation of the ions in between. Fragmentation of the analytes is necessary for structure elucidation, as each molecule has a "fingerprint" in the mass spectrum caused by the fragments. MS/MS has a major contribution to the identification of compounds in complex mixtures without chromatographic separations, as well as the elucidation of fragmentation pathways. The general principle of MS/MS is that a precursor ion is decomposed into smaller product ions in a collision cell, often followed by the loss of a neutral fragment. In this study, fragmentation was performed by a TQMS.

The TQ consists of two quadrupoles in a series (Q_1 and Q_3), combined with a collision cell (q_2) in the middle. The main process of MS/MS is that ions with specific *m/*z-values are selected in Q_1, and provided with high kinetic energy as they collide with gas ions (usually N_2 or Ar) in q_2, in a process called collision induced dissociation (CID). The q_2 has an RF-only field, *i.e.* all selected ions will pass through while CID is applied, and transmission to Q_3 is ensured [128]. There are several different modes of fragmentation; mass spectrum scan, product ion scan, precursor ion scan, neutral loss scan and selected reaction monitoring (SRM). A schematic illustration of the different scan modes in MS is shown in **Figure 63** in **Appendix 7.5**. In this study, a variant of SRM was carried out; multiple reaction monitoring (MRM).

In SRM, the mass selection is carried out at two levels, both in Q_1 and in Q_3. Q_1 is set to select a predefined *m/z*-value that corresponds to the analyte and Q_3 is set to monitor one or more specific fragment ions of the analyte, whereas q_2 serves as a collision cell. If Q_1 is set to select several *m/z*-values and Q_3 is set to monitor several fragments, the mode is called MRM [131]. An illustration of the TQMS operated in MRM mode is shown in **Figure 16**.

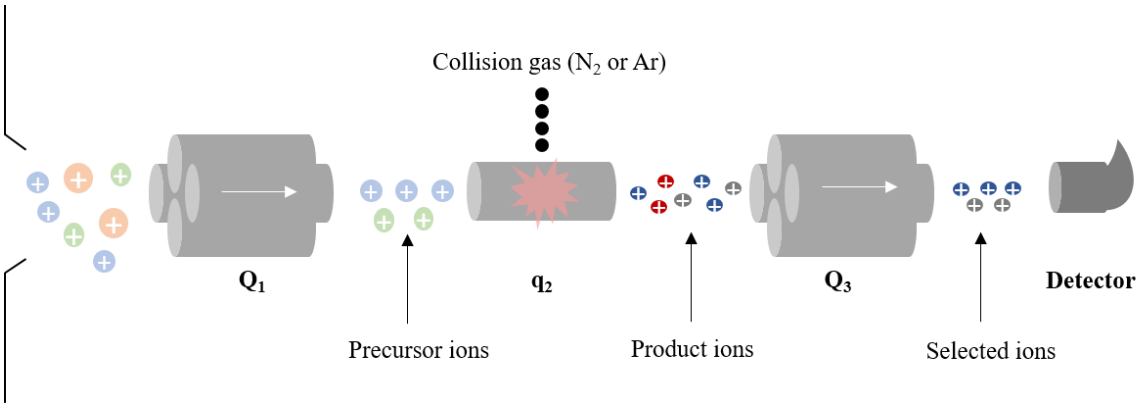

Figure 16. The TQMS operated in MRM mode. Q_1 selects ions with specific *m/z* (precursor ions). The precursor ions are transported to an RF-only collision cell, q_2 and the fragmentation is performed by collision with either N_2 or Ar. The fragments (product ions) are transported to Q_3, which selects specific fragments that are transported to the detector. Adapted from [132].

When the TQ is operated in MRM mode, it has exceptional sensitivity and selectivity. Thus, it has become a revolutionary tool for clinical application and biomarker validation of *e.g.* blood plasma [128, 133]. Quadrupole analyzers are considered robust and require low maintenance compared to other mass analyzers. In addition, their cost is relatively low and they are relatively small.

When performing measurements of isomeric oxysterols, the oxysterols must be separated prior to ionization and detection in the MS. The separation can be performed by LC.

2.6 Liquid chromatography

LC is an analytical technique used for separation, identification, and quantification of different components in a mixture [134]. The instrumentation mainly consists of an analytical column filled with a stationary phase (SP), a pump that transports the mobile phase (MP) along with the sample through the column, and a detector that detects the signal for each compound. The LC system is shown in **Figure 17**.

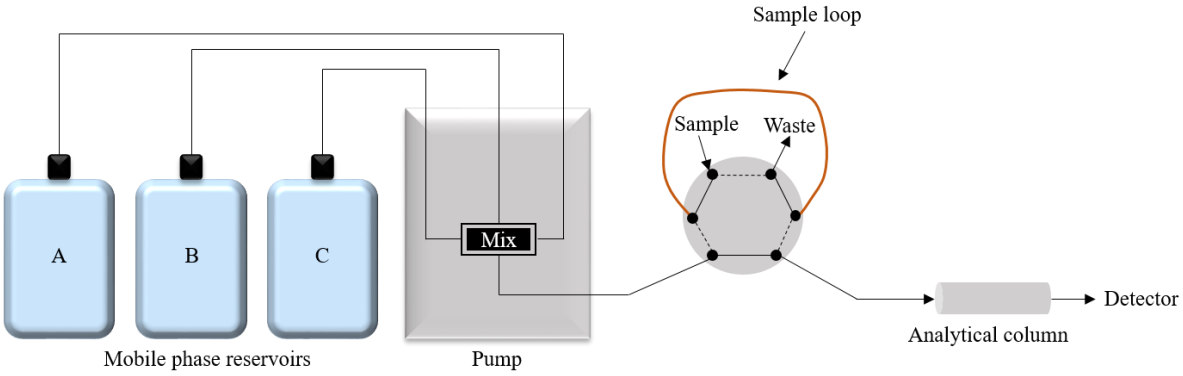

Figure 17. Illustration of an LC system, with three MP reservoirs, a pump, a 2-position 6-port injector, and an analytical column. The pump has three channels for mixing different solvents (A, B and C). The injector is illustrated with manual injection, where the sample is injected with a syringe to a sample loop before the compounds are separated in an analytical column and detected by a detector.

The sample components are separated based on different affinities to the SP; a compound with a stronger affinity to the SP will be more retained than a compound with a lower affinity. The retardation of the components depends on their chemical properties, as well as the nature of the SP and the composition of the MP [135]. Hence, the compounds will migrate through the column with different speed, and reach the detector at different times (**Figure 18A**). The migration time of a compound is defined as its retention time (t_R) [124]. Once the analytes reach the detector, their intensity is measured and they appear as peaks in a chromatogram. The chromatogram shows the signal of the compounds as a function of time (**Figure 18B**). The signal measured is proportional to the concentration of the analytes, and compounds that are more abundant will have higher peaks than less abundant compounds.

The MP composition can be varied during the analysis; this is called gradient elution and is usually applied for complex samples. If the MP composition is constant during the run, the elution is said to be isocratic. The choice of solvents and gradient depends on the type of SP and the analyte(s).

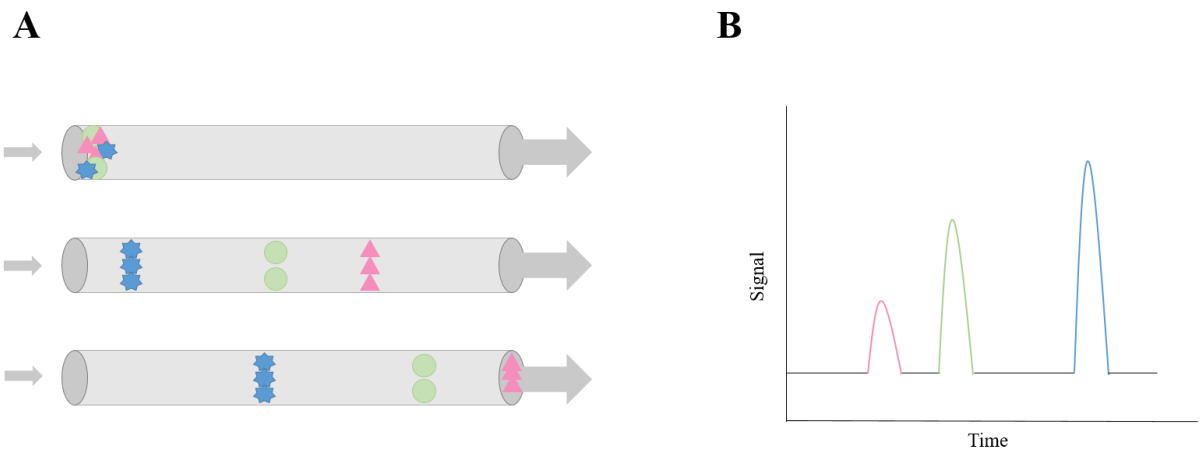

Figure 18. The compounds of interest have different migration time through the analytical column (**A**). Compounds with the strongest affinity to the column (blue) will have a longer t_R than the ones with lower affinity (pink and green). The intensity of each compound is measured as a peak in the chromatogram (**B**).

Totally porous particles have traditionally been used as column material for determination of oxysterols [50]. However, the previous work of McDonald has shown improved chromatographic performance when using core-shell particles [89]. Core-shell particles consist of a solid core and a porous layer (typically 0.2 – 0.7 μm) and have been increasingly used for highly efficient separation with fast flow rate and relatively low back pressure [136]. The smaller pore volume of core-shell particles compared to totally porous particles reduces the volume present for band broadening from longitudinal diffusion, and the short diffusion path length (a thin porous layer) gives faster mass transfer of the analyte between the MP and SP [137-139]. As the mass transfer takes place in a thin layer, larger core-shell particles can be applied and higher flow rates can be used, resulting in faster analyses with the same efficiency as smaller totally porous particles [139-141]. However, due to the reduced surface area, core-shell particles suffer from lower loading capacity than totally porous particles [142].

2.6.1 Reversed-phase liquid chromatography

The term "reversed-phase" was coined by Howard and Martin in 1950, and has evolved to become the most widely used separation principle in LC [143, 144]. In reversed phase-liquid chromatography (RPLC), the most common SP is hydrophobic carbon chains (often C_8 and C_{18}) bonded to silica particles, as illustrated in **Figure 19** [145]. The retention mechanism is not yet fully understood, but it is believed to be based on hydrophobicity, and that hydrophobic

interactions occur between the solutes and the SP. Hence, more hydrophobic analytes will interact more strongly with the SP, and elute later than less hydrophobic analytes. The MP is hydrophilic and often consists of miscible combinations of pH-adjusted water and organic liquids, with acetonitrile (ACN) and methanol (MeOH) being the most common. For oxysterol measurements, mixtures of ACN and MeOH have previously been used, but their effect on selectivity has not been fully elucidated [78, 89].

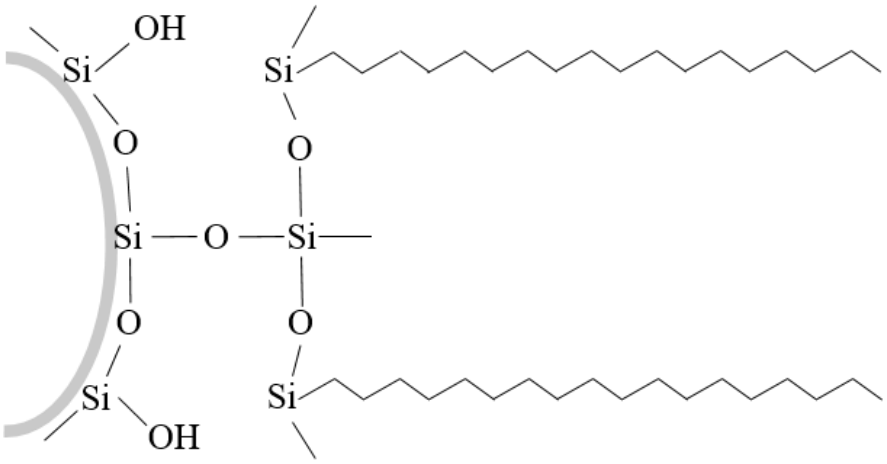

Figure 19. An illustration of a C18 SP bonded to silica particles. Figure adapted from [124].

Griffiths *et al.* have reported several successful methods for the separation of hydrophobic oxysterols with RPLC [50, 88]. However, the oxysterols to be determined in this thesis are isomers, *e.g.* different structure with the same mass. The molecular weight of the oxysterols in this study is 402.65, and they are only differentiated by the placement of the hydroxyl group on the side-chain. The first-choice separation principle for isomers is usually normal-phase liquid chromatography (NPLC) [146 (p. 172)].

In NPLC, the SP is hydrophilic and hence the main types of interactions include ionic and polar interactions, such as hydrogen bonding and dipole-dipole interactions [147]. Since the placement of the hydroxyl group in the oxysterols differentiates them, their separation has been reported as more successful when performed with NPLC [148]. Nevertheless, the solvents typically used in NPLC are non-polar (*e.g.* heptane) mixed with a more polar solvent (*e.g.* chloroform), and NPLC is, therefore, less compatible with ESI-MS [149]. Consequently, RPLC is the choice for separation in this study.

2.6.2 Stationary phase: selectivity for oxysterols

Many oxysterols (*e.g.* 24S- and 25-OHC) exhibit similar precursor to product ion fragmentation and often SRM/MRM can not differentiate them [118, 150]. Therefore, the LC separation of these oxysterols is extremely important for quantification. The most favored choice of SP for oxysterol separation is C18 bonded to silica particles, due to the hydrophobic interactions between the silica and the steroid rings [82, 151, 152]. Silica-based RP phases have a wide range of selectivity because the SP can be chemically bonded to the surface in various ways and various compositions, and hence provide different retention, *e.g.* C8, C18 and phenyl-containing phases.

Many minor unidentified sterols are present in biological samples, and the complete separation of all sterols by a single chromatographic run is, as of today, impossible to accomplish [119]. Thus, the SP and MP must be selected in regards to the target sterols of interest. The selectivity for 22R-hydroxycholesterol (22R-OHC), 24S-, 25-, and 27-OHC on different SPs in RPLC-MS was explored by Solheim *et al.*, who achieved sufficient separation of the oxysterols using a phenyl-hexyl SP [153]. Pataj *et al*. have also reported a separation of oxysterols with rapid analysis time using a biphenyl SP [154]. The structure of the phenyl-hexyl SP is illustrated in **Figure 20**.

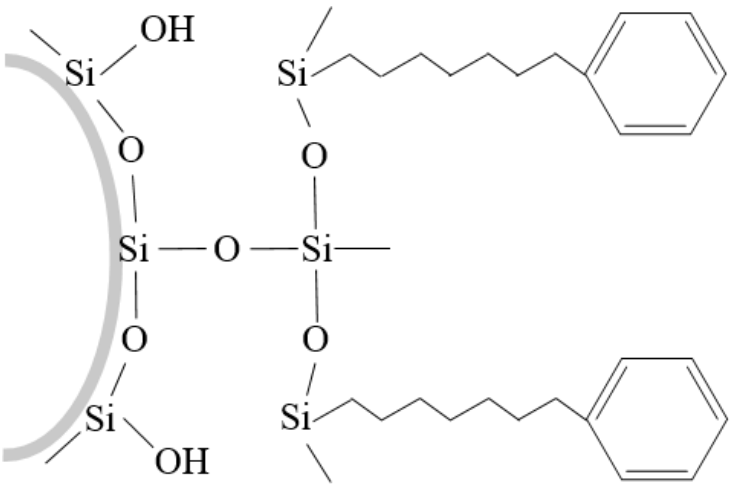

Figure 20. The structure of the phenyl-hexyl SP, with a phenyl group attached to the C8-chain.

2.6.3 On-line sample clean up

As explained in **Section 2.4.3**, a derivatization of the oxysterols is necessary for determination by ESI-MS. However, the derivatization reagent (*e.g.* Girard T) is added in excess to the sample, and it is crucial to remove the reagent before loading the sample to the LC system, in order to avoid an overload of the analytical column (which may cause peak broadening [155]) or clogging of the system with precipitation of the derivatization reagent. In addition, if the derivatization reagent reaches the MS, the instrument may be contaminated. Biological samples (*e.g.* blood plasma) contain particles, *e.g.* from protein precipitation and cell debris, which may clog the system as well, and must be removed prior to analysis.

The sample clean up procedure is often carried out with off-line solid phase extraction (SPE). However, in order to decrease the sample preparation time, the SPE can be done on-line with a 10-port valve system, by using an SPE column before the analytical column. The SPE switching system allows for large volume injection, as the analytes are loaded with high flow by a loading pump with a non-eluting MP, before being trapped and enriched in the SPE column.

The SPE column is exposed to contaminations from the unwanted particles in the sample, and the column switching is prone to the buildup of backpressure [156]. The aforementioned challenges can be solved by implementing a robust automatic filtration and filter flush (AFFL) system [151, 157-159]. An illustration of the system is shown in **Figure 21**. In position 1, the sample containing the analytes (oxysterols) and the excess derivatization reagent (Girard T) are loaded by a loading pump (pump 1) on the SPE column after passing the stainless steel (SST) filter. The analytes are trapped on the RP SPE column, the unwanted particles are held by the filter and the hydrophilic compounds are eluted to waste along with the derivatization reagent. When the 10-port valve switches to position 2, the LC pump (pump 2) with the MP elutes the analytes to the analytical column (front-flush), while the loading pump flushes the unwanted particles from the filter to waste. The analytes can also be back-flushed to the analytical column, which improves the peak shape, but the SPE is consequently more prone to clogging.

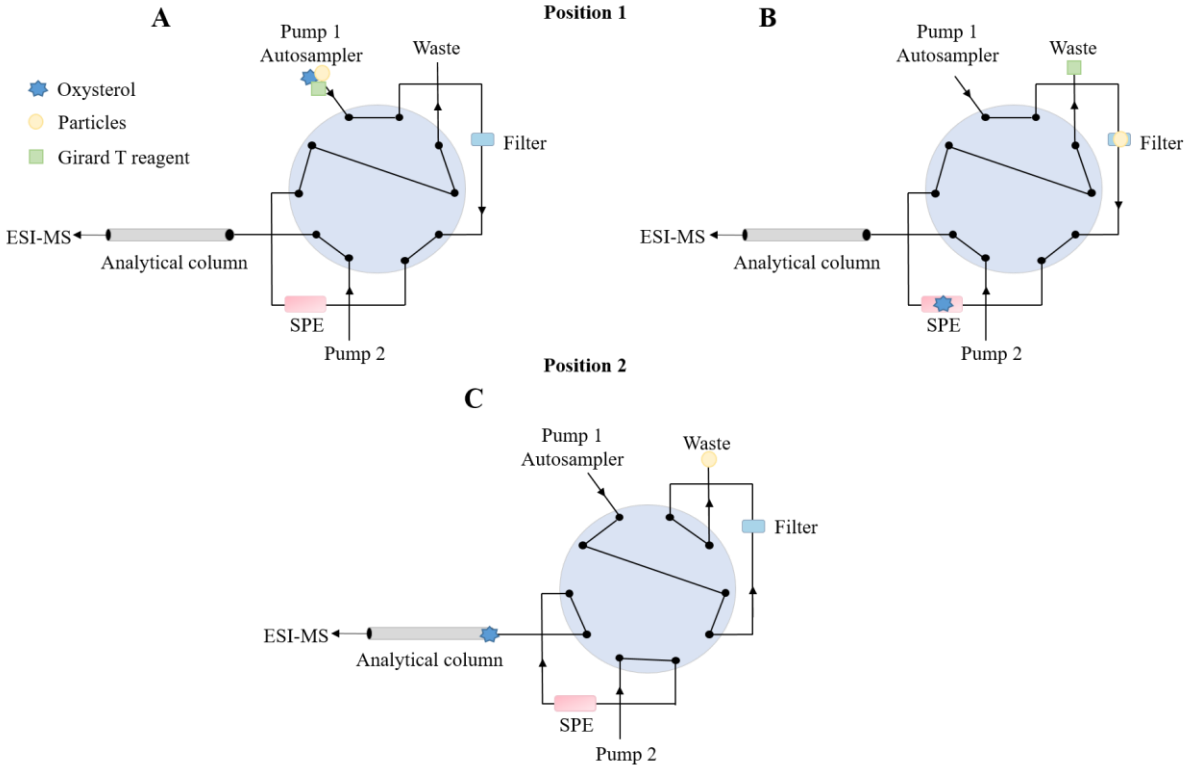

Figure 21. An illustration of the AFFL-SPE system. The sample is transported by a loading pump (pump 1) in position 1 (**A**). The unwanted particles (yellow) are trapped in the SST filter, while the oxysterols (blue) are trapped on the hydrophobic SPE column and the Girard T-reagent (green) is flushed to waste (**B**). In position 2 of the 10-port valve, the unwanted particles are back-flushed to waste by the loading pump, while the oxysterols are front-flushed on to the analytical column by the LC pump (**C**). Adapted from [158].

2.7 Aim of study

Oxysterols have shown to affect BC in several ways, and more rapid methods for sample preparation for the determination of these compounds in biological samples are needed. Our current method uses derivatization with Girard T and employs KOH for hydrolysis of oxysterols esters in biological samples, and the method is quite laborious and time-consuming (> 1 day). It was hypothesized that the method could be faster (*i.e.* < 1 day) by using an alternative derivatization technique (derivatization with picolinic acid or thiyl radical-based charge tagging) and/or hydrolysis technique (enzymatic hydrolysis with ChE).

Thus, the aim of this study was to improve the current sample preparation procedure in our method for determination of side-chain oxysterols in BC tumors, especially in terms of time consumption. Human plasma was chosen as a sample matrix for the method improvement due to limited amounts of tumors. The hydrolysis step was addressed measuring 24S-, 25-, and 27-OHC in human plasma, by implementing large-volume injection performed by the AFFL-SPE-LC-MS system. The derivatization step was addressed by derivatization using standard solutions (cholesterol and selected oxysterols). The aim of study is illustrated in ***Figure 22****.*

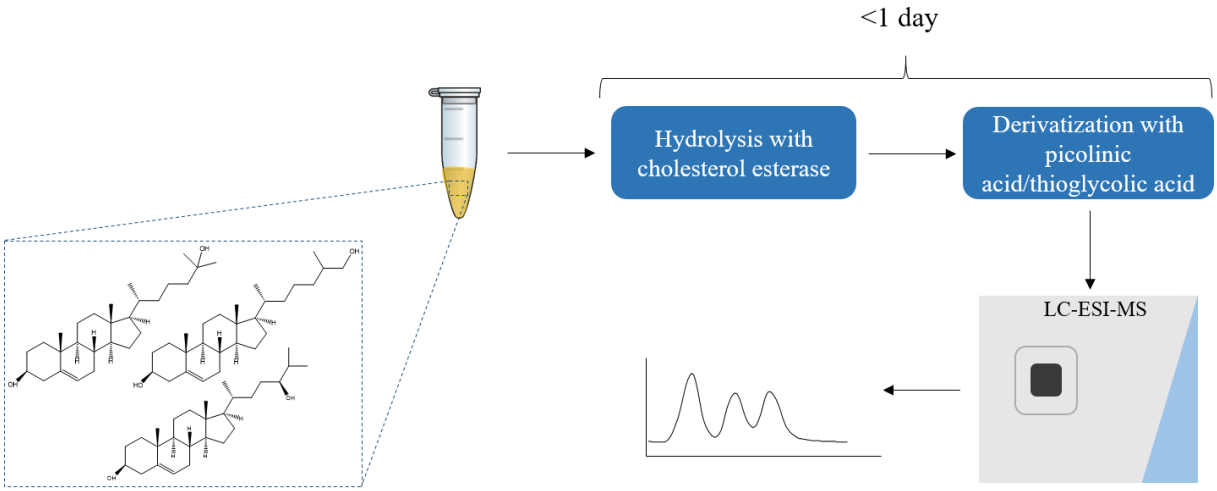

Figure 22. Graphical illustration of the aim of study. The hypothesis was that a sample preparation time of < 1 was obtainable after enzymatic hydrolysis with ChE and derivatization with picolinic acid or thiyl radical-based charge tagging.

3 Experimental

In this section, the focus will be on the preparation of plasma for hydrolysis of 24S-, 25-, and 27-OHC following derivatization with Girard T. The alternative derivatization techniques investigated are described briefly in **Section 3.5**, and further elaborated in **Appendix 7.1**.

The water used was either type 1 water acquired from a Milli-Q® Integral water purification system from Merck-Millipore (Billerica, MA, USA) or HPLC grade water from VWR (Radnor, PA, USA). If not otherwise specified, type 1 water will from now on be referred to as "H_2O".

3.1 Chemicals

ACN (LC-MS grade, 99.9%), MeOH (HPLC gradient grade, ≥ 99.8%) and 2-propanol (IPA) were purchased from VWR. Formic acid (FA, LC-MS grade, 98%), glacial acetic acid, NaOH pellets (> 99%) and n-hexane were from Merck (Darmstadt, Germany). 27-OHC (cholest-(25R)-5-ene-3β,27-diol), 24S-OHC (cholest-5-ene-3β,24(S)-diol), 27-OHC-d_6 (cholest-5-ene-3β,27-diol(d6)) and 25-OHC-d_6 (cholest-5-ene-3β,25-diol(d6)) were from Avanti Polar Lipids (Alabaster, AL, USA). 25-OHC (cholest-5-ene-3β,25-diol), 22R-OHC (cholest-5-ene-3β,22(R)-diol), cholesterol-25, 26, 27 ^{13}C (^{13}C-cholesterol), ChE from *Pseudomonas sp.*, ChX from *Streptomyces sp*., Girard's reagent T (99%), cholic acid from ox or sheep bile (≥ 98%), KH_2PO_4, TX-100 and human plasma were obtained from Sigma Aldrich (St. Louis, MO, USA).

3.2 Equipment for preparation of samples and solutions

Centrifugation was carried out in a 5424 R centrifuge from Eppendorf and sample drying was done in a centrifugal evaporator (Concentrator Plus; hereafter referred to as a SpeedVac), also from Eppendorf. The E2M2 vacuum pump for the SpeedVac was from Edwards (Crawley, Sussex, England, UK). All stirring was performed on an MS2 Minishaker vortex mixer or on a Topolino magnet stirrer, both from IKA (Staufen, Germany).

Sample incubation was carried out on a PHMT PSC-20 thermoshaker from Grant-Bio (20x2.0 mL, Grant Instruments, Shepreth, Cambridgeshire, UK) or in a GC-17A oven from Shimadzu (Kyoto, Japan). Ultrasonic treatments were performed in an ATM-40 ultrasonic cleaner from ATU Ultrasonidos (0.7 L, Paterna, Valencia, Spain).

A Titrino plus 877 pH meter from Metrohm (Herisau, Switzerland), equipped with a Primatrode pH electrode (also from Metrohm), was used for pH measurements of the phosphate buffers. All weighing was performed on an AT200 analytical balance from Mettler-Toledo (Grefiensee, Switzerland).

All pipettes were from Thermo Scientific (Waltham, MA, USA). Oasis PRiME HLB SPE columns (30 mg, 1 cm^3) for off-line SPE were from Waters (Milford, MS, USA).

Containers and glassware

Eppendorf safe-lock 1.5 mL tubes (hereafter referred to as Eppendorf tubes) were from Eppendorf (Hamburg, Germany). The volumetric flasks were from Schott (Mainz, Germany) and the measuring cylinders were from Kimble (Fisher Scientific, part of Thermo Scientific). The autosampler vials (0.3 mL Microvials) with screw caps (Snap Ring Cap, 9 mm), the autosampler glass vials (1.5 mL) with lids (11 mm), the centrifuge tubes with flat caps (15 mL), and the MP flasks (1000 mL) were from VWR.

3.3 Preparation of solutions

3.3.1 Stock- and working solutions

The stock solutions of hydroxycholesterol and the working solution with 25-OHC-d_6 and 27-OHC-d_6 (solution C) were previously made by Dr. Hanne Røberg-Larsen. 25-OHC-d_6 was used as internal standard (IS) for 25- and 24S-OHC, and 27-OHC-d_6 was used as IS for 27-OHC. An appropriate dilution of the stock solutions was performed in order to prepare two working solution with each oxysterol (solution A and B). The solutions and corresponding concentrations are shown in **Table 2**. A desired amount of the working solutions was added to human plasma, as further explained in **Section 3.4**.

Table 2. Concentrations of stock- and working solutions of 22R-, 25-, 24S- and 27-OHC and concentrations of working solutions of 25-OHC-d_6 and 27-OHC-d_6.

Hydroxycholesterol/IS	Stock solutions (µM)		Working solution (nM)*	Working solution (µM)**	Working solution (nM)	Referred to as
22R-OHC	248	→	1.0	1.0		***A**
25-OHC	467					****B**
24S-OHC	248					
27-OHC	1242					
25-OHC-d_6					1.5	**C**
27-OHC-d_6						

3.3.2 Evaluation solutions

For the evaluation solutions, plasma was spiked with the desired concentrations of working solution A and B. The concentrations are shown in **Table 3** and **Table 4**. For determination of concentration limit of quantification (cLOQ) with IS, plasma was spiked with the desired concentrations of working solution C, shown in **Table 5**. The sample preparation of plasma is described in **Section 3.4**.

Table 3. Spiked volumes in plasma of working solution A, concentrations in injection solution and concentrations in 5 µL plasma.

Volume from working solution A (µL)	Concentration in 735 µL (injection solution) (pM)	Corresponds to concentration in 5 µL plasma (nM)
74	100	15
147	200	30
221	300	45
294	400	60
368	500	75

Table 4. Spiked volumes in plasma of working solution B, concentrations in injection solution and concentrations in 5 µL plasma.

Volume from working solution B (µL)	Concentration in 735 µL (injection solution) (nM)	Corresponds to concentration in 5 µL plasma (µM)
74	100	15
147	200	30
221	300	45
294	400	60
368	500	75

Table 5. Spiked volumes in plasma of working solution C, concentrations in injection solution and concentrations in 5 µL plasma.

Volume from working solution C (µL)	Concentration in 735 µL (injection solution) (pM)	Corresponds to concentration in 5 µL plasma (pM)
0.50	1.0	150
1.4	3.0	450
2.4	5.0	750
4.8	10	1500
9.5	20	3000
14	30	4500

3.3.3 Phosphate buffers, derivatization solution and solvents

The phosphate buffer with ChE was prepared according to the procedure of Mendiara *et al.* [96]. The 50 mM buffer was made by dissolving 1.0 g KH_2PO_4 and 15 mg (0.25 M) cholic acid in 100 mL H_2O with magnetic stirring. Due to the insolubility of cholic acid, the solution was stirred in a sealed volumetric flask for approximately 48 hours at room temperature. A quantity of 125 µg ChE from *Pseudomonas sp.* was added to the solution, along with 50 mL H_2O, achieving the final concentration of 25 units (UN) ChE. Further, 1 M NaOH was added dropwise while monitoring the pH to pH 7. An aliquot of 50 µL TX-100 was added to 10 mL of the prepared buffer, obtaining a 0.5% TX-100 solution. The buffer was stored at -80 °C.

The 50 mM phosphate buffer containing ChX was prepared according to the procedure of Solheim [153]. The 50 mM buffer was made by dissolving 885 mg KH_2PO_4 in 130 mL H_2O with 4 mg ChX from *Streptomyces sp.* Further, 1 M NaOH was added dropwise while monitoring the pH to pH 7. The buffer was stored at -80 °C.

The Girard T derivatization solution was prepared by mixing 15 mg Girard T reagent with 15 µL glacial acetic acid and 500 µL MeOH. Solvents A, B, and C (shown in **Table 9** in **Section 3.6.2**) in were made by mixing HPLC grade water, MeOH and ACN, respectively, with FA, and the volumes were measured separately in a measuring cylinder.

3.4 Preparation of plasma solutions

The sample preparation procedure, including oxidation with ChX, hydrolysis with KOH and derivatization with the Girard T is the same as the procedure of Røberg-Larsen *et al*. [110, 158] which is based on the procedure described by Griffiths and co-workers [2], and modified by Solheim [153].

An aliquot of 5 µL plasma was transferred to an Eppendorf tube and mixed with 100 µL of solution C (IS, 204 pM) and 5 µL 6 µM ^{13}C-cholesterol (for monitoring autoxidation). For the evaluation solutions, the desired amount (µL) of solution A was added. Further, the sample solution was vortexed, and then exposed to either alkaline or enzymatic hydrolysis.

Alkaline hydrolysis

An aliquot of 35 µL saturated KOH in MeOH was transferred to the sample solution. The sample solution was incubated at 60 °C for 2 hours in a GC-oven. An LLE was carried out three times by adding 200 µL H_2O and 150 µL n-hexane. The hexane layers were mixed and evaporated to dryness before the dry sample was resolved in 200 µL IPA. Further, the sample solution was applied to an Oasis PRiME HLB column, and it was eluted with 200 µL MeOH.

Enzymatic hydrolysis

The sample solution was firstly evaporated to dryness. An aliquot of 200 µL 50 mM phosphate buffer with ChE from *Pseudomonas sp.* and 0.25 mM cholic acid (and eventually 0.5% TX-100) was added, and the sample solution was incubated at 37 °C for 1 hour. Further, the sample solution was applied to an Oasis PRiME HLB column, and it was eluted with 200 µL IPA and 200 µL MeOH.

After hydrolysis, the sample solution was evaporated to dryness and resolved in 20 µL IPA. An aliquot of 200 µL 50 mM phosphate buffer with ChX from *Streptomyces sp*. was added to the sample solution before incubation at 37 °C for 1 hour.

Derivatization with Girard T

An aliquot of 515 µL of the Girard T derivatization solution was added to the sample solution before storage overnight in the dark, at room temperature. Further, the sample solution was transferred to an autosampler vial (0.3 or 1.5 mL).

The sample preparation with enzymatic hydrolysis and derivatization with Girard T of plasma is illustrated in **Figure 23**. The concentrations of 25- and 27-OHC-d_6 is shown in **Table 6**.

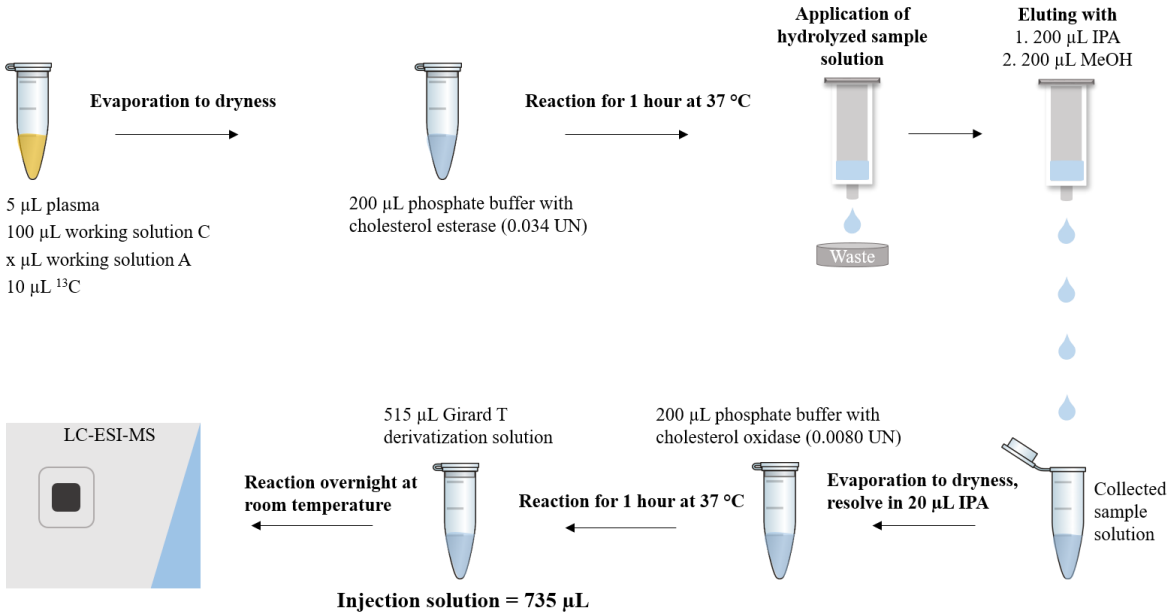

Figure 23. Illustration of the sample preparation of plasma with enzymatic hydrolysis and derivatization with Girard T.

Table 6. The concentration of the IS from working solution C in injection solution and in 5 µL plasma added to every plasma solution.

Volume from working solution C (µL)	Concentration in 735 µL (injection solution) (pM)	Corresponds to concentration in 5 µL plasma (nM)
100	204	30.6

3.5 Derivatization of standards

Derivatization with picolinic acid

The derivatization procedure is based on the method described by Honda *et al.* [118], which is based on the method described by Yamashita *et al.* [160].

The derivatization solution was prepared by transferring 100 mg 2-methyl-6-nitrobenzoic anhydride (MNBA), 60 mg picolinic acid, 1.8 mL pyridine and 200 µL N,N-diisopropylethylamine (Hünig's base) to a glass container covered with aluminum foil during magnetic stirring (solution #1). The same amount together with 30 mg 4-dimethylaminopyridine (DMAP) was added to another glass container (solution #2).

An amount of 18 Eppendorf vials with 100 µL 10 ng/mL 25-OHC (from working solution A) and 25-OHC-d_6 was prepared. An aliquot of 170 µL derivatization solution #1 was added to 9 of the vials, while an aliquot of 170 µL derivatization solution #2 was added to the remaining 9 vials. The sample solutions were homogenized, and 3 replicates of each were incubated at either 20 °C in a thermoshaker, or 60 °C or 80 °C in a GC oven for 30 minutes. The sample solutions were evaporated to dryness and resolved in 500 µL MeOH + 0.1% FA. The sample preparation is illustrated in **Figure 24**. For chemicals and equipment, see **Appendix 7.1.1** and **7.1.2.** For MS settings, see **Appendix 7.1.4**.

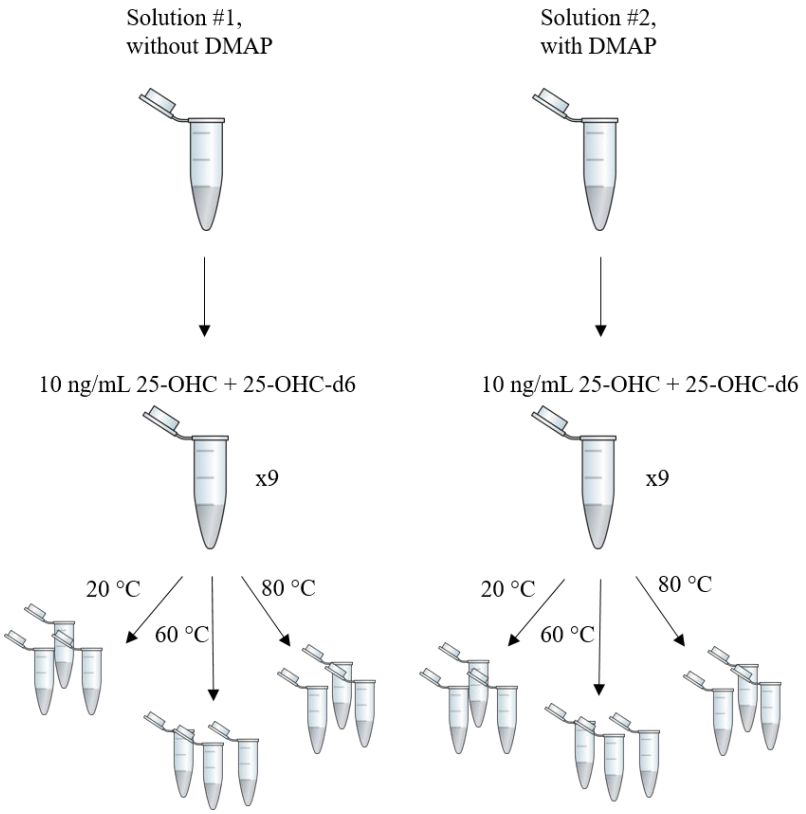

Figure 24. The sample preparation steps for the derivatization of 25-OHC with picolinic acid with and without DMAP.

Thiyl radical-based charge tagging

The derivatization procedure is the same as described by Adhikari and Xia [120]. The working solutions prepared are shown in **Table 7**. The working solutions of 24S- and 25-OHC was prepared from the stock solutions shown in **Table 2** in **Section 3.3.1**. The working solution of cholesterol was made from weighing in an appropriate amount of cholesterol and diluting in dimethylformamide (DMF).

Table 7. Working solutions of cholesterol, 25-OHC, and 24S-OHC.

Compound	Concentration (µM)	Solvent
Cholesterol	0.001	DMF
25-OHC	100	DMF
24S-OHC	100	DMF

An appropriate dilution of the working solutions was added to separate volumetric flasks, in order to achieve concentrations of 5 µM or 100 µM. The desired amount of TGA and 2,2-dimethoxy-2-phenylacetophenone (DMPA) was added to the flask, achieving the concentrations of 100 mM and 1 mM/10 mM, respectively. The sample solution was homogenized and sonicated for 5 minutes. An aliquot of 5 mL was transferred to quartz vials and irradiated by different UV lamps for 60 minutes. An illustration of the sample preparation is shown in **Figure 25**. The different UV lamps tested are shown in **Figure 64** in **Appendix 7.5**.

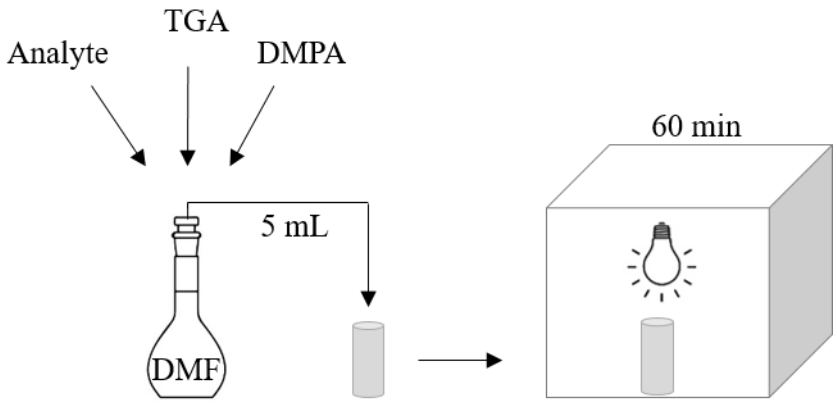

Figure 25. An illustration of the sample preparation for thiyl radical-based charge tagging. The analyte (cholesterol/25-OHC/24S-OHC), DMPA, and TGA is solved in DMF. An aliquot of 5 mL is transferred to a quartz cuvette and irradiated for 60 minutes by UV-light.

An aliquot of 1 mL NaOH and 1 mL ethyl acetate was added, and phase separation was obtained. The top layer was extracted, evaporated to dryness and resolved in ACN or MeOH + 0.1% FA. An illustration of the phase separation in LLE is shown in **Figure 26**. The SPE was carried out with an Oasis PRiME HLB column and eluted with 0.5 mL MeOH + 0.1% FA before direct injection MS in negative ionization mode. The solutions were injected with a 250 µL syringe (Hamilton Robotics, Reno, NV, USA) at a flow rate of 5 µL/min. For chemicals and equipment see **Appendix 7.1.1** and **7.1.2.** The MS settings were based on the recommended settings from Thermo Scientific, as shown in **Table 15** in **Appendix 7.2.1**.

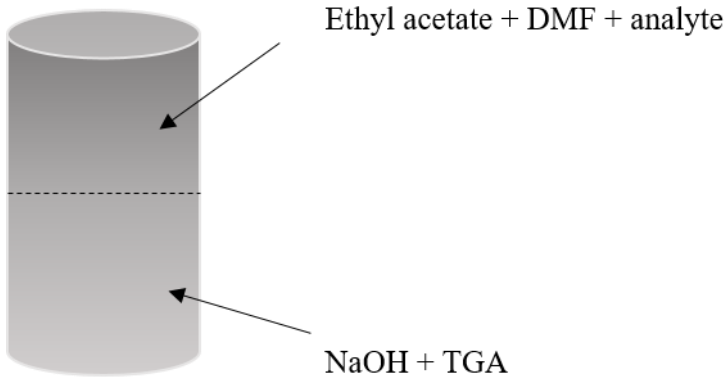

Figure 26. Illustration of the phase separation during LLE. The analyte, along with ethyl acetate and DMF is partitioned in the top layer, while the NaOH and TGA are present in the bottom layer.

3.6 Liquid chromatography-mass spectrometer instrumentation

A Dionex UltiMate 3000 liquid chromatograph with an LPG3400SD pump with a degasser, a column oven, MP reservoirs, and a WPS3000 autosampler (4 °C) was coupled to a TSQ Vantage TQ MS equipped with a heated electrospray interface (HESI-II). All of the equipment above was from Thermo Scientific.

3.6.1 TSQ Vantage mass spectrometer settings

The settings for the ESI-MS (*i.e.* fragmentation energy, position for the MS lenses, *etc.*) was optimized by Solheim [153] by direct injection of Girard T derivatized cholesterol, and the settings were according to his optimization. The suggested fragmentation reactions for the oxysterols are shown in **Figure 59** in **Appendix 7.2.2**. The tune settings (*i.e.* sheath gas pressure, ESI spray voltage, capillary temperature, *etc.*) are shown in **Table 8** and are based on the recommendations from Thermo Scientific (**Table 15** in **Appendix 7.2.1**).

Table 8. Tune settings (spray voltage, capillary temperature, vaporizer temperature, sheath gas, auxiliary gas flow, collision gas pressure) for the TSQ Vantage MS.

Spray voltage (V)	3000
Capillary temperature (°C)	380
Vaporizer temperature (°C)	300
Sheath gas (psi)	60
Auxiliary gas flow (arbitrary units)	10
Collision gas pressure (mTorr)	1

3.6.2 Solvent program

The LC pump can mix solvents from up to four MP reservoirs simultaneously. Three of the reservoirs were used; see **Table 9**. The MP composition was 56/11/33/0.1 H_2O/MeOH/ACN/FA (v/v/v/v), before changing to 50/50/0.1 MeOH/ACN/FA (v/v/v) for a washing step, as shown in **Figure 27**. The flow rate was 650 µL/min before changing to 700 µL/min during the washing step.

Table 9. The solvents and reservoirs used in this study. The starred (*) solvent is HPLC grade water.

Reservoir	Solvent
A	H_2O* + 0.1% FA
B	MeOH + 0.1% FA
C	ACN + 0.1% FA

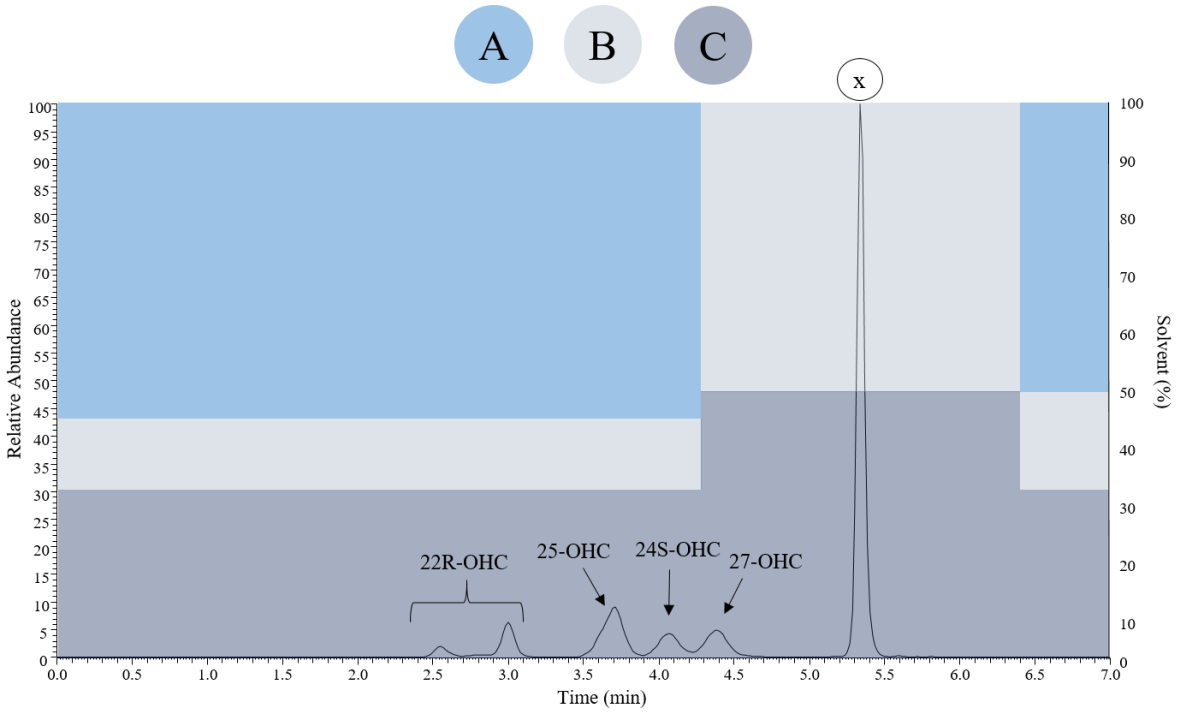

Figure 27. A graphic illustration of the gradient program, also showing at which MP composition the oxysterols eluted. The peak marked as (x) is explained in **Section 4.2.3**.

3.6.3 The automatic filtration and filter flush system

In addition to the Dionex UltiMate 3000 pump, an AFFL system, which utilized a Hitachi L-7110 loading pump from Merck, was included in the system. The loading pump contained H_2O with 0.1% FA and was operated at 500 µL/min. Column switching was performed with a CapLC® 10-port 2-position selector valve from Waters. The filter was a Screen 2SR1 2 µm filter from VICI Valco (Houston, TX, USA).

The two analytical columns operated at 55 °C are shown in **Table 10.** The columns are packed with 2.5 µm core-shell particles and acquired from VWR. The columns will be referred to as column **A** and column **B** from now. The HotSep Kromasil C18 (1.0 x 5.0 mm inner diameter (ID)) SPE pre-column with 5 µm particles was from G&T Septech AS (Ski, Norway).

Table 10. The two ACE UltraCore SuperPhenylHexyl (SPH) 150 x 2.1 mm ID analytical columns with serial numbers and batch numbers used in the study.

Column		Serial number	Batch number	Suggested interactions
A	ACE UltraCore SPH 150 x 2.1 mm ID	A183921	V15-8818	Hydrophobic interactions, π - π and dipole-dipole interactions
B	ACE UltraCore SPH 150 x 2.1 mm ID	A226044	V17-1702	

Connections and couplings for the AFFL-SPE-LC-MS system

The connections and couplings used in the AFFL-SPE-LC-MS system are shown in **Figure 28**. The SST vipers were from Thermo Scientific. The 1/16'' unions and steel nuts were from VICI Valco. The PEEK tubings were from Teknolab (Ski, Norway).

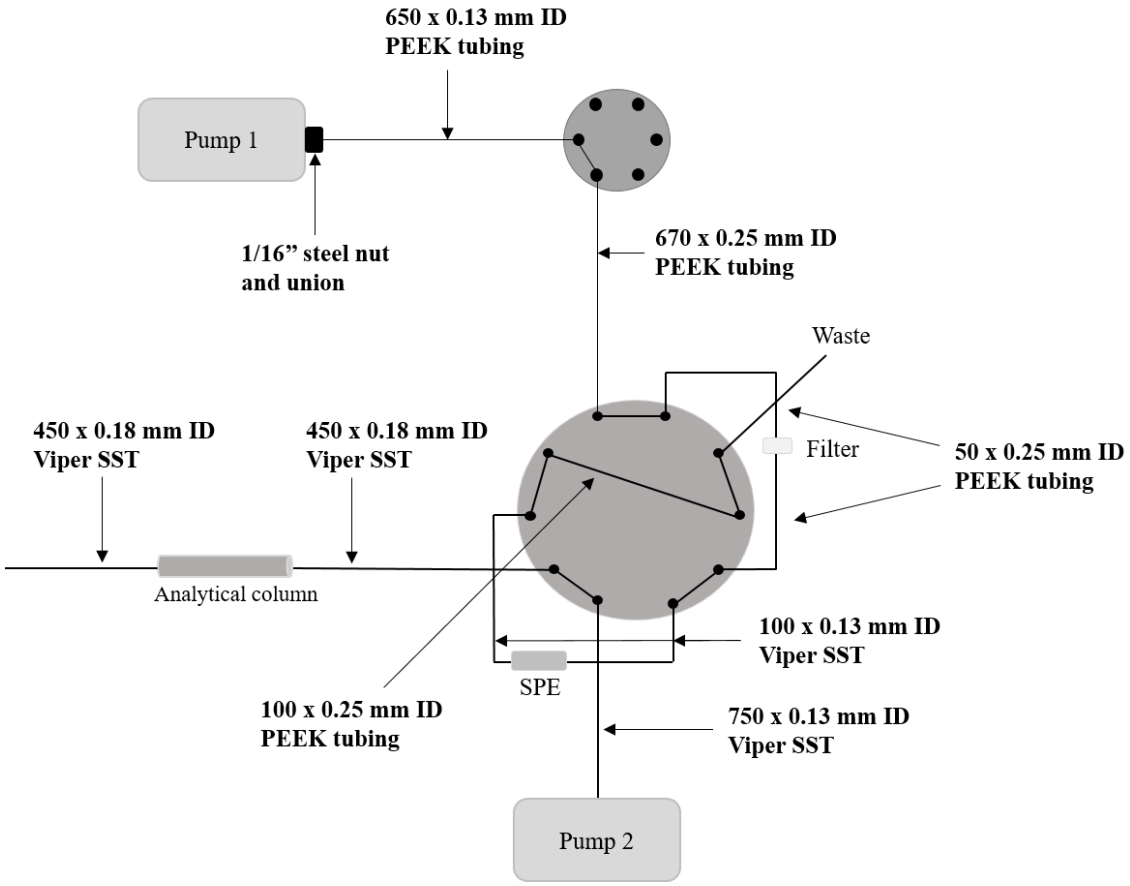

Figure 28. An illustration of the connections and couplings in the AFFL-SPE-LC-MS system.

3.6.4 Data handling

The Thermo Xcalibur software (Xcalibur, version 2.0) was used to set up the method and sequence for the TSQ Vantage MS. Thermo TSQ Tune master (version 2.3.0.1214 SP3) was used to control the TSQ Vantage MS equipped with the HESI-II source. Xcalibur was used for data handling of the mass spectra and the chromatograms, *i.e.* identifying the t_R, peak area and resolution (Rs). The Dionex Ultimate 3000 pump with the column oven and the autosampler was controlled with Chromeleon Express (version 6.80 SR13).

Microsoft Excel (2016 version) was used to calculate means, standard deviations and relative standard deviations in percentage (%RSD) for t_R, peak area, and Rs, and to create bar charts, scatter plots and curves. Rs was calculated by using **Equation 1** [161 (p. 615)]. All figures in this thesis, except **Figure 6**, are made with Microsoft PowerPoint (2016 version). **Figure 6** is created with PyMol Molecular Graphics System (version 1.8.6.2). All molecular structures are made in ChemDraw Professional 16.0.

Equation 1.

$$Rs = \frac{0.589(t_2 - t_1)}{0.5w(av)}$$

4 Results and discussion

In the present study, the aim was to improve our established sample preparation procedure for the determination of oxysterols in BC tumors. The main goals were to shorten the sample preparation time, reduce the sample handling, and reduce the environmental impact due to the use of alkaline solutions.

Two alternative derivatization methods for oxysterols were investigated using standard solutions containing cholesterol and selected oxysterols, and compared to our established method, which is derivatization with Girard's reagent T. The results of the derivatization experiments will be presented first.

Subsequently, the experiments using pooled plasma samples for hydrolysis of oxysterol esters by the enzyme ChE and the comparison to our established method, which uses KOH (alkaline hydrolysis) will be presented. Human plasma was used due to limited amounts of cancer tumors.

A graphical illustration of the workflow is presented in **Figure 29**. The blue boxes present the sample matrix. The black boxes describe experiments carried out using column A and the red boxes describe experiments carried out with column B (explained in **Experimental 3.6.3**).

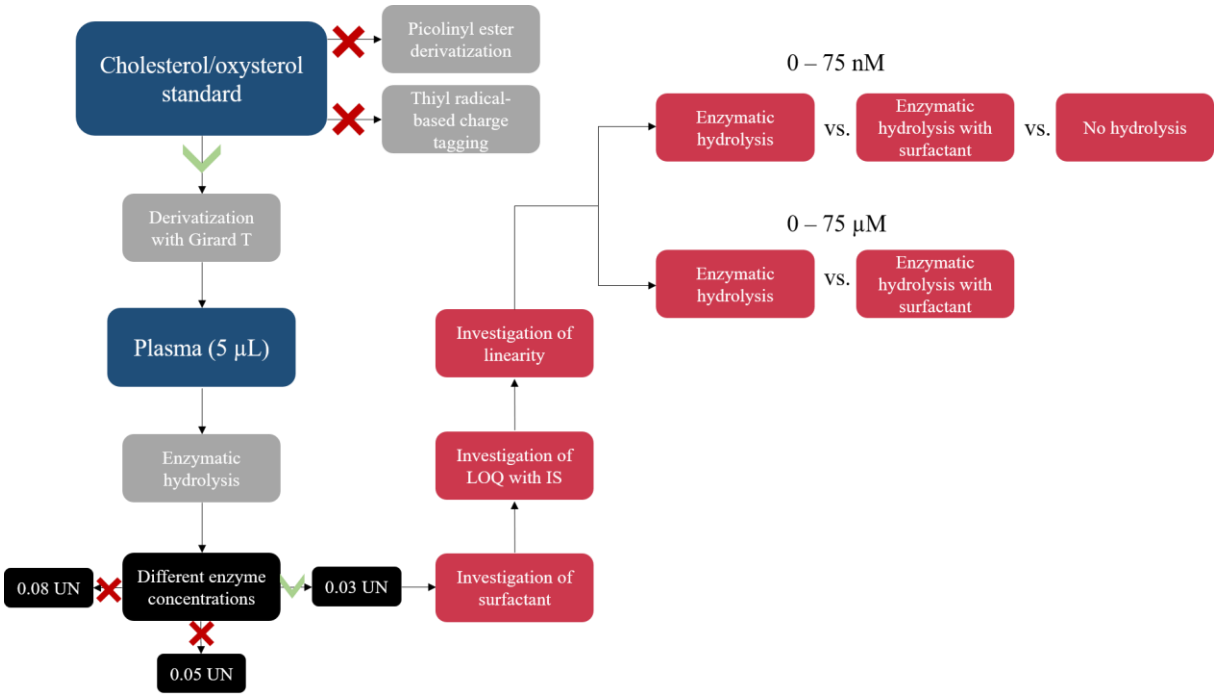

Figure 29. The workflow of the experiments carried out.

4.1 Charge tagging of cholesterol and selected oxysterols

The derivatization methods assessed in this study were charge tagging (derivatization) with picolinic acid into picolinyl esters, and charge tagging with TGA through a click-chemistry reaction (thiyl radical-based charge tagging).

4.1.1 Derivatization of cholesterol into picolinyl esters proved to be challenging

The derivatization experiments were carried out in collaboration with former bachelor student Maria Schüller. The proposed structures for the ester derivates of cholesterol, 25-OHC and 25-OHC-d_6 (cholesterol, 25-OHC, 25-OHC-d_6 picolinate) with corresponding *m/z* values are shown in **Figure 30**.

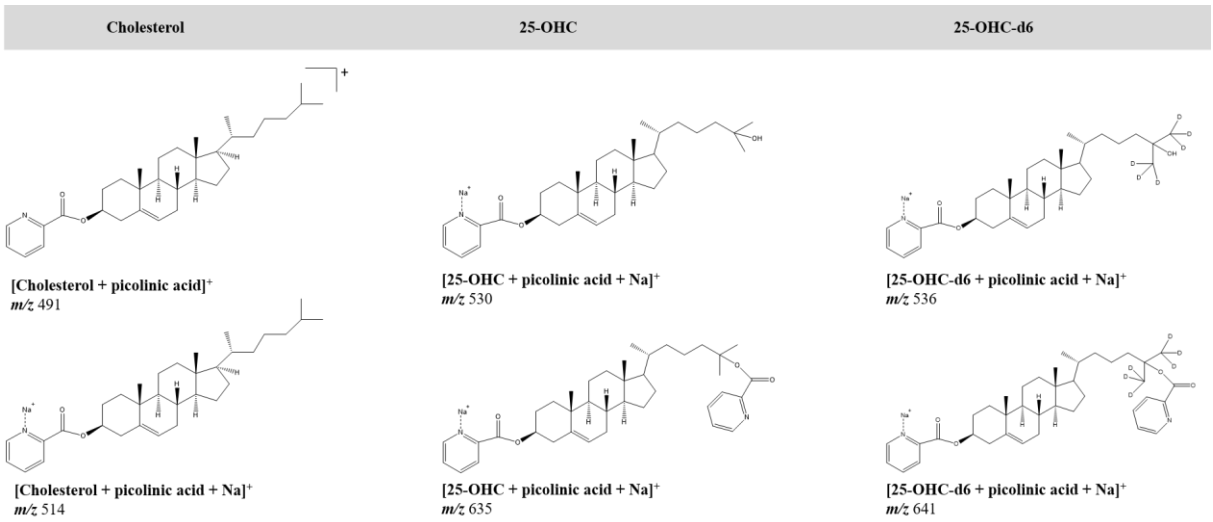

Figure 30. The predicted *m/z* and structures for cholesterol and 25-OHC(-d_6) after derivatization with picolinic acid.

Neither cholesterol picolinate, nor cholesterol was detected by direct injection MS in full scan mode after following the initial procedure of Honda [118]. Therefore, several modifications of the procedure were made, as shown in **Table 12** in **Appendix 7.1.3**. After advice from former master student Ingvild Comfort Hvinden, who had experience with this derivatization reaction, triethylamine was replaced by Hünig's base as base and tetrahydrofuran (THF) was excluded, due to THF causing precipitation when added to the dried sample solution. Pyridine was also added. The latter is in accordance with a later publication of Honda *et al*. [116]. DMAP was eventually removed from the reaction mixture, due to its toxicity and hazardous effects on the skin. However, the changes mentioned above did not prove to be successful, as no detectable signal of cholesterol picolinate was observed.

Optimization of the derivatization procedure was further pursued with experimental design by Schüller [162], who eventually achieved detectable signals for cholesterol picolinate in full scan mode. However, the signal for cholesterol itself had a sometimes higher intensity than for the picolinate derivative, meaning that the yield was poor or that the derivatization did not take place. Arbitrary formation of mono- and dipicolinate derivatives when performing the derivatization on selected oxysterols was also experienced, probably due to the presence of two hydroxyl groups in the oxysterols, and thereby two possible placements for the picolinyl moiety (see **Figure 30**). Thus, the placement of the picolinyl group seemed to be difficult to control. The concentration of cholesterol and the oxysterols was suggested to be the decisive factor for

picolinyl ester formation, as a detectable signal for 22S-hydroxycholesterol (22S-OHC) was achieved when the concentration was increased to 100 μg/mL [162].

The complicated role of 4-dimethylaminopyridine

As mentioned, DMAP was removed from the derivatization solution. However, DMAP is a useful nucleophilic catalyst for various esterification reactions, because of its basicity and thereby electron-donating abilities. Along with MNBA, DMAP allegedly plays an important role in the picolinyl esterification. The proposed mechanism for the derivatization is based on the Shiina esterification, which forms carboxylic esters from carboxylic acids and alcohols, in the presence of carboxylic acid anhydrides [163]. The reaction mechanism of the derivatization is shown in **Figure 31**. However, the detailed mechanism for the role of DMAP in organic synthesis has not been fully elucidated [164], and hence the mechanism shown here is merely a proposition.

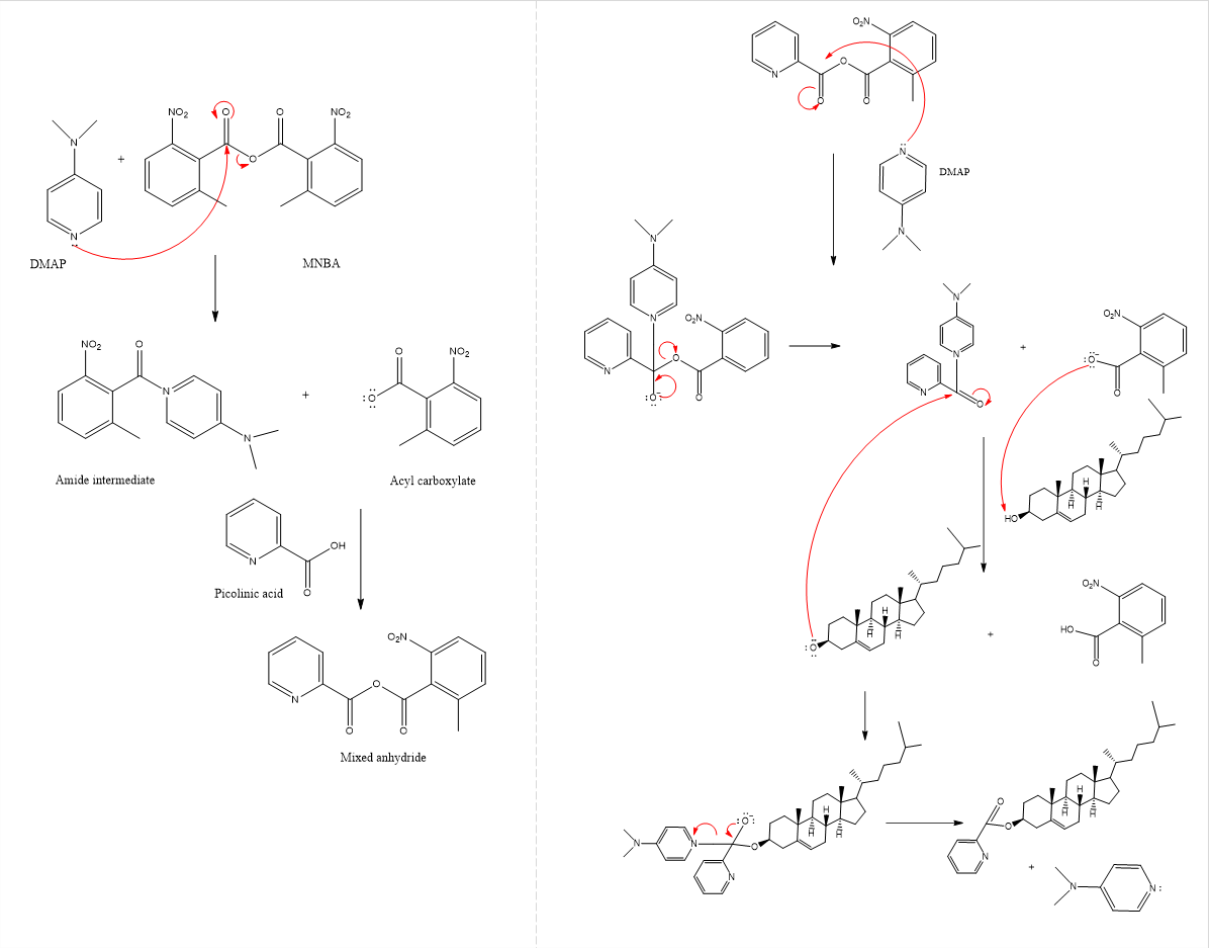

Figure 31. The proposed reaction mechanism of the derivatization of cholesterol with picolinic acid.

The reaction is started by cleavage of MNBA, performed by a nucleophilic attack of DMAP, which suggests that the reaction is DMAP dependent. In order to further investigate the effects of DMAP, the derivatization was carried out with and without DMAP for 25-OHC and 25-OHC-d_6 for different temperatures: 20 °C, 60 °C and 80 °C, with the optimized conditions of Schüller. The oxysterols 25-OHC and 25-OHC-d_6 were chosen instead of cholesterol in order to assess the problem with the arbitrary formation of mono- and dipicolinate derivatives. The chromatograms are shown in **Figure 32**.

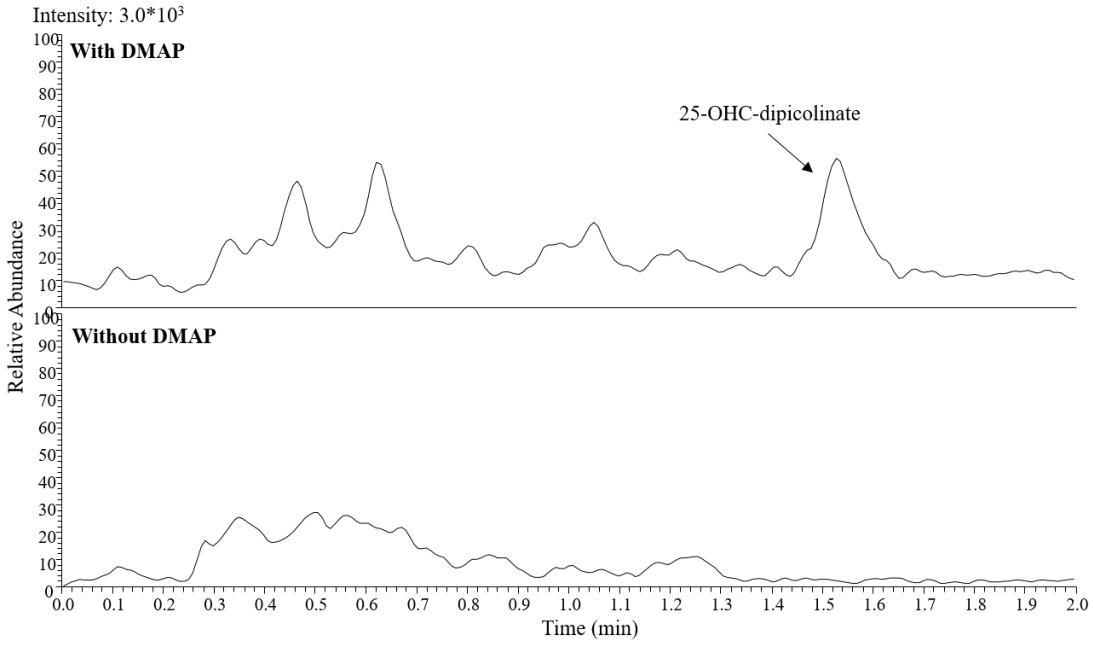

Figure 32. Total ion current (TIC) chromatograms (7 points smoothing) of *m/z* 635 -> 146, 512 of 25-OHC (10 ng/mL) after charge tagging with picolinic acid. Separation was done with an ACE Excel CN-ES (50 x 2.1 mm ID, 1.7 µm particle size) column. The MP was 70/30/0.1 (ACN/H_2O/FA, v/v/v), the flow rate was 800 µL/min at 25 °C, and the injection volume was 10 µL.

As observed from the chromatogram, a weak signal for 25-OHC-dipicolinate was observed when DMAP was included. 25-OHC-monopicolinate was not observed (data not shown). An explanation for the successful derivatization of 25-OHC- and 25-OHC-d_6-picolinate without DMAP by Honda is that pyridine *de facto* may have worked as a substitute nucleophile, as they are structurally similar, as shown in **Figure 33**.

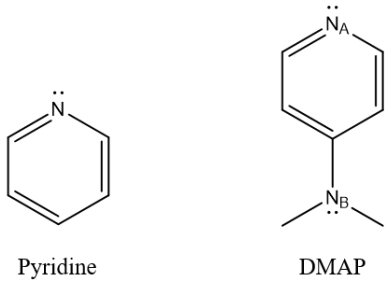

Figure 33. The structures of pyridine and DMAP.

The basicity of DMAP and pyridine is determined by two factors. Firstly, the lone pair on the nitrogen in pyridine is delocalized due to resonance stabilization in the aromatic system and is, therefore, less available for a nucleophilic attack. Secondly, the positive charge on the nitrogen after protonation will not be stabilized as the resonance stability is disrupted. DMAP has lone pairs on N_A and N_B, but the nucleophilic attack would presumably occur on N_A, as the electrons on N_B will help resonance stabilize the positive charge after protonation. Hence, DMAP is a stronger nucleophile than pyridine, yet pyridine may have performed a nucleophilic attack on MNBA. In other words, the derivatization is not impossible to perform when removing DMAP and adding pyridine, but DMAP would perhaps be the optimal choice of the catalyst due to the aforementioned reasons.

To summarize, several modifications were made to the procedure of Honda, and experimental design was performed to optimize the picolinyl esterification [162]. However, poor yield, an arbitrary formation of mono- and dipicolinate derivatives, and issues with sensitivity was experienced. The role of DMAP was further investigated, but the derivatization was not successful. The derivatization is, by our hands, challenging to reproduce, and was therefore abandoned.

4.1.2 Thiyl radical-based charge tagging: too good to be true?

The proposed structure of the charge tagged derivate of cholesterol (^{TGA}-cholesterol) is shown in **Figure 34**. The initial procedure of Adhikari [120] did not prove to be successful; therefore, several modifications were carried out, *i.e.* increased analyte concentrations, different UV lamps, and SPE in addition to LLE.

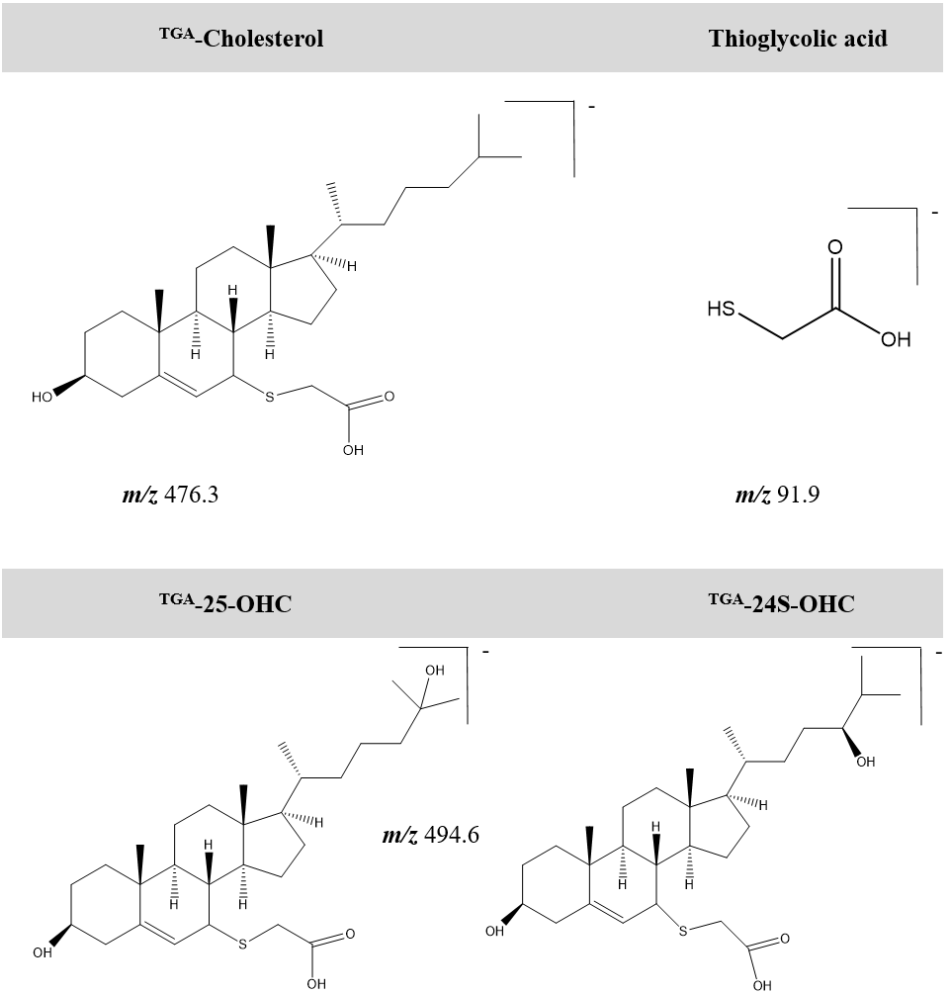

Figure 34. The predicted structures with corresponding *m/z* for ^{TGA}-cholesterol, ^{TGA}-25-OHC, and ^{TGA}-24S-OHC.

TGA was added in high concentration to the reagent mixture and is expected to cause signal suppression in the ESI-MS analysis if not removed sufficiently. However, according to Adhikari, an LLE with ethyl acetate and NaOH should remove the excess TGA. The extraction volumes were specified neither in the article, nor in the supplementary information, and the author of this thesis experienced issues with phase separation during extraction, even after centrifugation. A signal for TGA (*m/z* = 91.9) was repeatedly observed in the mass spectrum (**Figure 35**). Even when SPE was carried out post LLE, the TGA was still present. The recurring observation of TGA in the mass spectrum could give a reason to believe that TGA was suppressing the signal for the ^{TGA}-cholesterol. Nevertheless, a signal at *m/z* = 387 for intact cholesterol was observed in positive ionization mode, indicating that the reaction may not have taken place.

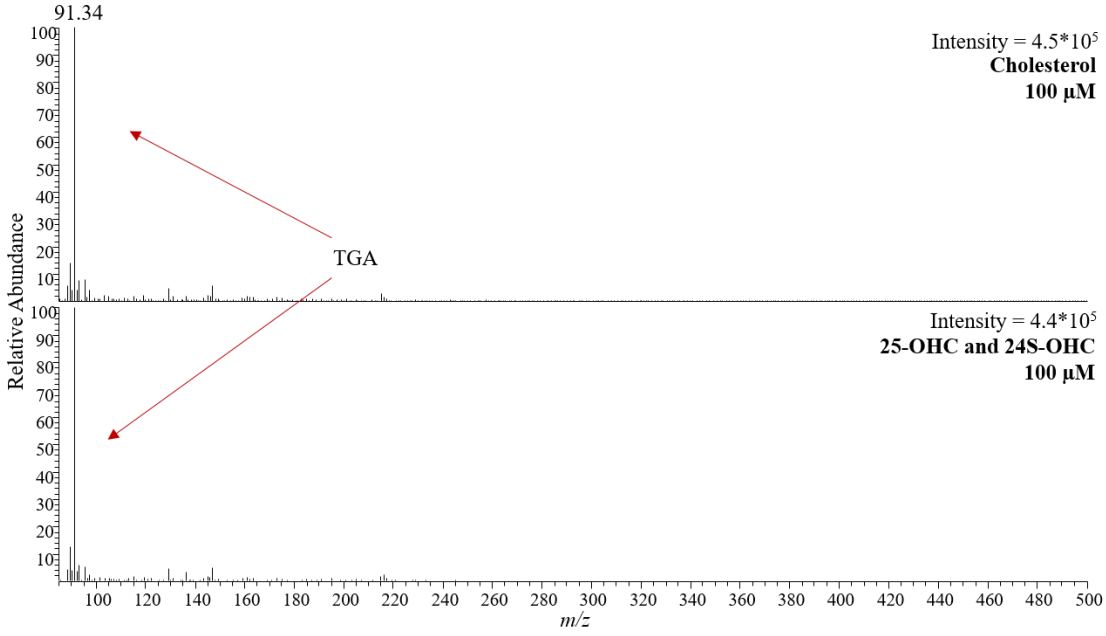

Figure 35. Mass spectra of cholesterol, 25-OHC and 24S-OHC (100 µM) in full scan negative ESI mode by direct injection after thiyl radical-based charge tagging.

Due to the suspicion that the charge tagging did not occur, different UV lamps and irradiation times were tested. Adhikari [120] performed irradiation for 15-20 minutes with a low-pressure mercury lamp at 351 nm; however, the lamp model reported used by Adhikari can not provide this wavelength. Hence, the information in [120] is conflicting. Two of the three UV lamps tested in the present study had unidentifiable wavelengths, and the third was a deuterium lamp operated at 351 nm, as these were the only available lamps in the laboratory. The irradiation times tested were 30 and 60 minutes, but there was no signal for ^{TGA}-cholesterol, only for TGA itself. Photochemical reactions have shown to proceed more rapidly if the photon absorption efficiency is increased [165], and a flow microreactor should have been investigated. Due to the limited amount of time however, this was not prioritized.

Different concentrations of cholesterol (5 µM and 100 µM) and different concentrations of the photoinitiator DMPA (1 mM and 10 mM) were investigated, but a signal for ^{TGA}-cholesterol was still not obtained. DMPA was chosen as the photoinitiator as Adhikari experienced successful derivatization, and also because DMPA has proven to be efficient for several thiol-ene click reactions [166]. However, different photoinitiators could be investigated further.

To summarize, thiyl-radical based charge tagging of cholesterol, 25-OHC, and 24S-OHC was investigated. Several modifications of the initial procedure of Adhikari were carried out, i.e.

different extraction techniques (LLE/SPE), UV lamps, photoinitiator concentrations, and analyte concentrations, without success. Thus, the derivatization procedure is, by our hands, challenging to reproduce, and was not further pursued in this study.

Hence, it was decided to keep the established Girard T derivatization procedure, and rather assess the hydrolysis step in the sample preparation method.

4.2 Hydrolysis of oxysterols in human plasma

Our established hydrolysis method for oxysterol esters in biological samples uses an alkaline solution (KOH) and is time-consuming and tedious due to the two hour reaction time. The method is laborious, as an LLE must be carried out prior to SPE in order to remove the alkaline compound. Consequently, an alternative enzymatic hydrolysis method with the enzyme ChE based on the work by Mendiara *et al.* was investigated [96].

Enzymatic hydrolysis of the esterified oxysterols 24S-, 25-, and 27-OHC in pooled plasma samples was carried out with the enzyme ChE and evaluated by using the AFFL-SPE-LC-MS system. As mentioned, human plasma was used because tumors were available in very small amounts. All the chromatograms in the following sections are shown in the time range of 1 – 5 minutes as the target oxysterols elute in this time range, even though the analysis time was 7 minutes.

4.2.1 Preliminary investigation of chromatographic performance

Human plasma does not only contain 24S-, 25-, and 27-OHC, but also other bound and free oxysterols, *e.g.* 22S-OHC, 7β-OHC and 7-ketocholesterol [78, 167, 168]. In addition, oxysterols have shown to be substrates for cytosolic sulfotransferases, which are enzymes that catalyze sulfation of the sterols (*i.e.* the transfer of a sulfo group) [169, 170]. Therefore, it may be possible that other unidentifiable bound (or free) oxysterols with the same mass and fragmentation patterns as 24S-, 25-, and 27-OHC, either esterified or sulfated, could appear in the chromatograms with similar t_R as 24S-, 25-, and 27-OHC.

In order to assess the above-mentioned assertion, as well as the chromatographic performance, human plasma was analyzed by the two methods at two following days. The performance was evaluated in terms of peak area, $t_{R,}$ and Rs between the oxysterols. As the peak area is

proportional to the analyte concentration, it was also desirable to check whether alkaline or enzymatic hydrolysis provided the highest concentration of oxysterols, *i.e.* amount of hydrolyzed oxysterols. A standard solution of oxysterols in IPA was also exposed to enzymatic hydrolysis, in order to investigate if the enzyme had a direct impact on the chromatography. **Figure 36** shows the chromatograms obtained following both hydrolysis procedures on human plasma and the standard solution (400 pM) on the two days.

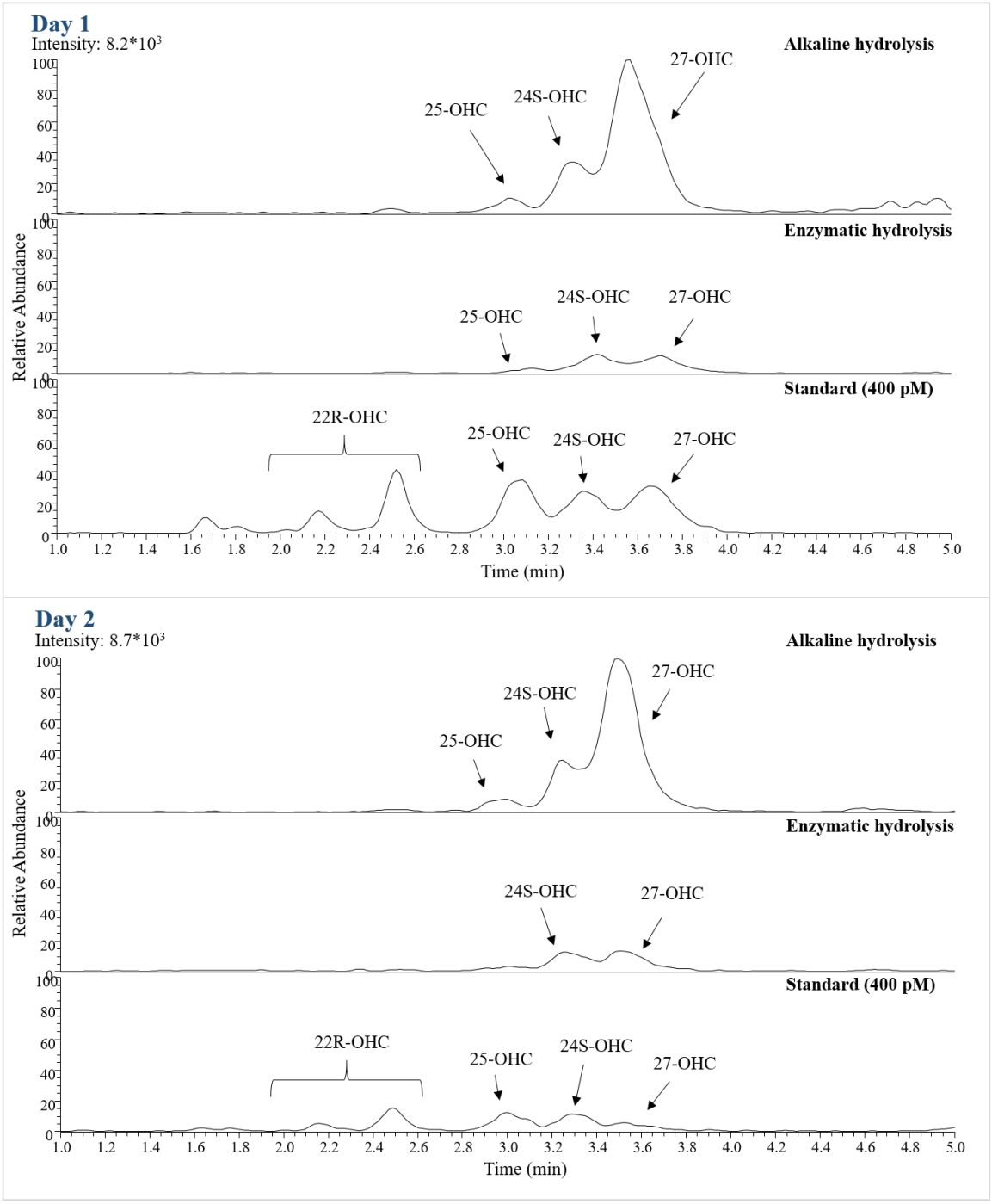

Figure 36. TIC chromatograms (7 points smoothing) of *m/z* 514 -> 433, 461 of 5 µL plasma with 24S-, 25-, and 27-OHC following alkaline and enzymatic hydrolysis, and a standard solution with 22R-, 24S-, 25-, and 27-OHC (400 pM) after enzymatic hydrolysis. Separation was done with the ACE UltraCore SPH (150 x 2.1 mm ID, 2.5 µm core-shell particles) column A with a C18 SPE column, by using the AFFL-SPE system described in **Section 3.6.3**. The MP was 57/10/33/0.1 (H_2O/MeOH/ACN/FA, v/v/v/v), the flow rate was 650 µL/min at 55 °C, and the injection volume was 60 µL.

As observed from the chromatograms at day 1, alkaline hydrolysis provided highest peak areas and best Rs. However, the Rs for alkaline hydrolysis was poor (Rs for 25/24S-OHC ≈ 1.0 and for 24S/27-OHC ≈ 0.75), and did not reach the value of 1.5, which is the threshold for baseline separation (see **Table 19** in **Appendix 7.6**). Baseline separation was not achieved for 24S-, 25-, and 27-OHC neither for the enzymatic hydrolysis nor for the standard. Consequently, the peak areas were challenging to measure, and for day 2, 25-OHC could not even be determined from the chromatogram for enzymatic hydrolysis. All the oxysterols were harder to determine for the enzymatic hydrolysis.

22R-OHC was included in the standard solution for a reference, but the oxysterol is apparently not present in the plasma, as observed. No other oxysterols can be observed in the chromatograms with the same fragmentation patterns as 25-, 24S-, and 27-OHC.

To summarize, the peak areas of 24S-, 25-, and 27-OHC were largest for alkaline hydrolysis and difficult to measure for the enzymatic hydrolysis and the standard. The Rs was poor for both hydrolyses and baseline separation was not achieved. For enzymatic hydrolysis, 24S-, 25-, and 27-OHC were harder to identify.

In order to pursue higher peak areas for enzymatic hydrolysis, it was hypothesized that a higher concentration of ChE would perhaps be able to hydrolyze a higher concentration of oxysterols.

4.2.2 Increased concentration of cholesterol esterase gave larker peak areas

The concentration added to plasma for the experiment addressed in the previous subsection was 0.0080 UN, as this concentration was the same Solheim [153] used for the enzyme ChX (for oxidation of the hydroxyl group in the oxysterols, see **Section 2.4.3**) in 5 µL plasma. Although the enzymes are different, it was desired to use the smallest enzyme concentration as possible to reduce the cost.

The initial ChE concentration used by Mendiara *et al.* [96] was 1.6 UN in 100 µL plasma (0.016 UN/µL), which corresponds to 0.080 UN in 5 µL plasma. Hence, it was of interest to compare the use of 0.0080 UN (Solheim) and 0.080 UN (Mendiara). As the concentration used by Solheim had already been assessed in the previous experiment (**Section 4.2.1**) and provided poor intensity and chromatography, other concentrations were also investigated; 0.034 UN and 0.051 UN. The concentrations were chosen in order to get suitable pipetting volumes, and to

keep the buffer volume < 500 µL to reduce the cost and as the sample vials were 1.5 mL. The concentrations of ChE investigated in this study are shown in **Table 11**.

Table 11. The concentrations (UN) of ChE added to 5 µL plasma

Concentration (UN)
0.034
0.051
0.080

The peak areas for 24S-, 25- and 27-OHC with the standard deviation between sample replicates given as error bars plotted against injection number (n = 6) for 0.034, 0.051 and 0.080 UN ChE are shown in **Figure 37A**. The ChE concentration of 0.034 UN provided larger peak areas for every oxysterol, *i.e.* a higher concentration of oxysterols were hydrolyzed at this concentration. This observation was especially noticeable for 27-OHC, which is the most abundant oxysterol in blood plasma (discussed further in **Section** Error! Reference source not found.) [78, 96]. As shown in **Table 20** in **Appendix 7.6**, the lowest average relative standard deviation in percentage (%RSD) between the sample replicates for the areas of 24S- and 25-OHC were 8.8% and 11%, respectively, and achieved with 0.034 UN ChE. For 27-OHC, the lowest %RSD (6.3%) was achieved with 0.051 UN.

The chromatograms for 24S-, 25- and 27-OHC following enzymatic hydrolysis with 0.034, 0.051 and 0.080 UN are shown in **Figure 37B**. As observed, the ChE concentration of 0.034 UN provided higher intensity and smoother peaks. Baseline separation was almost achieved between 25-OHC and 24S-OHC for all concentrations (Rs ≈ 1.2, 1.3 and 1.2 for 0.034, 0.051 and 0.080 UN, respectively). The average Rs between 25-OHC and 27-OHC (n = 6) was *de facto* better for the concentration of 0.080 UN (Rs ≈ 1.02). For 0.034 UN and 0.051 UN, the Rs between 25-OHC and 27-OHC was 0.83 and 0.85, respectively. The Rs for 24S-, 25-, and 27-OHC with a standard deviation between injection numbers given as error bars plotted against injection number (n = 6) is shown in **Figure 38**. The raw data is shown in **Table 20** in **Appendix 7.6**.

Because the concentration of 0.034 UN ChE provided largest peak areas for the oxysterols, and hence a higher concentration of hydrolyzed oxysterols, the concentration was chosen for further experiments. This concentration is also beneficial in terms of cost.

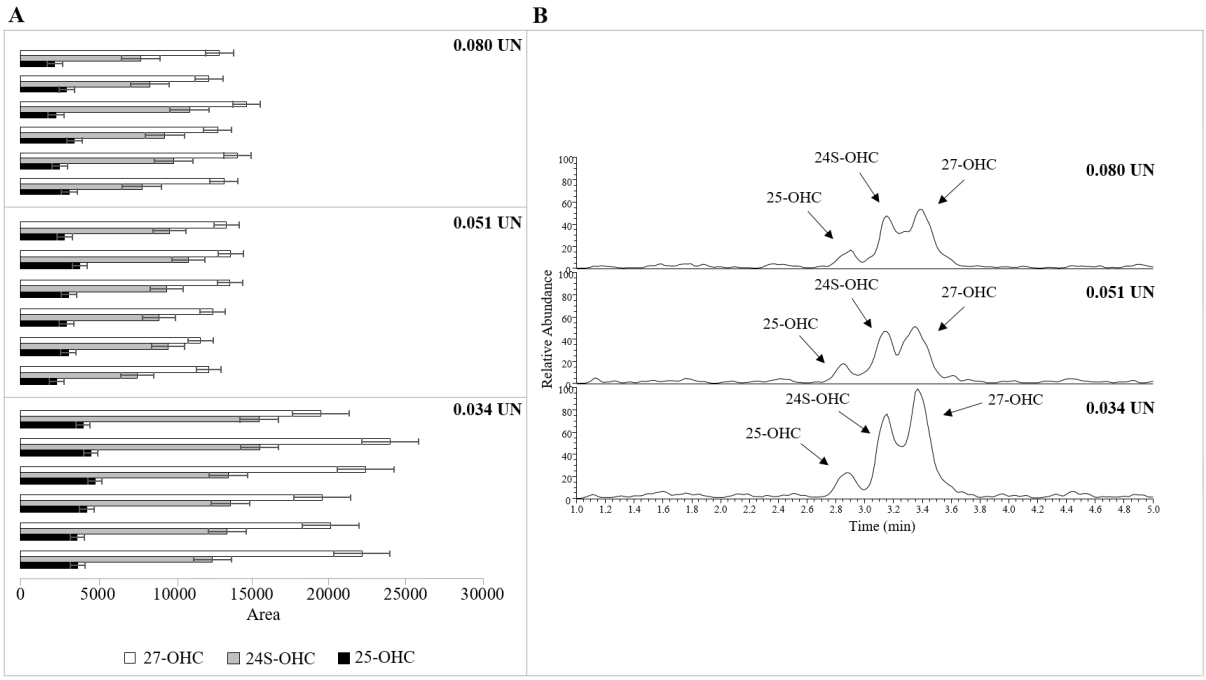

Figure 37. A. Peak areas plotted against injection number (n = 6) with standard deviation between the sample replicates given as error bars for 24S-, 25-, and 27-OHC after enzymatic hydrolysis of 5 µL plasma with 0.034, 0.051 and 0.080 UN ChE. **B**. TIC chromatograms (7 points smoothing) of *m/z* 514 -> 433, 461 of 5 µL plasma with 24S-, 25-, and 27-OHC following enzymatic hydrolysis with 0.034, 0.051 and 0.080 UN. Separation was done with the ACE UltraCore SPH (150 x 2.1 mm ID, 2.5 µm core-shell particles) column A with a C18 SPE column, by using the AFFL-SPE system described in **Section 3.6.3**. The MP was 57/10/33/0.1 (H_2O/MeOH/ACN/FA, v/v/v/v), the flow rate was 650 µL/min at 55 °C, and the injection volume was 60 µL

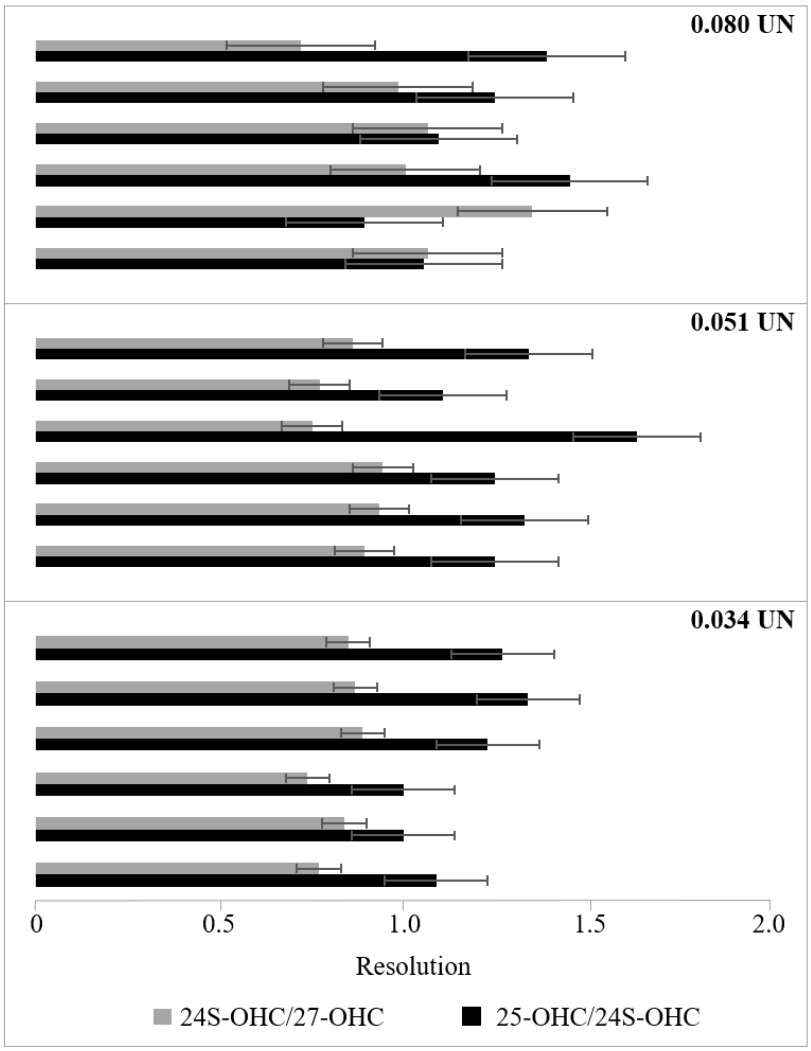

Figure 38. Rs plotted against injection number (n = 6) with standard deviation between the sample replicates given as error bars for 24S-, 25-, and 27-OHC after enzymatic hydrolysis of 5 µL plasma with 0.034, 0.051 and 0.080 UN ChE. Separation was done with the ACE UltraCore SPH (150 x 2.1 mm ID, 2.5 µm core-shell particles) column A with a C18 SPE column, by using the AFFL-SPE system described in **Section 3.6.3**. The MP was 57/10/33/0.1 (H_2O/MeOH/ACN/FA, v/v/v/v), the flow rate was 650 µL/min at 55 °C, and the injection volume was 60 µL

To summarize, the ChE concentration of 0.034 UN provided higher peak areas and smoother peaks for 24-, 25-, and 27-OHC. Baseline separation between 25- and 24S-OHC was almost achieved for every ChE concentration. The concentration of 0.034 UN was chosen for further experiments.

In order to pursue a higher Rs and better peak shapes for the oxysterols, a new analytical column was tested.

4.2.3 The change of analytical column led to improved peak shape

In order to improve the peak shapes and the Rs, the column used for the previous experiments (column A) was replaced with a new column (column B). The columns are shown in **Table 10** in **Experimental 3.6.3**.

Plasma was spiked with 400 pM 24S-, 25-, and 27-OHC prior to enzymatic hydrolysis. An unwanted result was that the t_R of the oxysterols was increased on column B, which resulted in longer analysis time. Hence, the MP composition previously used, 57/10/33/0.1 (H_2O/MeOH/ACN/FA, v/v/v/v), had to be adjusted.

In RPLC, the retention decreases with an increasing amount of organic solvent. According to Snyder's selectivity triangle, the solvent strength increases when changing the organic solvent from MeOH to ACN, *i.e.* ACN will elute hydrophobic analytes faster than MeOH [171]. In addition, when mixed with water, the pressure for MeOH increases more than the pressure for ACN. However, as the back pressure did not cause any troubles for the analysis, and because ACN is more toxic than MeOH, a small increase of MeOH was performed.

The MP compositions tested were 56/11/33/0.1 (H_2O/MeOH/ACN/FA, v/v/v/v) and 55/12/33/0.1 (H_2O/MeOH/ACN/FA, v/v/v/v), *i.e.* an increase of 1% and 2% MeOH, respectively. **Figure 39** shows chromatograms of plasma spiked with 400 pM 22R-, 24S-, 25-, and 27-OHC following enzymatic hydrolysis with 0.034 UN ChE for the different MP compositions.

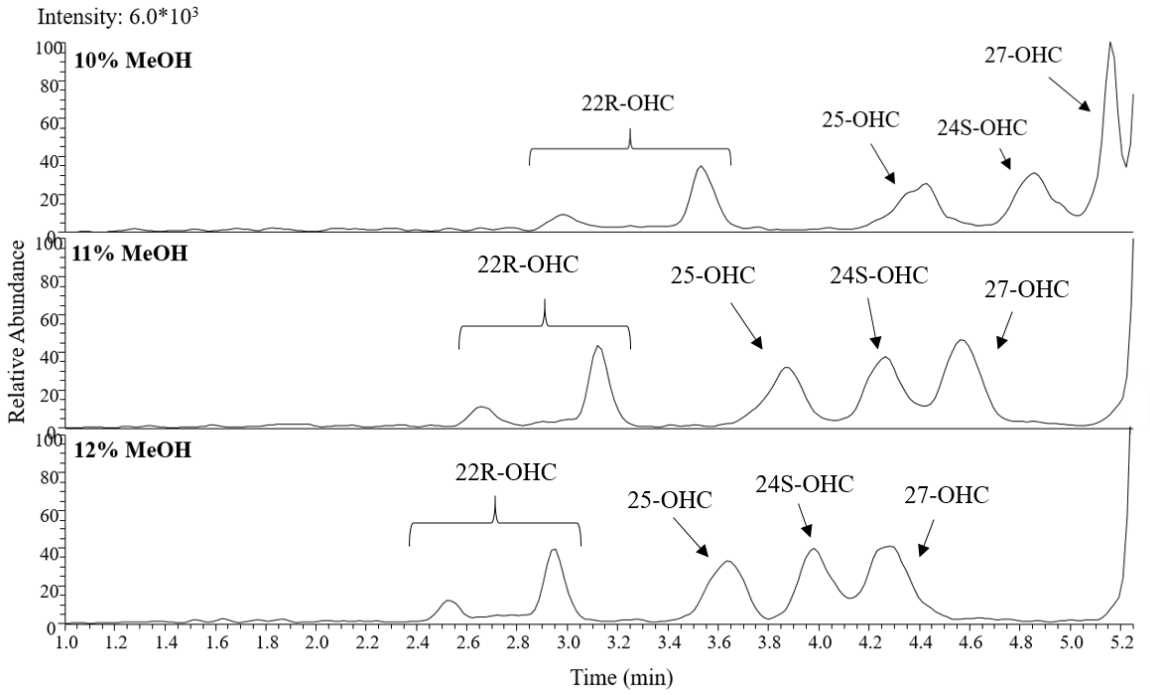

Figure 39. TIC chromatograms (7 points smoothing) of m/z 514 -> 433, 461 of 5 µL plasma spiked with 22R-, 24S-, 25-, and 27-OHC (400 pM) following enzymatic hydrolysis. Separation was done with the ACE UltraCore SPH (150 x 2.1 mm ID, 2.5 µm core-shell particles) column B with a C18 SPE column, by using the AFFL-SPE system described in **Section 3.6.3**. The MPs were 57/10/33/0.1, 56/11/33/0.1 and 55/12/33/0.1 (H_2O/MeOH/ACN/FA, v/v/v/v), the flow rate was 650 µL/min at 55 °C, and the injection volume was 60 µL.

As seen from the chromatogram, the increase to 11% and 12% MeOH in the MP expectedly led to less retention. The peak observed after 5.3 minutes (also shown in **Figure 27** in **Experimental 3.6.2**) at the initial composition of 10% MeOH partly co-eluted with 27-OHC, and hence this MP composition could not be used further. The peak is presumably a combination of oxysterols with the hydroxyl group on the steroid ring and cholesterol which autoxidizes in the ionization source. Cholesterol is in such a high amount that the peak is present even in blanks and standards, due to carry over.

The t_R for each oxysterol for the different MP compositions are given as scatter plots in **Figure 40**. The Rs between the oxysterols are presented as bar charts in **Figure 41** and in **Table 21** in **Appendix 7.6**. The initial composition of 57/10/33/0.1 (H_2O/MeOH/ACN/FA, v/v/v/v) provided the highest Rs between 25-OHC/24S-OHC and 24S-OHC/27-OHC (Rs ≈ 1.5 for both). However, as the peak of 27-OHC partly co-eluted with the interfering peak at 5.3 minutes, the MP composition with 11% MeOH, which provided second best Rs (1.4 between 25-OHC/24S-OHC and 1.1 between 24S-OHC/27-OHC) was chosen for further experiments.

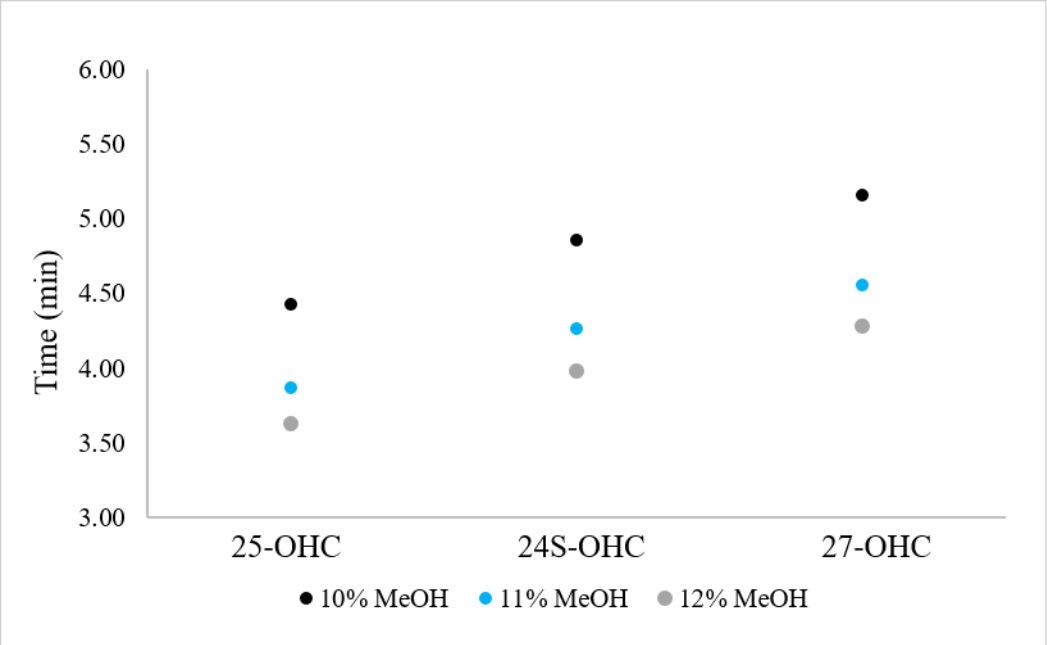

Figure 40. t_R for derivatized oxysterols in 5 µL plasma spiked with 400 pM of 25-, 24S-, and 27-OHC following enzymatic hydrolysis, for the MP compositions 57/10/33/0.1, 56/11/33/0.1 and 55/12/33/0.1 (H_2O/ACN/MeOH/FA, v/v/v/v), using the ACE UltraCore SPH (150 x 2.1 mm ID, 2.5 µm core-shell particles) column B with a C18 SPE column, by using the AFFL-SPE system described in **Section 3.6.3**. The flow rate was 650 µL/min and the injection volume was 60 µL.

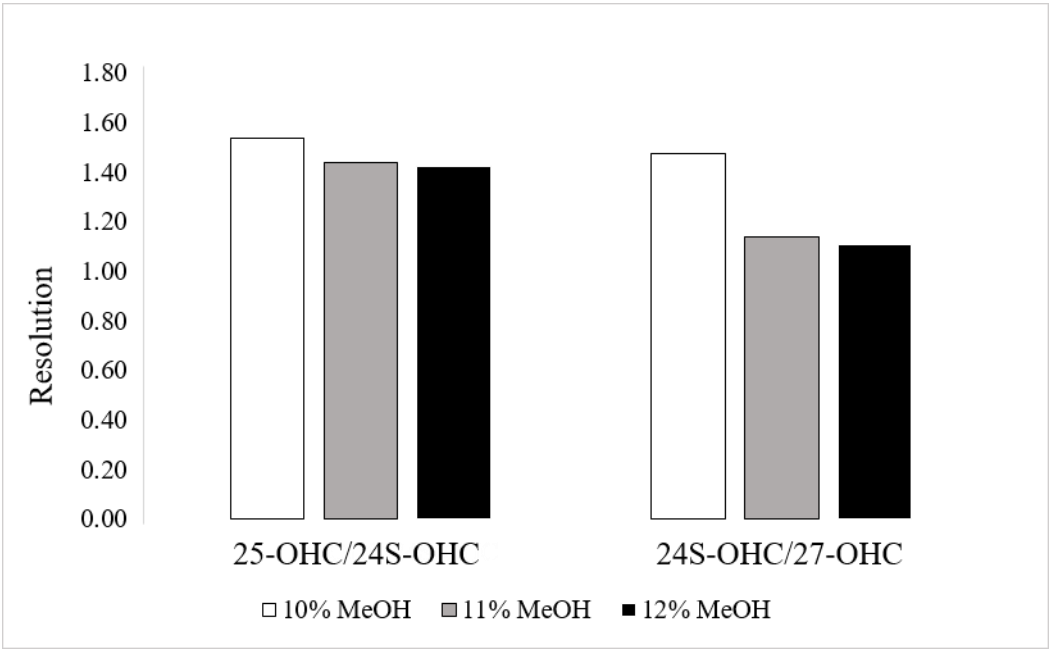

Figure 41. Rs between derivatized oxysterols in 5 µL plasma, spiked with 400 pM of 25-, 24S-, and 27-OHC following enzymatic hydrolysis, for the MP compositions 57/10/33/0.1, 56/11/33/0.1 and 55/12/33/0.1 (H_2O/MeOH/ACN/FA, v/v/v/v), using the ACE UltraCore SPH (150 x 2.1 mm ID, 2.5 µm core-shell particles) column B with a C18 SPE column, by using the AFFL-SPE system described in **Section 3.6.3**. The flow rate was 650 µL/min and the injection volume was 60 µL.

To summarize, the amount of MeOH in the MP was increased with 1% and 2% for column B. The initial MP composition of 57/10/33/0.1 (H_2O/MeOH/ACN/FA, v/v/v/v was changed to 56/11/33/0.1 (H_2O/MeOH/ACN/FA, v/v/v/v), which provided second best Rs (1.4 for 25-OHC/24S-OHC and 1.1 for 25-OHC/27-OHC).

4.2.4 Hydrolysis with a surfactant improved the oxysterol yield

It was suspected that the low peak areas observed for the oxysterols (and thereby the low concentrations of hydrolyzed oxysterols) after enzymatic hydrolysis might be a result of ChE not being able to approach the oxysterols properly. As mentioned, oxysterol esters are stored in LDL, whose membrane needs to be solubilized for ChE to reach the oxysterols. The solubilization can be performed by a surfactant.

Mendiara *et al.* carried out enzymatic hydrolysis in the presence of 0.5% of the surfactant TX-100) [96]. Surfactants may cause ion suppression and may adsorb on an RPLC column, presumably by their hydrophobicity [172]. Consequently, TX-100 was excluded from the procedure for the experiments previously addressed. The structure of TX-100 is shown in **Figure 42**.

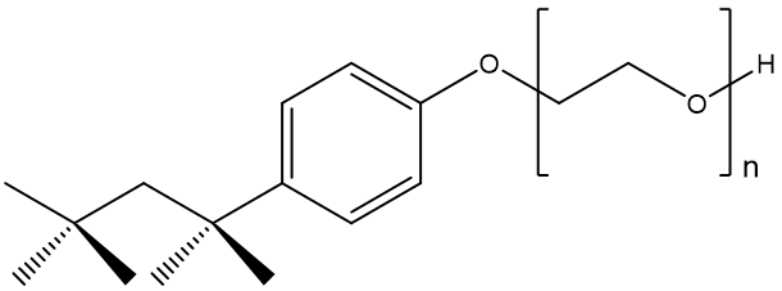

Figure 42. The structure of TX-100.

The possible effect of TX-100 on the enzymatic hydrolysis of 24S-, 25-, and 27-OHC in plasma was investigated and compared to enzymatic hydrolysis without TX-100 and no hydrolysis (*i.e.* free oxysterol measurement, as a reference). The chromatograms are shown in **Figure 43**. The peak areas for each oxysterol are presented as bar charts with corresponding standard deviations between the sample replicates given as error bars in **Figure 44**.

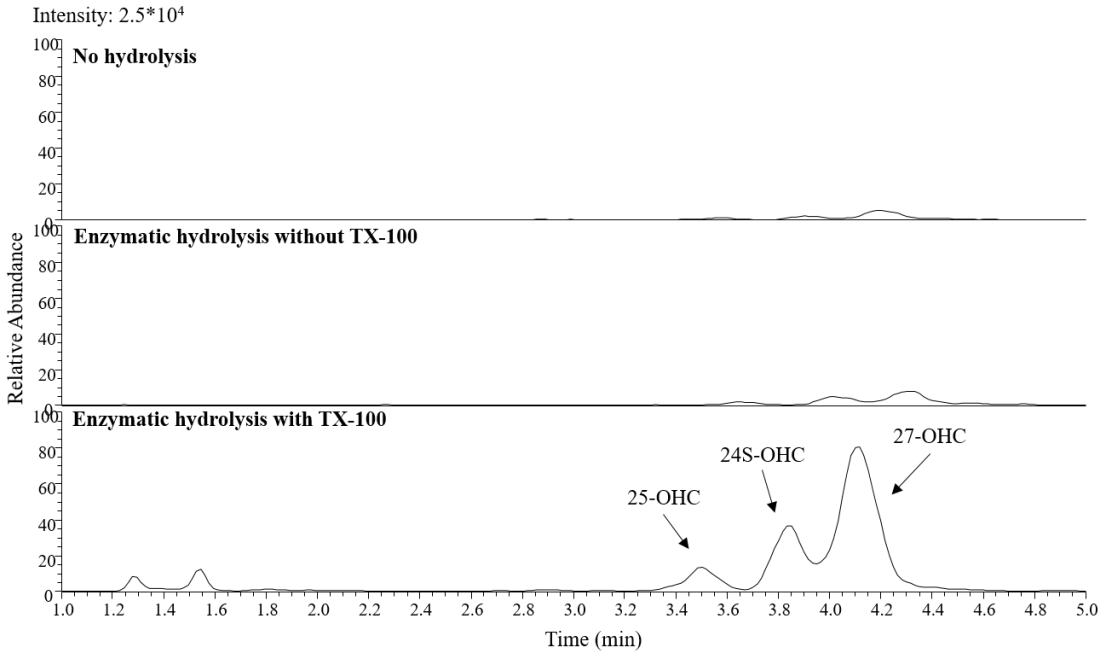

Figure 43. TIC chromatograms (7 points smoothing) of *m/z* 514 -> 433, 461 of 5 µL plasma after enzymatic hydrolysis with and without TX-100, and no hydrolysis. Separation was done with the ACE UltraCore SPH (150 x 2.1 mm ID, 2.5 µm core-shell particles) column B with a C18 SPE column, by using the AFFL-SPE system described in **Section 3.6.3**. The MP was 56/11/33/0.1 (H_2O/MeOH/ACN/FA, v/v/v/v), the flow rate was 650 µL/min at 55 °C, and the injection volume was 60 µL.

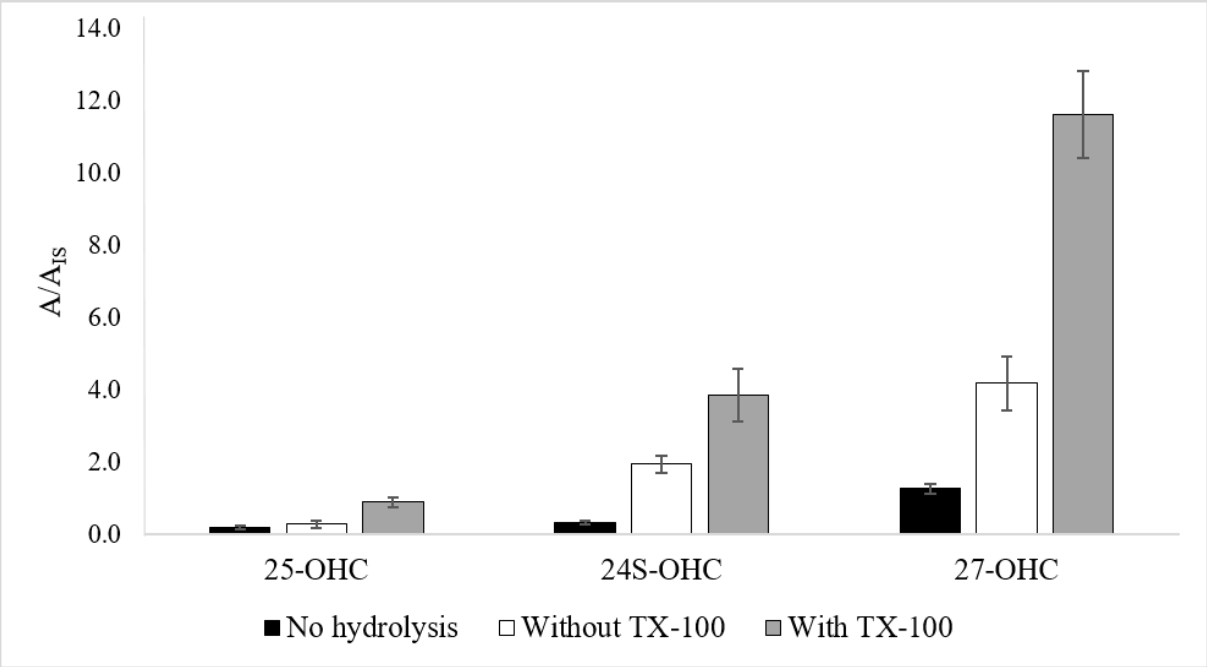

Figure 44. A/A_{IS} for 25-, 24S-, and 27-OHC after enzymatic hydrolysis with and without TX-100 and no hydrolysis of 5 µL plasma, with standard deviations between sample replicates given as error bars (n = 3 for hydrolysis without TX-100 and no hydrolysis, n = 4 for hydrolysis with TX-100). Separation was done with the ACE UltraCore SPH (150 x 2.1 mm ID, 2.5 µm core-shell particles) column B with a C18 SPE column, by using the AFFL-SPE system described in **Section 3.6.3**. The MP was 56/11/33/0.1 (H_2O/MeOH/ACN/FA, v/v/v/v), the flow rate was 650 µL/min at 55 °C, and the injection volume was 60 µL.

As observed from the chromatograms and the bar charts, the peak area for 27-OHC after enzymatic hydrolysis with TX-100 was undoubtedly improved compared to hydrolysis without TX-100. An improvement in the peak area for 24S-OHC can also be observed. The increased peak areas indicate that ChE hydrolyzes a higher concentration of bound oxysterols in plasma in the presence of TX-100, and hence the oxysterol yield is improved with the surfactant.

The peak area for 25-OHC after enzymatic hydrolysis without TX-100 is almost as small as the peak area obtained after no hydrolysis. The reason for the similar peak areas is that most of 25-OHC presumably exists as a free oxysterol in plasma, and a smaller relative amount of this oxysterols is bound compared to 24S- and 27-OHC [89, 173]. The free and total oxysterol concentrations in plasma reported by McDonald and Griffiths are shown in **Table 17** in **Appendix 7.2.3** [78, 89, 173]. As observed, 27-OHC has a higher relative concentration bound in plasma, which also corresponds to the peak area of the oxysterol having the highest increase with enzymatic hydrolysis with TX-100 in this thesis.

The fact that 27-OHC provided the highest A/A_{IS} corresponds to previous reports about the oxysterol being more abundant than 24S- and 25-OHC in plasma [50, 96]. According to Mendiara *et al.*, 24S-OHC is the second most abundant oxysterol in plasma, followed by 25-OHC [96], as can also be observed in the bar chart. The aforementioned observations about the concentrations of 24S-, 25-, and 27-OHC in plasma were also reported by McDonald and Griffiths (**Table 17**, **Appendix 7.2.3**) [89, 173].

To summarize, the peak areas for 24S-, 25-, and 27-OHC increased when enzymatic hydrolysis was performed with TX-100, i.e. the oxysterol yield increased compared to hydrolysis without TX-100. The increase was most significant for 27-OHC, which corresponds to the reports that a higher amount of this oxysterol is bound compared to 24S- and 25-OHC in plasma. Thus, enzymatic hydrolysis was more successful in terms of yield with TX-100, than without.

4.2.5 Significantly higher yields were obtained with enzymatic hydrolysis

Compared to alkaline hydrolysis, enzymatic hydrolysis with TX-100 provided larger peak areas for 25-, 24S-, and 27-OHC, and especially for the latter two. **Figure 45** presents the A/A_{IS} as bar charts with corresponding standard deviations between sample replicates for 25-, 24S-, and 27-OHC after alkaline hydrolysis and enzymatic hydrolysis with TX-100. The areas for the oxysterols and the IS are shown in **Table 22** in **Appendix 7.6**.

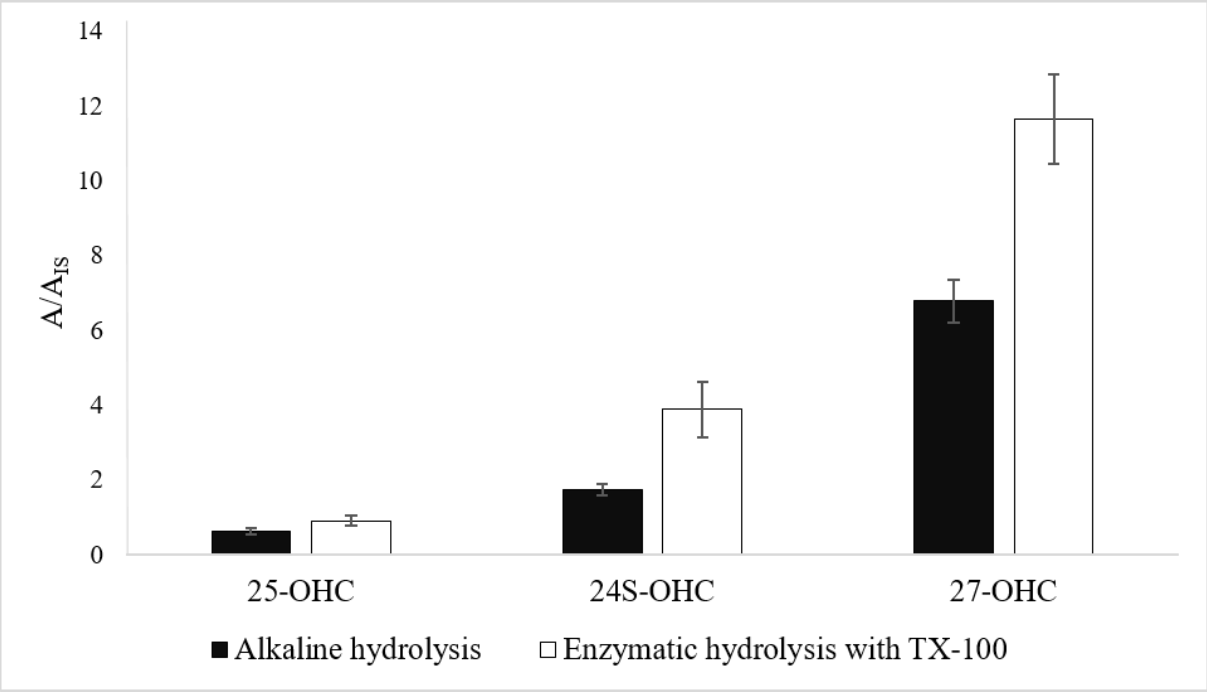

Figure 45. A/A_{IS} for 25-, 24S-, and 27-OHC after enzymatic hydrolysis with (n = 4) and without TX-100 (n = 3) and no hydrolysis (n= 3) of 5 µL plasma, with standard deviations between sample replicates given as error bars. Separation was done with the ACE UltraCore SPH (150 x 2.1 mm ID, 2.5 µm core-shell particles) column B with a C18 SPE column, by using the AFFL-SPE system described in **Section 3.6.3**. The MP was 56/11/33/0.1 (H_2O/MeOH/ACN/FA, v/v/v/v), the flow rate was 650 µL/min at 55 °C, and the injection volume was 60 µL.

The increase in the peak areas show that hydrolysis with ChE give higher yields than alkaline hydrolysis. Mendiara *et al.* [96] reported higher concentrations for 24S-, 25-, and 27-OHC after enzymatic hydrolysis compared to alkaline hydrolysis as well. Higher yields may indicate that ChE hydrolyzes a larger concentration of oxysterols in plasma However, another possible reason is that the chance of thermal degradation of the oxysterols decreases due to a lower hydrolysis temperature and a shorter reaction time for ChE (37 °C for 1 hour) compared to alkaline hydrolysis (60 °C for 2 hours). Park *et al*. reported a greater thermal degradation of 7-ketocholesterol at 45 – 75 °C during saponification [93], and Mendiara *et al*. reported degradation for 25-OHC after incubation at 120 min, even at lower temperatures than 60 °C [96]. Another possible reason for the high peak areas for the oxysterols after enzymatic hydrolysis with TX-100 is that the LLE step prior to alkaline hydrolysis is removed, and the risk of losing analytes during sample preparation is therefore reduced.

The chromatograms of 25-, 24S-, and 27-OHC after alkaline hydrolysis and enzymatic hydrolysis with TX-100 of plasma are shown in **Figure 46**. The chromatograms show higher intensities and more narrow peaks for the oxysterols after enzymatic hydrolysis. An interesting

observation is the two compounds eluting at ~ 1.3 and 1.5 minutes in the chromatogram for enzymatic hydrolysis. The peaks are similar to the ones for 22R-OHC, an oxysterol that gives two separate peaks due to stereoisomerism (explained in **Section 2.4.3**) [112, 113, 155]. However, the t_R of the peaks do not correspond to the t_R for 22-OHC (shown in **Figure 39**) Thus, the unidentified peaks could give reason to believe that ChE may hydrolyze more esterified oxysterols than alkaline hydrolysis does.

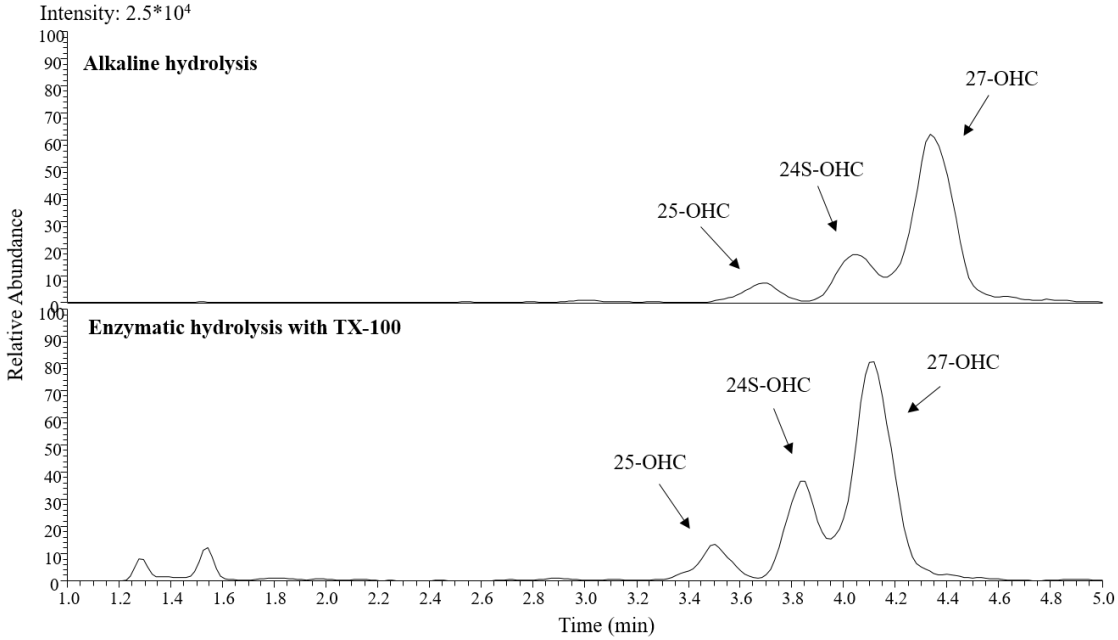

Figure 46. TIC chromatograms (7 points smoothing) of *m/z* 514 -> 433, 461 of 5 µL plasma after alkaline hydrolysis and enzymatic hydrolysis with TX-100. Separation was done with the ACE UltraCore SPH (150 x 2.1 mm ID, 2.5 µm core-shell particles) column B with a C18 SPE column, by using the AFFL-SPE system described in **Section 3.6.3**. The MP was 56/11/33/0.1 (H_2O/MeOH/ACN/FA, v/v/v/v), the flow rate was 650 µL/min at 55 °C, and the injection volume was 60 µL.

A two-tailed t-test was performed in order to establish if the A/A_{IS} for enzymatic hydrolysis was significantly different from alkaline hydrolysis (details for the t-test is presented in **Appendix 7.3**). The results from the t-test (**Table 18** in **Appendix 7.3**) showed a significant difference for 24S- and 27-OHC at a confidence interval of 99% and for 25-OHC at a confidence interval of 98%, *i.e.* the methods are significantly different at the 1% and 2% level. Thus, enzymatic hydrolysis with TX-100 gave significantly higher yields than alkaline hydrolysis.

To summarize, enzymatic hydrolysis gave larger peak areas for 24S-, 25-, and 27-OHC than alkaline hydrolysis, i.e. a higher oxysterol yield was obtained with enzymatic hydrolysis compared to alkaline hydrolysis. Possible explanations are the decreased risk of thermal degradation and the loss of oxysterols during sample preparation, or that ChE de facto hydrolyzes a higher concentration of oxysterols. A t-test was performed, and the A/A_{IS} of the oxysterols were significantly different between the hydrolysis methods.

Triton X-100 and 27-hydroxycholesterol-d_6: a brief consideration

The peak for the IS 27-OHC-d_6 (204 pM) was not detectable in several replicates when TX-100 was excluded from the enzymatic hydrolysis of plasma. When TX-100 was included, a peak for 27-OHC-d_6 was always present in the chromatograms. **Figure 47** shows the chromatograms of 25-OHC-d_6 and 27-OHC-d_6 (204 pM) in 5 μL plasma after enzymatic hydrolysis with and without TX-100. The peak for 25-OHC-d_6 is considerably smaller without TX-100, and the peak for 27-OHC-d_6 can not be observed. Peak areas for 25- and 27-OHC-d_6 plotted as bar charts with corresponding standard deviations between sample replicates are presented in **Figure 48**. The peak areas for 25-OHC-d_6 are similar for hydrolysis without TX-100 and after no hydrolysis, whereas a decrease in the peak area for 27-OHC-d_6 is observed when TX-100 was excluded compared to when no hydrolysis was performed.

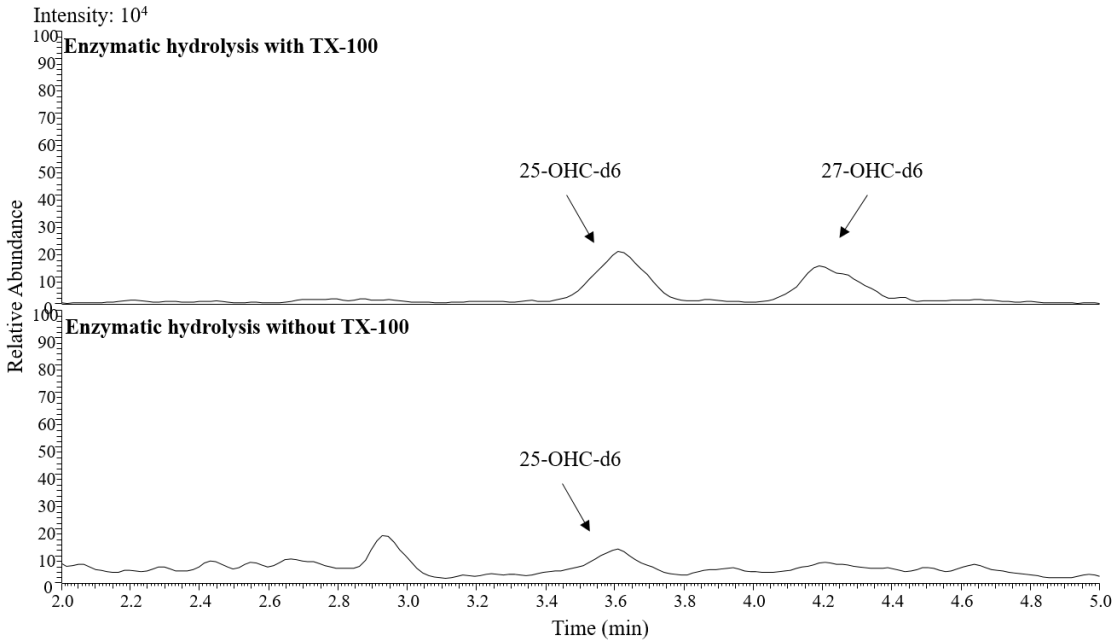

Figure 47. TIC chromatograms (7 points smoothing) of m/z 520 -> 433, 461 of 25-OHC-d6 and 27-OHC-d6 (204 pM) in 5 µL plasma following enzymatic hydrolysis with and without TX-100. Separation was done with the ACE UltraCore SPH (150 x 2.1 mm ID, 2.5 µm core-shell particles) column B with a C18 SPE column, by using the AFFL-SPE system described in **Section 3.6.3**. The MP was 56/11/33/0.1 (H_2O/MeOH/ACN/FA, v/v/v/v), the flow rate was 650 µL/min at 55 °C, and the injection volume was 60 µL.

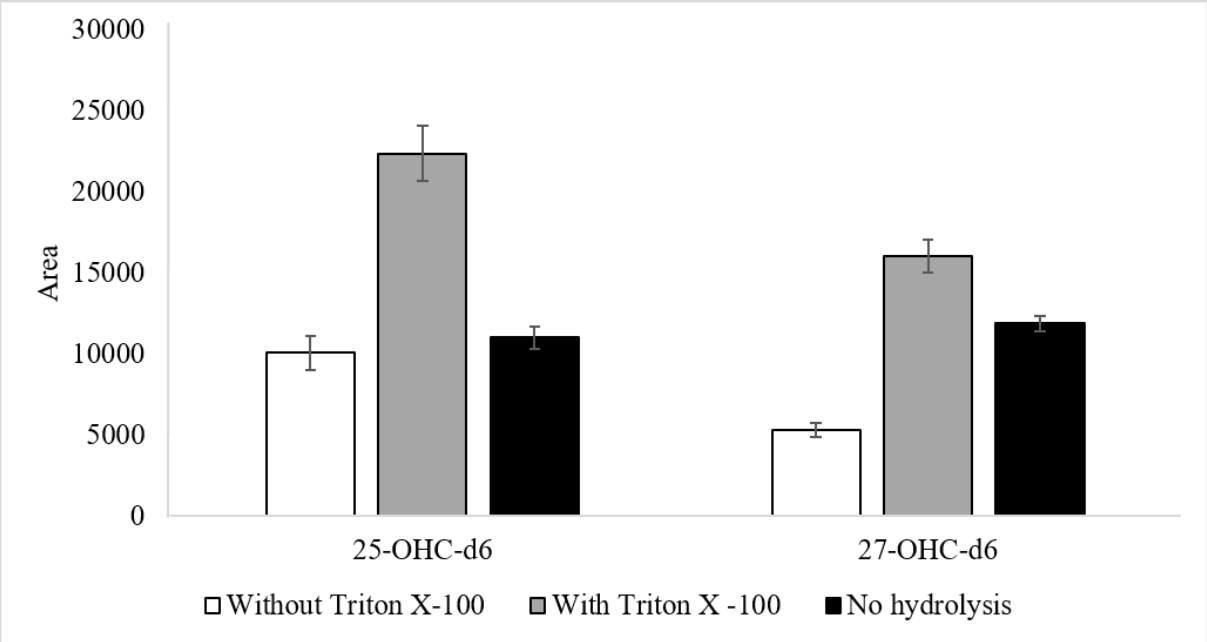

Figure 48. Areas for 25- and 27-OHC-d_6 after enzymatic hydrolysis with (n =4) and without TX-100 (n = 3), and no hydrolysis (n = 3) of 5 µL plasma, with standard deviations between sample replicates given as error bars. Separation was done with the ACE UltraCore SPH (150 x 2.1 mm ID, 2.5 µm core-shell particles) column B with a C18 SPE column, by using the AFFL-SPE system described in **Section 3.6.3**. The MP was 56/11/33/0.1 (H_2O/MeOH/ACN/FA, v/v/v/v), the flow rate was 650 µL/min at 55 °C, and the injection volume was 60 µL.

27-OHC-d_6 was used by Mendiara *et al.* [96], and issues with this IS was not reported. Human plasma is a complex sample matrix that consists of *e.g.* cells and proteins, and it may be possible that 27-OHC-d_6 was bound to other components of the plasma when TX-100 was excluded. The absence of 27-OHC-d_6 led to some challenges when enzymatic hydrolysis was evaluated.

The IS 27-OHC-d_6 was not always detectable in the chromatograms after enzymatic hydrolysis without TX-100, and the peak for 25-OHC-d_6 had less intensity. The concentration of 27-OHC-d_6 decreased without TX-100 and increased with TX-100, compared to the concentration after no hydrolysis was performed.

4.3 Evaluation of enzymatic hydrolysis

Enzymatic hydrolysis was evaluated in terms of the cLOQ and linearity. The preparation of the evaluation solutions is described in **Section 3.3.2**.

4.3.1 Investigating limit of quantification

The cLOQ is the smallest concentration of the analyte that is quantifiable and is defined as the concentration giving a signal 10 times the noise [174]. The method cLOQ for the oxysterols in plasma after enzymatic hydrolysis could not be determined with the analytes themselves, because they already are abundant in plasma. Therefore, the cLOQ was investigated with the IS 25-OHC-d_6 and 27-OHC-d_6. The signal-to-noise ratios (SNRs) were measured from the peak areas obtained for 25- and 27-OHC-d_6, and are shown in **Table 23** in **Appendix 7.6**. However, the experiments were carried out without TX-100, and hence there were challenges with detection of 27-OHC-d_6. The chromatograms of plasma spiked with different concentrations of 25- and 27-OHC-d_6 after enzymatic hydrolysis without TX-100 are shown in **Figure 49**.

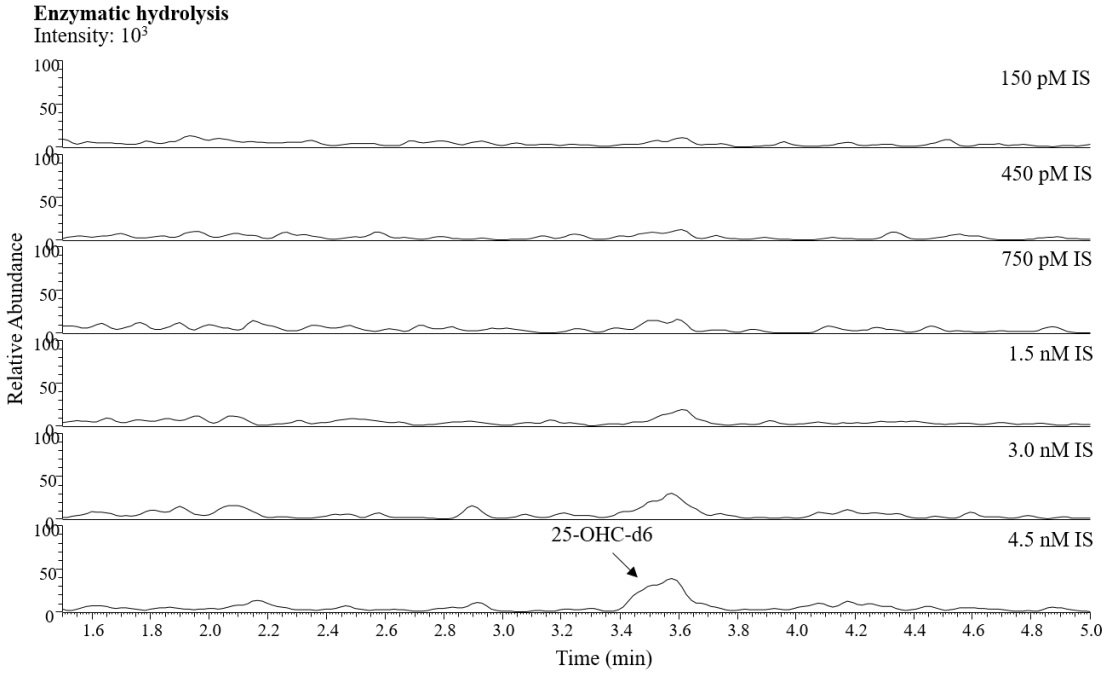

Figure 49. A TIC chromatogram (7 points smoothing) of m/z 520 -> 433, 461 of 5 µL plasma spiked with different concentrations of 25- and 27-OHC-d_6, after enzymatic hydrolysis without TX-100. Separation was done with the ACE UltraCore SPH (150 x 2.1 mm ID, 2.5 µm core-shell particles) column B with a C18 SPE column, by using the AFFL-SPE system described in **Section 3.6.3**. The MP was 56/11/33/0.1 (H_2O/MeOH/ACN/FA, v/v/v/v), the flow rate was 650 µL/min at 55 °C, and the injection volume was 60 µL.

As observed, 27-OHC_6 did not give a detectable signal for the concentrations investigated. For the concentration of 4.5 nM, an SNR = 13 and 10 could be observed for two of the replicates (n = 10). However, the %RSD (97%, **Table 23** in **Appendix 7.6**) between the replicates for this concentration was large. For 25-OHC-d_6, the concentration of 3.0 nM gave an SNR > 10 for all replicates (n = 6) with a %RSD of ~ 20% (**Table 23**). Nevertheless, as 27-OHC-d_6 gave SNRs

of 13 and 10 for 4.5 nM, the cLOQ was determined to be 4.5 nM. A scatterplot of the SNRs for each replicate (n = 10) and the average SNR for 25- and 27-OHC-d_6 (4.5 nM) is shown in **Figure 50**.

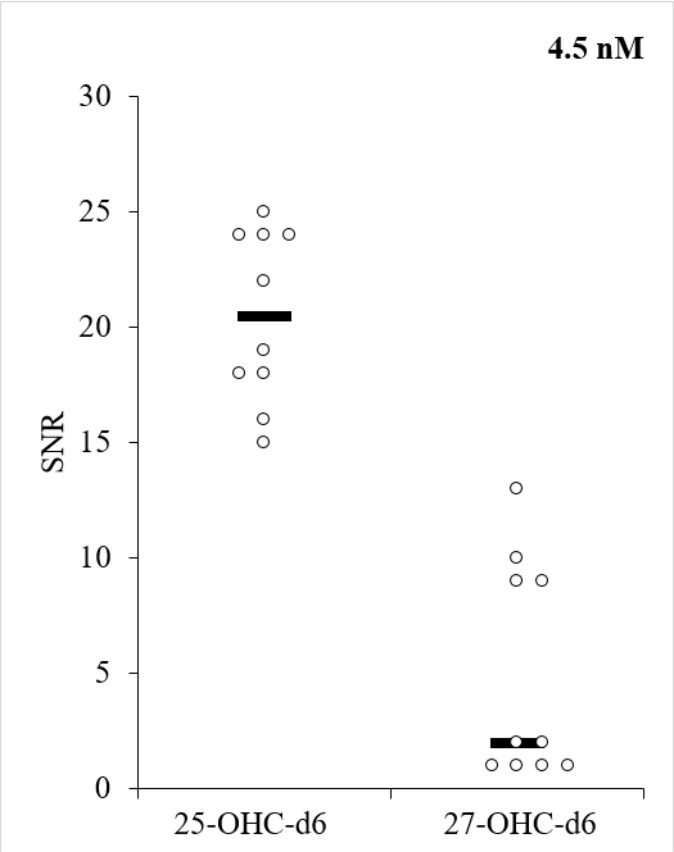

Figure 50. A scatterplot of the SNRs for 25- and 27-OHC-d_6 (4.5 nM, n = 10) in 5 µL plasma after enzymatic hydrolysis without TX-100. Separation was done with the ACE UltraCore SPH (150 x 2.1 mm ID, 2.5 µm core-shell particles) column B with a C18 SPE column, by using the AFFL-SPE system described in **Section 3.6.3**. The MP was 56/11/33/0.1 (H_2O/MeOH/ACN/FA, v/v/v/v), the flow rate was 650 µL/min at 55 °C, and the injection volume was 60 µL.

To summarize, the cLOQ was determined to be 4.5 nM with 25- and 27-OHC-d_6, albeit with a high %RSD for 27-OHC-d_6 (97%).

4.3.2 Enzymatic hydrolysis with Triton X-100 gave linearity for 25-OHC in a 0 - 75 nM range in plasma

The linearity of the method with and without the use of TX-100 was investigated with spiked plasma samples. The total oxysterol concentrations of 25-, 24S-, and 27-OHC in plasma are 29.3, 139, 376 nM (**Table 17** in **Appendix 7.2.3**), and hence the spiked concentrations were chosen hereafter. In addition, the linearity for 24S-, 25-, and 27-OHC without any hydrolysis in plasma was investigated as a reference, *i.e.* only spiked and free oxysterols present in plasma were measured.

The peak A/A_{IS} of the oxysterols after enzymatic hydrolysis with and without TX-100, as well as no hydrolysis, are presented as bar charts with corresponding standard deviations between the sample replicates in **Figure 51**. Chromatograms are shown in **Figure 60** - **Figure 62** in **Appendix 7.4**. The areas for the oxysterols and the IS after hydrolysis with and without TX-100, and no hydrolysis are shown in **Table 24 - Table 26** in **Appendix 7.6**.

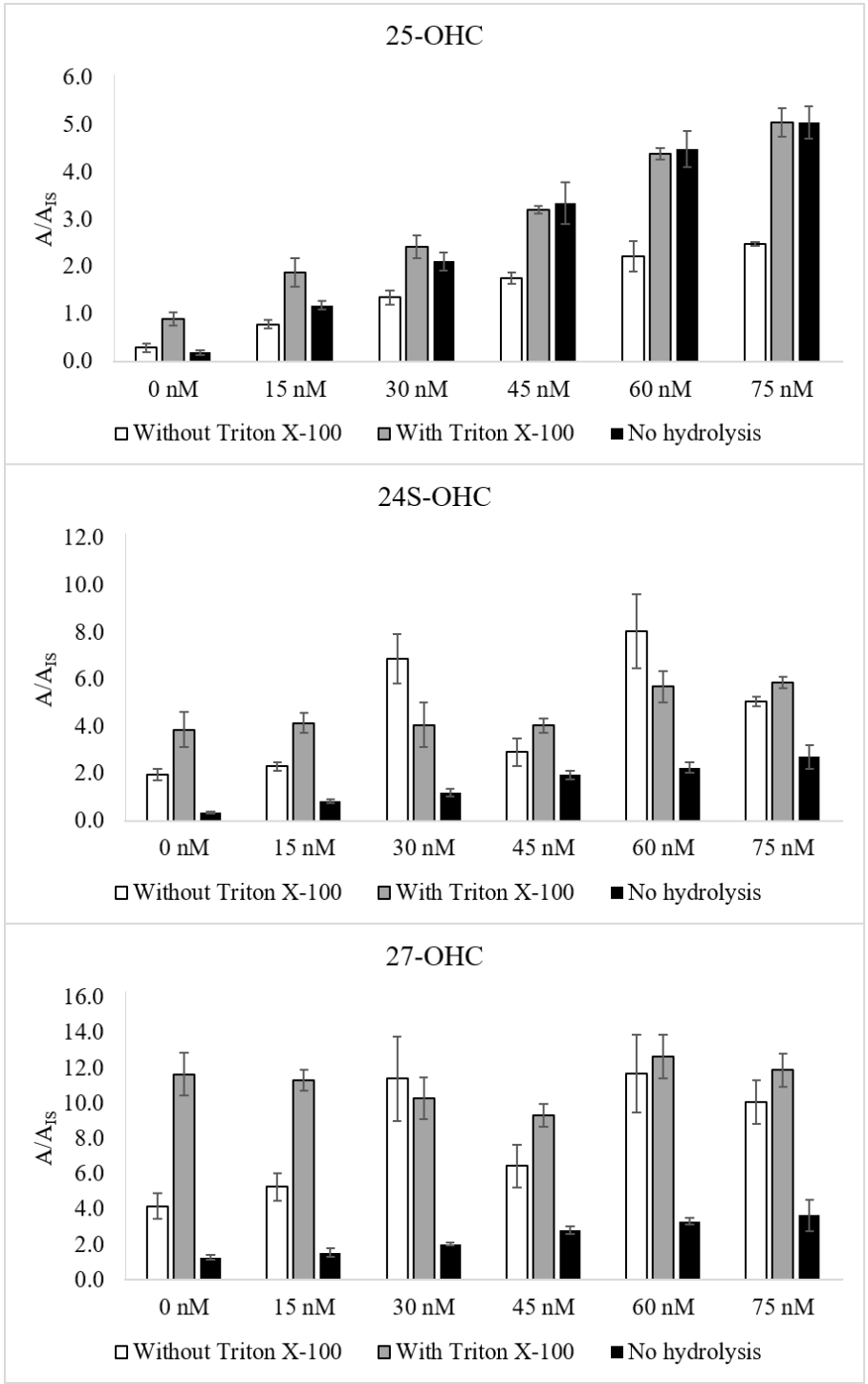

Figure 51. A/A_{IS} plotted against the spiked concentration (nM) of 24S-, 25-, and 27-OHC added to 5 µL plasma presented as bar charts with standard deviation between the sample replicates given as error bars after enzymatic hydrolysis with (n = 4) and without (n = 3) TX-100, and no hydrolysis (n = 3). Separation was done with the ACE UltraCore SPH (150 x 2.1 mm ID, 2.5 µm core-shell particles) column B with a C18 SPE column, by using the AFFL-SPE system described in **Section 3.6.3**. The MP was 56/11/33/0.1 (H_2O/MeOH/ACN/FA, v/v/v/v), the flow rate was 650 µL/min at 55 °C, and the injection volume was 60 µL.

Linearity was expectedly achieved for all the oxysterols in spiked plasma after no hydrolysis was performed. The curves for 24S- and 27-OHC are shown in **Figure 52**, and the curve for 25-OHC is shown in **Figure 53C**. For 24S- and 27-OHC, linearity was not achieved with enzymatic hydrolysis neither without TX-100 nor with TX-100 (the curves are also shown in **Figure 52**). The lack of linearity is presumably due to the high concentrations of esterified 24S- and 27-OHC in human plasma (discussed in **Section 4.2.4**), and thus the spiked concentrations were exceeded by the concentrations present in the plasma itself (and hydrolyzed by ChE).

For 25-OHC, however, a linear relationship was obtained for enzymatic hydrolysis with and without TX-100, and the curves are presented in **Figure 53**. The correlation coefficients (R^2) were satisfying (≥ 0.99), albeit smallest for hydrolysis without TX-100. The intercept for the curve in **Figure 53B** (0.90) is higher than for the curve in **Figure 53A** (0.40), meaning that higher amounts of esterified oxysterols were hydrolyzed when TX-100 was present, as previously observed.

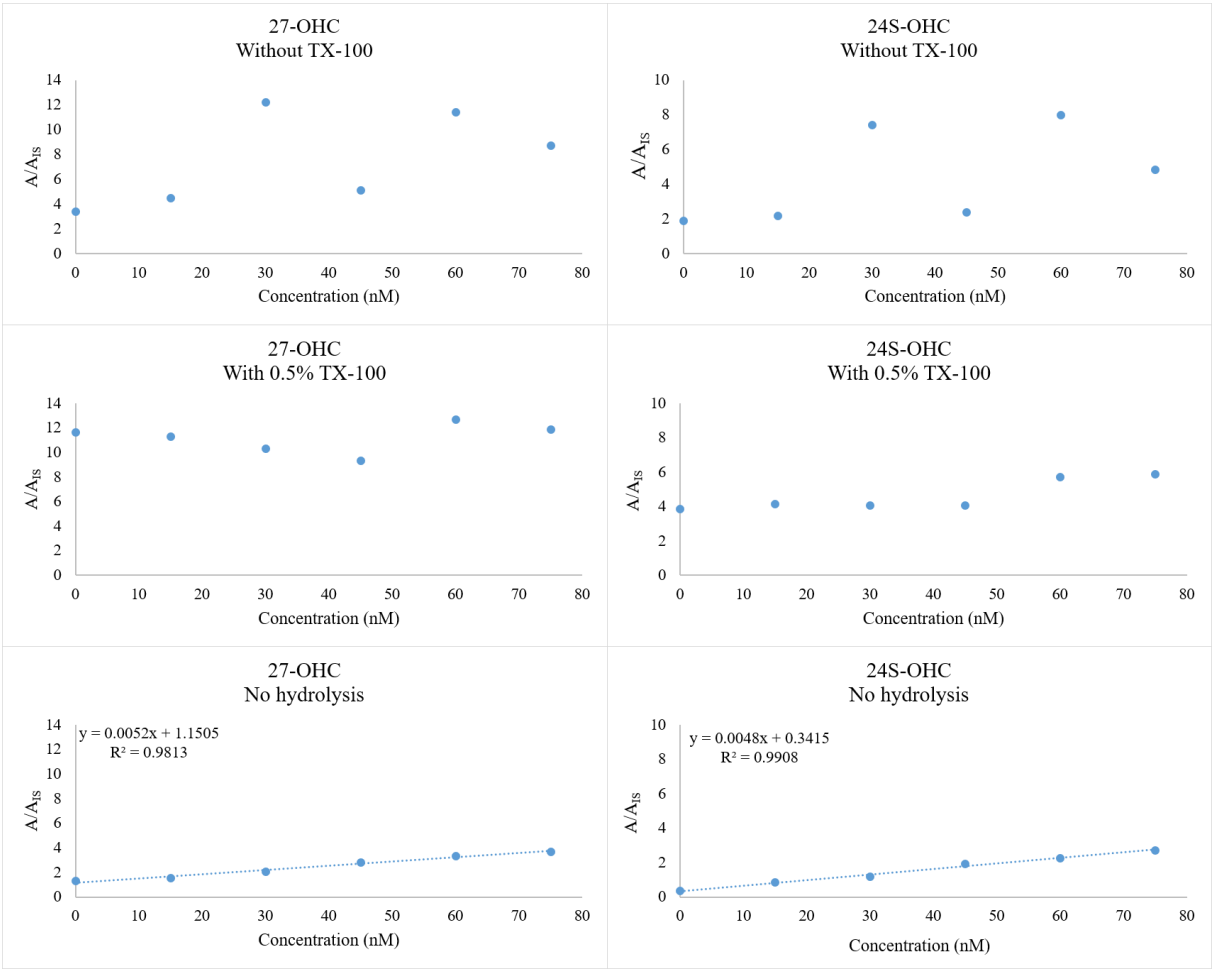

Figure 52. A/A_{IS} plotted against concentration (nM) 24S- and 27-OHC added tot 5 µL plasma after enzymatic hydrolysis with (n = 4) and without TX-100 (n = 3) and after no hydrolysis (n = 3). Separation was done with the ACE UltraCore SPH (150 x 2.1 mm ID, 2.5 µm core-shell particles) column B with a C18 SPE column, by using the AFFL-SPE system described in **Section 3.6.3**. The MP was 56/11/33/0.1 (H_2O/MeOH/ACN/FA, v/v/v/v), the flow rate was 650 µL/min at 55 °C, and the injection volume was 60 µL.

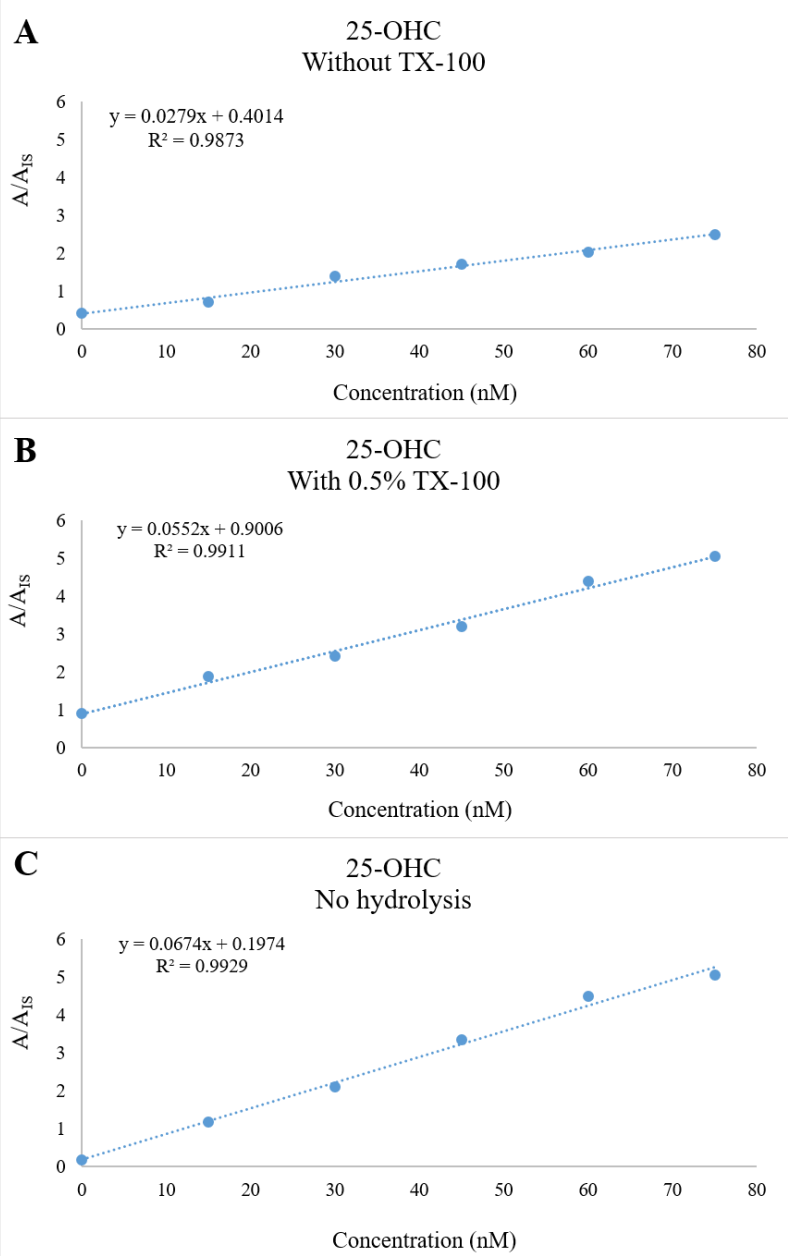

Figure 53. A/A_{IS} plotted against the concentrations (nM) of 25-OHC added to 5 µL plasma after enzymatic hydrolysis without (A, n = 3) and with (B, n = 4) TX-100, and no hydrolysis (C, n = 3). Separation was done with an ACE UltraCore SPH (150 x 2.1 mm ID, 2.5 µm core-shell particles) column with a C18 SPE column, by using the AFFL-SPE system described in **Section 3.6.3**. The MP was 56/11/33/0.1 (H_2O/MeOH/ACN/FA, v/v/v/v), the flow rate was 650 µL/min at 55 °C, and the injection volume was 60 µL.

To summarize, the linearity of enzymatic hydrolysis with and without TX-100 was investigated in a 0 – 75 nM range for 25-, 24S-, and 27-OHC. Linearity was only achieved for 25-OHC, which supports the fact that this oxysterol is the least abundant in plasma of the three. The linearity was best for hydrolysis with TX-100 (R^2 > 0.99), and hence a calibration curve containing these concentrations should be used for quantification of 25-OHC in plasma.

4.3.3 Linearity was achieved for 24S- and 27-OHC in a 0 – 75 µM range in plasma

Linearity for 24S- and 27-OHC was intended to be pursued in a 100 – 500 nM range, as the total oxysterol concentrations of 24S- and 27-OHC in plasma are reported to be 139 nM and 376 nM, respectively (**Table 17** in **Appendix 7.2.3**). However, due to a mistake during the sample preparation, the concentrations were 0 – 75 µM. Chromatograms are shown in **Figure 54** and **Figure 55**, and A/A_{IS} for the different concentrations of 25-, 24S-, and 27-OHC is plotted as bar charts with standard deviations in **Figure 56**. The peak areas for the oxysterols and the IS after hydrolysis with and without TX-100 are shown in **Table 27** and

Table 28 in **Appendix 7.6**, respectively.

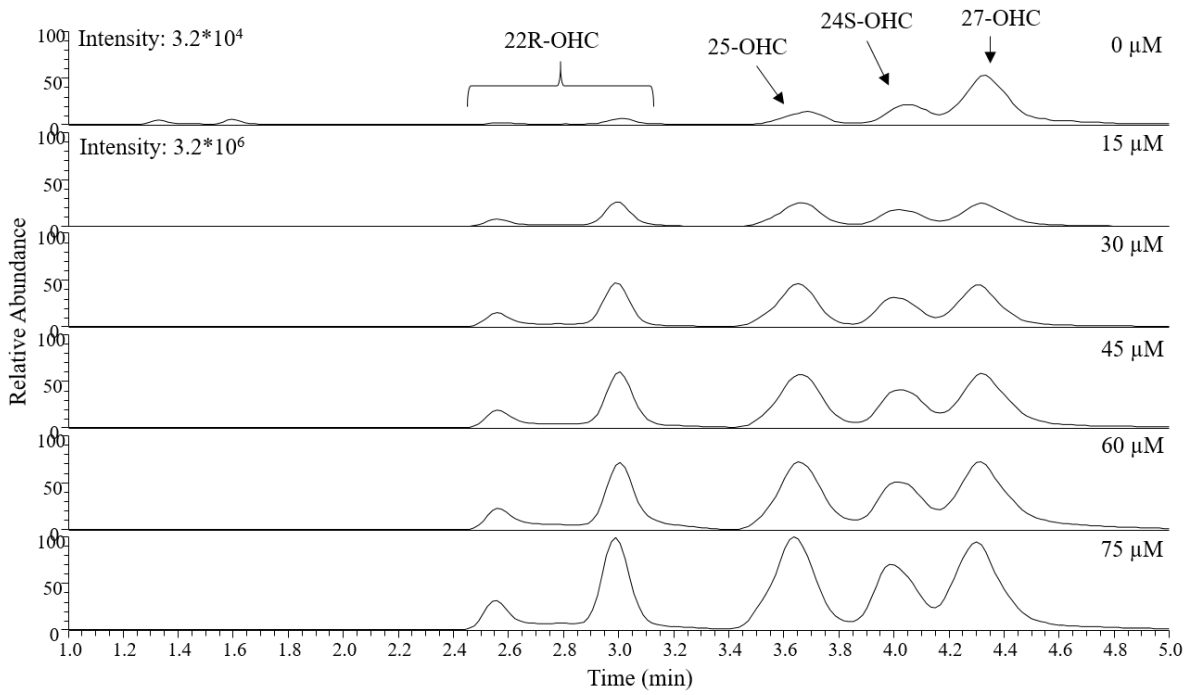

Figure 54. TIC chromatograms (7 points smoothing) of m/z 514 -> 433, 461 of 5 µL plasma spiked with 0 – 75 µM 22R-, 24S-, 25-, and 27-OHC after enzymatic hydrolysis **with TX-100**. Separation was done with the ACE UltraCore SPH (150 x 2.1 mm ID, 2.5 µm core-shell particles) column B with a C18 SPE column, by using the AFFL-SPE system described in **Section 3.6.3**. The MP was 56/11/33/0.1 (H_2O/MeOH/ACN/FA, v/v/v/v), the flow rate was 650 µL/min at 55 °C, and the injection volume was 60 µL.

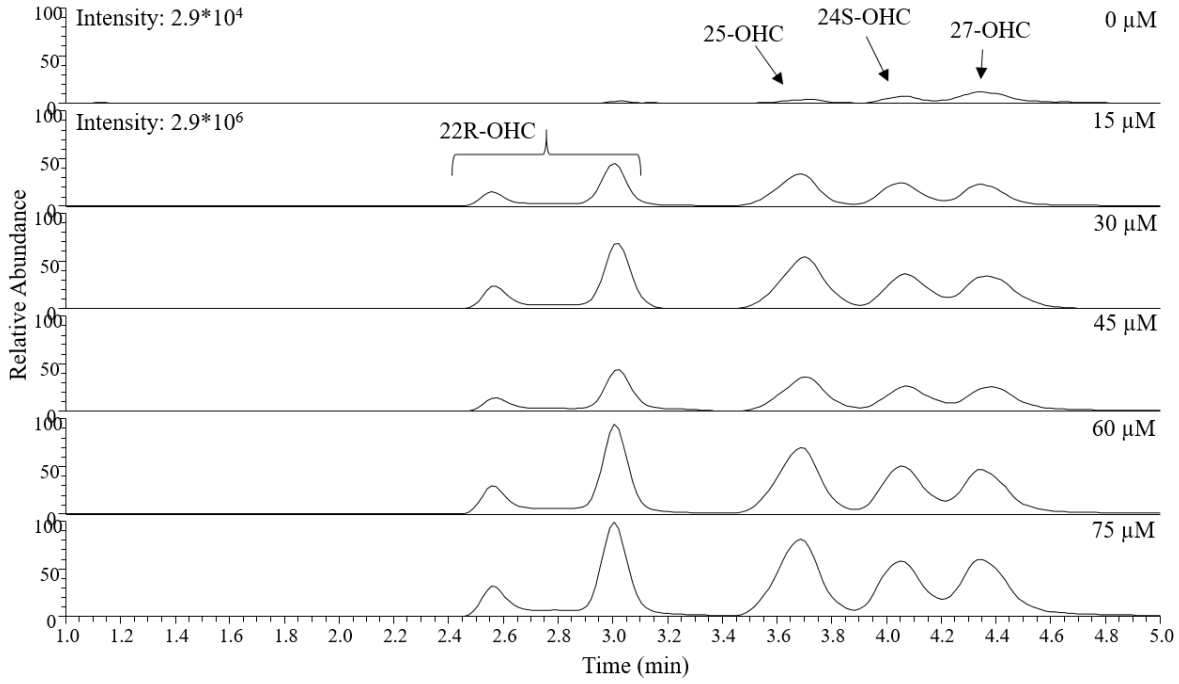

Figure 55. TIC chromatograms (7 points smoothing) of m/z 514 -> 433, 461 of 5 µL plasma spiked with 0 – 75 µM 22R-, 24S-, 25-, and 27-OHC after enzymatic hydrolysis **without TX-100**. Separation was done with the ACE UltraCore SPH (150 x 2.1 mm ID, 2.5 µm core-shell particles) column B with a C18 SPE column, by using the AFFL-SPE system described **in Section 3.6.3**. The MP was 56/11/33/0.1 (H_2O/MeOH/ACN/FA, v/v/v/v), the flow rate was 650 µL/min at 55 °C, and the injection volume was 60 µL.

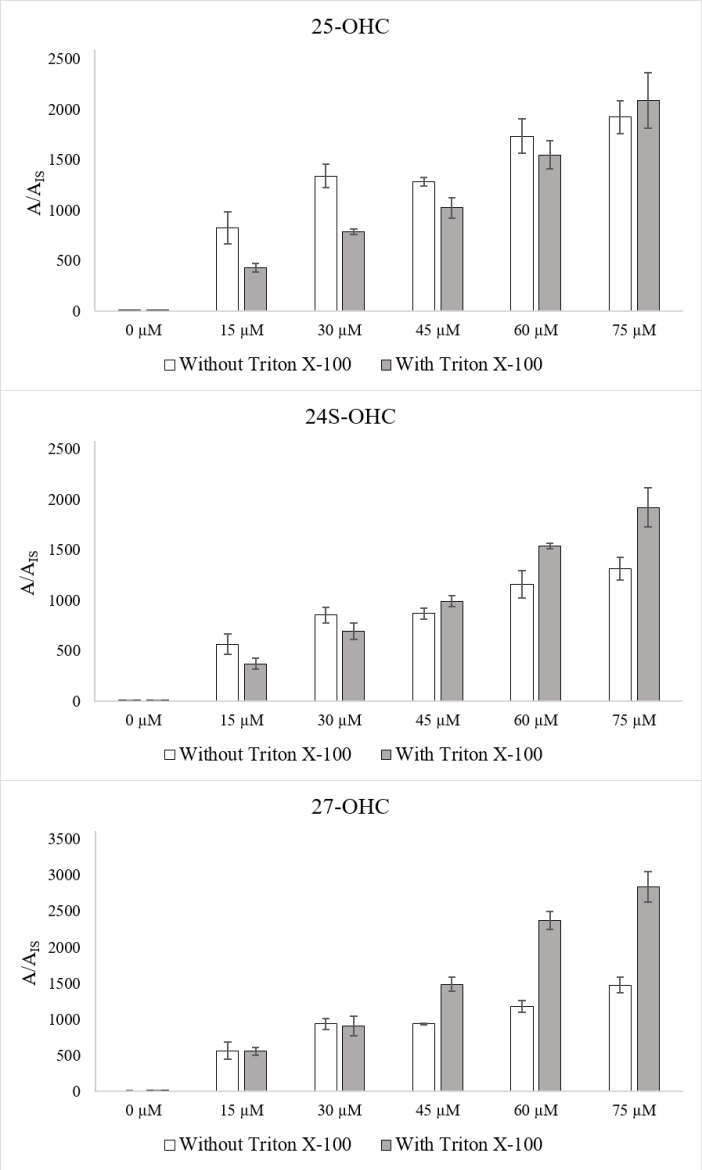

Figure 56. A/A_{IS} plotted against the spiked concentrations (µM) of 24S-, 25-, and 27-OHC added to 5 µL plasma presented as bar charts with standard deviation between sample replicates given as error bars for 24S-, 25-, and 27-OHC, after enzymatic hydrolysis with and without TX-100 (n = 3). Separation was done with the ACE UltraCore SPH (150 x 2.1 mm ID, 2.5 µm core-shell particles) column B with a C18 SPE column, by using the AFFL-SPE system described in **Section 3.6.3**. The MP was 56/11/33/0.1 (H_2O/MeOH/ACN/FA, v/v/v/v), the flow rate was 650 µL/min at 55 °C, and the injection volume was 60 µL.

The bar charts show that the peak A/A_{IS} *de facto* is larger without TX-100, for the 15 – 30 µM concentrations of 24S- and 27-OHC, and for the 15 – 60 µM concentrations of 25-OHC. These observations may indicate that ChE hydrolyzes arbitrary concentrations of oxysterols without TX-100 and that the enzyme activity is improved in the presence of the surfactant. Curves for 24S-, 25-, and 27-OHC are shown in **Figure 57**.

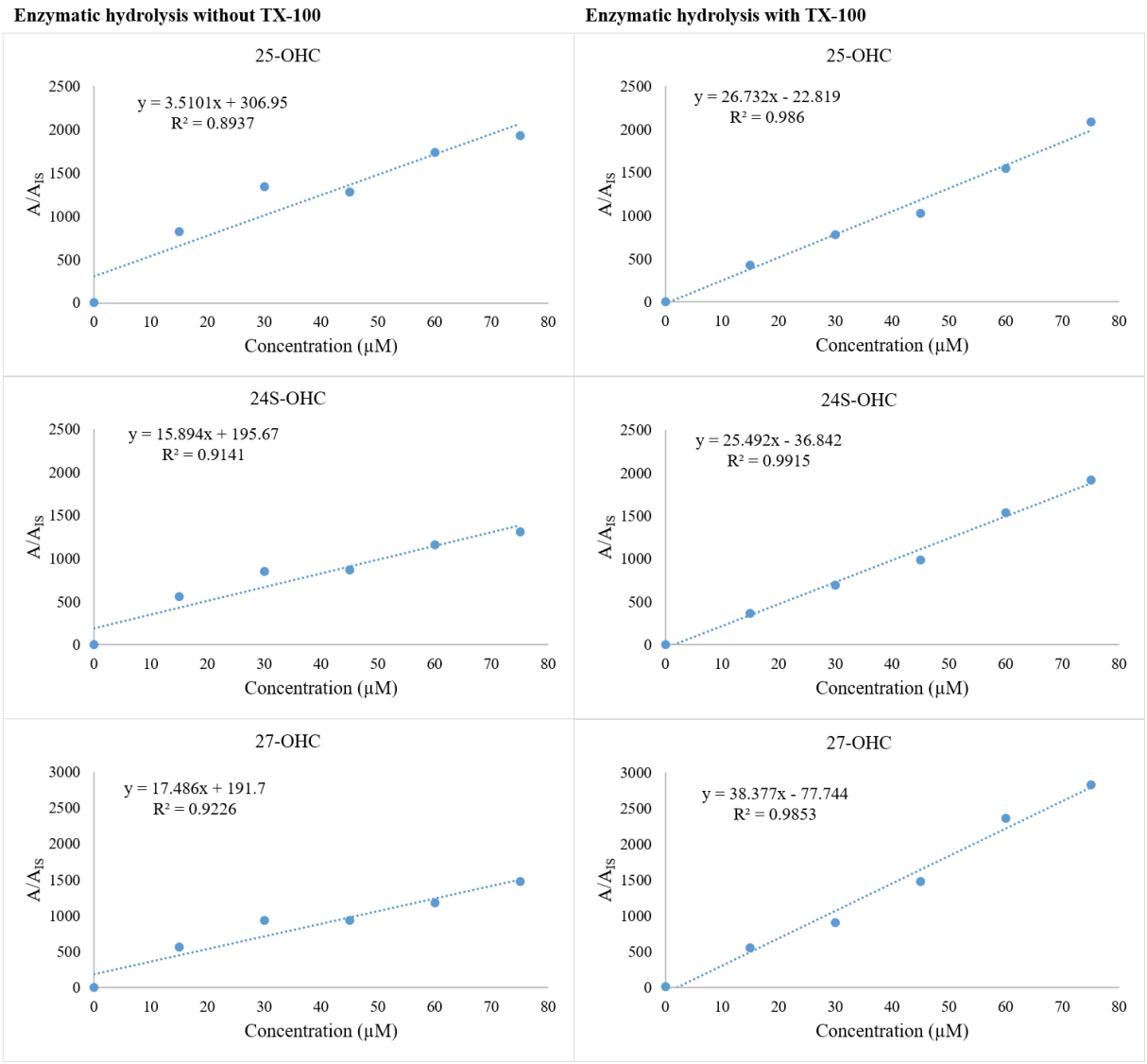

Figure 57. A/A_{IS} plotted against the concentrations (µM) of 25-, 24S-, and 27-OHC added to 5 µL plasma after enzymatic hydrolysis with and without TX-100 (n = 3). Separation was done with the ACE UltraCore SPH (150 x 2.1 mm ID, 2.5 µm core-shell particles) column B with a C18 SPE column, by using the AFFL-SPE system described in **Section 3.6.3**. The MP was 56/11/33/0.1 (H_2O/MeOH/ACN/FA, v/v/v/v), the flow rate was 650 µL/min at 55 °C, and the injection volume was 60 µL

The curves show greater linearity for 24S-, 25-, and 27-OHC when TX-100 was included in the hydrolysis. The R^2 values are 0.99 with TX-100, while they vary between 0.89 – 0.92 without TX-100. The poor linearity without TX-100 can also be observed by the fact that the intercepts for 25- and 24S-OHC are greater than for 27-OHC (307 and 196 compared to 192), which implies that 27-OHC is less abundant in plasma than 24S- and 25-OHC. The slopes of the curves with TX-100 is greater for every oxysterol compared to the ones without TX-100, which supports the observations from the bar charts.

To summarize, linearity for 24S- and 27-OHC was achieved in the 0 – 75 µM range. The linearity was poor without TX-100 (R^2 = 0.89 – 0.92), and satisfying with TX-100 (R^2 = 0.99) for every oxysterol. The ChE activity is seemingly increased in the presence of TX-100.

4.4 A personal view on sample preparation of oxysterols

As mentioned in **Section 2.4**, the methods for sample preparation of oxysterols mostly include alkaline hydrolysis followed by different derivatization methods, *i.e.* derivatization with Girard T/Girard P, derivatization into picolinyl esters, and also derivatization with N,N-dimethylglycine [78, 88, 154]. The sample amounts are often > 50 µL plasma, which may be too much, as biosamples usually are available in limited amounts. Even though Honda *et al.* developed a rapid sample preparation method (< 1 day) for LC-MS quantification of oxysterols in 5 µL serum, the method suffers from the use of alkaline solutions, organic solvents and sample handling due to the LLE step, and a risk of thermal degradation of the oxysterols [116, 118].

Enzymatic hydrolysis would as mentioned, be able to remove the aforementioned drawbacks. As far as the author of this thesis knows, only Mendiara *et al.* [96] have performed enzymatic hydrolysis on 100 µL plasma for detection with LC-MS, but the sample amount is still an issue. Hence, the sample preparation of oxysterols is complicated and a combination of the methods by Honda *et al.* [118] and Mendiara *et al.* [96] would perhaps be the most promising method (*i.e.* enzymatic hydrolysis followed by picolinyl ester derivatization on 5 µL plasma) for LC-MS detection.

Reflecting on the results of this thesis, *i.e.* higher oxysterol yields from enzymatic hydrolysis compared to alkaline hydrolysis of 5 µL human plasma, the enzymatic hydrolysis is indeed a faster and less laborious hydrolysis method that outranks alkaline hydrolysis. The sample preparation time was decreased by 2 hours, and sample handling was reduced compared to alkaline hydrolysis. Thus, the method should be of importance to the oxysterol community, which undoubtedly lacks rapid sample preparation methods with limited sample handling on small amounts of biosamples.

5 Conclusion

A partial answer to the hypothesis that a faster (< 1 day) and less laborious sample preparation method for measurements of oxysterols can be achieved with an alternative hydrolysis and/or derivatization technique, was provided. The sample preparation method became faster (by 2 hours), although not as fast as the time that was pursued.

Two alternative derivatization techniques were investigated; derivatization with picolinic acid and thiyl radical-based charge tagging with TGA. The derivatization with picolinic acid could not give detectable signals for cholesterol, but a signal was obtained for 25-OHC-dipicolinate after modifications and optimization of the procedure. However, poor yield and arbitrary formation of mono- and dipicolinate derivatives of 25-OHC in IPA were experienced, and the method was abandoned.

The thiyl radical-based charge tagging could not give detectable signals for cholesterol, 24S- or 22-OHC after direct injection MS. No modifications of the procedure resulted in detectable signals. A signal for TGA was frequently observed in the mass spectra, and it is suspected that TGA may suppress the analyte signal to some extent. The method was not pursued further, and it was decided to keep the established derivatization method with Girard T.

Enzymatic hydrolysis with ChE was investigated using human plasma and compared to the established hydrolysis with KOH (alkaline hydrolysis) for 24S-, 25-, and 27-OHC. The hydrolysis with ChE gave higher yields for all the oxysterols compared to alkaline hydrolysis if a surfactant (TX-100) was added to the hydrolysis solution. The linearity of the method was satisfying ($R^2 = 0.99$) in a 0 – 75 nM range for 25-OHC, and in a 0 – 75 µM range for 24S- and 27-OHC (which are naturally present at relatively high concentrations in human plasma). The cLOQ was determined to be 4.5 nM with 25- and 27-OHC-d_6.

To conclude, the developed sample preparation method was less laborious in terms of sample handling compared to our present method, as enzymatic hydrolysis (1 hour) of 24S-, 25-, and 27-OHC in the presence of TX-100 resulted in higher yields for the oxysterols compared to alkaline hydrolysis (3 hours). The method should be applicable to BC tumors and considered important to the oxysterol community for measurements of oxysterols in biosamples. The conclusion is illustrated in **Figure 58**.

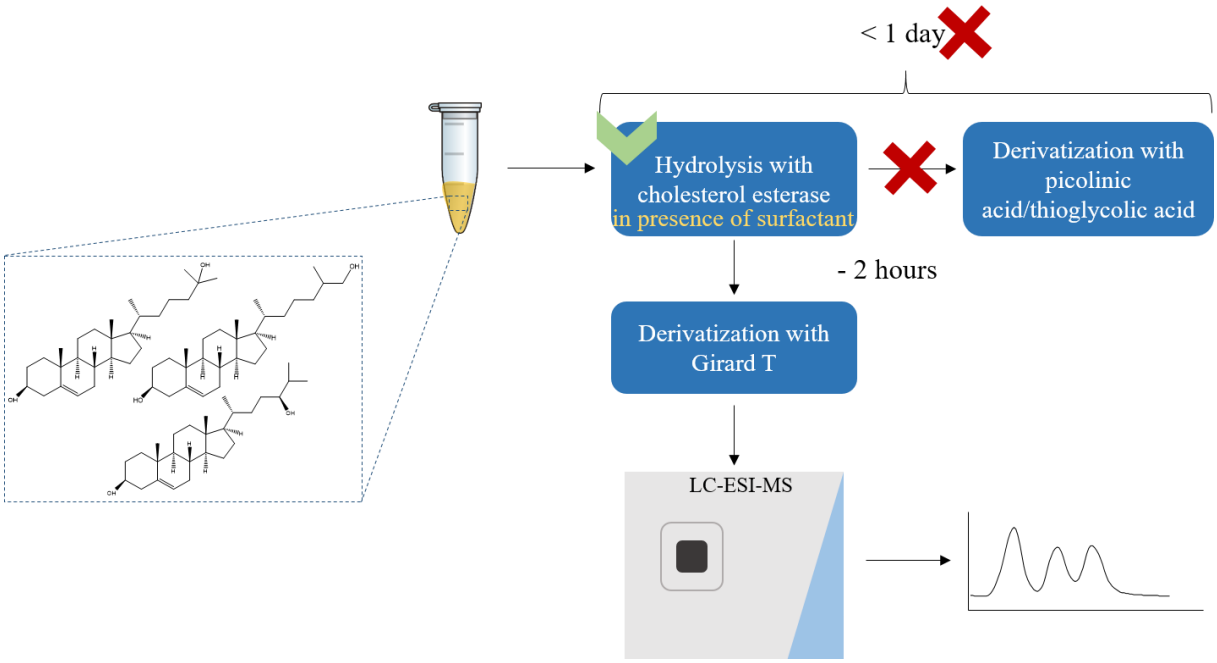

Figure 58. Illustration of the conclusion to the work in this thesis. The goal of a < 1 day sample preparation time was not achieved, although a 2 hour reduction in the sample preparation time was obtained.

5.1 Further work

The enzymatic hydrolysis with ChE should be validated in terms of inter-day and intra-day precision. The cLOQ and the concentration limit of detection (cLOD) should be investigated in presence of TX-100, and the recovery of the oxysterols should be calculated. A calibration curve in the concentration range 0 – 75 nM could be used for quantification of 25-OHC in plasma. The linearity for 24S- and 27-OHC could also be investigated for lower concentrations (nM range). Enzymatic hydrolysis could then be performed on 24S-, 25-, and 27-OHC in tumors from BC patients for a total oxysterol quantification.

A possible effect of TX-100 on the ACE UltraCore SPH column was not experienced in this thesis but should be investigated further.

6 References

[1] L. Pecorino, *Molecular Biology of Cancer: Mechanisms, targets, and therapeutics*, 4th ed., Oxford University Press, Oxford, **2016**.
[2] B. Alberts, J.H. Wilson, T. Hunt, *Molecular Biology of the Cell*, 6th ed., Garland Science, New York, **2015**.
[3] J. Ferlay, I. Soerjomataram, R. Dikshit, S. Eser, C. Mathers, M. Rebelo, D.M. Parkin, D. Forman, F. Bray, *Cancer incidence and mortality worldwide: Sources, methods and major patterns in GLOBOCAN 2012*, International Journal of Cancer 136 (**2015**) 359-386.
[4] N. Harbeck, M. Gnant, *Breast cancer*, The Lancet 389 (**2017**) 1134-1150.
[5] Cancer Registry of Norway, *Cancer in Norway 2017: Cancer incidence, mortality, survival and prevalence in Norway*. https://www.kreftregisteret.no/Generelt/Publikasjoner/Cancer-in-Norway/cancer-in-norway-2017/, **2018**).
[6] S. Masood, *Estrogen and progesterone receptors in cytology: A comprehensive review*, Diagnostic Cytopathology 8 (**1992**) 475-491.
[7] S. Mohibi, S. Mirza, H. Band, V. Band, *Mouse models of estrogen receptor-positive breast cancer*, Journal of Carcinogenesis 10 (**2011**) 35.
[8] G. Aron, D.G. Richard, *Breast cancer: Anastrozole and fulvestrant—combination to unlock efficacy*, Nature Reviews Clinical Oncology 9 (**2012**) 556-557.
[9] K.R. Bauer, M. Brown, R.D. Cress, C.A. Parise, V. Caggiano, *Descriptive analysis of estrogen receptor (ER)-negative, progesterone receptor (PR)-negative, and HER2-negative invasive breast cancer, the so-called triple-negative phenotype*, Cancer 109 (**2007**) 1721-1728.
[10] N.N. Pavlova, C.B. Thompson, *The Emerging Hallmarks of Cancer Metabolism*, Cell Metabolism 23 (**2016**) 27-47.
[11] D. Hanahan, R.A. Weinberg, *Hallmarks of Cancer: The Next Generation*, Cell 144 (**2011**) 646-674.
[12] M.G. Vander Heiden, R.J. Deberardinis, *Understanding the Intersections between Metabolism and Cancer Biology*, Cell 168 (**2017**) 657-669.
[13] O. Warburg, F. Wind, E. Negelein, *The metabolism of tumors in the body*, Journal of General Physiology 8 (**1927**) 519-530.
[14] M.G. Vander Heiden, L.C. Cantley, C.B. Thompson, *Understanding the Warburg effect: the metabolic requirements of cell proliferation*, Science 324 (**2009**) 1029-1033.
[15] A.C. Rob, W.M. Tak, *The current state of cancer metabolism*, Nature Reviews Cancer 16 (**2016**) 613-614.
[16] R. Zechner, R. Zimmermann, T.O. Eichmann, S.D. Kohlwein, G. Haemmerle, A. Lass, F. Madeo, *Fat signals - lipases and lipolysis in lipid metabolism and signaling*, Cell Metabolism 15 (**2012**) 279-291.
[17] E. Currie, A. Schulze, R. Zechner, T.C. Walther, R.V. Farese, *Cellular Fatty Acid Metabolism and Cancer*, Cell Metabolism 18 (**2013**) 153-161.
[18] J.A. Menendez, *Fine-tuning the lipogenic/lipolytic balance to optimize the metabolic requirements of cancer cell growth: Molecular mechanisms and therapeutic perspectives*, Biochimica et Biophysica Acta - Molecular and Cell Biology of Lipids 1801 (**2010**) 381-391.
[19] A.D. McNaught, A. Wilkinson, *Compendium of chemical terminology: IUPAC recommendations*, 2nd ed., Blackwell, Osney Mead, Oxford, **1997**.
[20] S. Subramaniam, E. Fahy, S. Gupta, M. Sud, R.W. Byrnes, D. Cotter, A.R. Dinasarapu, M.R. Maurya, *Bioinformatics and systems biology of the lipidome*, Chemical Reviews 111 (**2011**) 6452-6490.
[21] E. Fahy, S. Subramaniam, H.A. Brown, C.K. Glass, A.H. Merrill, R.C. Murphy, C.R.H. Raetz, D.W. Russell, Y. Seyama, W. Shaw, T. Shimizu, F. Spener, G. van Meer, M.S.

Vannieuwenhze, S.H. White, J.L. Witztum, E.A. Dennis, *A comprehensive classification system for lipids*, Journal of Lipid Research 46 (**2005**) 839-861.
[22] E. Fahy, S. Subramaniam, R.C. Murphy, M. Nishijima, C.R.H. Raetz, T. Shimizu, F. Spener, G. van Meer, M.J.O. Wakelam, E.A. Dennis, *Update of the LIPID MAPS comprehensive classification system for lipids*, Journal of Lipid Research 50 (**2009**) 9-14.
[23] E. Fahy, D. Cotter, M. Sud, S. Subramaniam, *Lipid classification, structures and tools*, Biochimica et Biophysica Acta 1811 (**2011**) 637-647.
[24] J.F. Wilson, *Long-suffering lipids gain respects*, Scientist 17 (**2003**) 34-36.
[25] M. Lagarde, A. Geloen, M. Record, D. Vance, F. Spener, *Lipidomics is emerging*, Biochimica et Biophysica Acta 1634 (**2003**) 61-61.
[26] X.L. Han, K. Yang, R.W. Gross, *Multi-dimensional mass spectrometry-based shotgun lipidomics and novel strategies for lipidomic analyses*, Mass Spectrometry Reviews 31 (**2012**) 134-178.
[27] S.J. Blanksby, T.W. Mitchell, *Advances in mass spectrometry for lipidomics*, Annual Review of Analytical Chemistry 3 (**2010**) 433-465.
[28] A. Kloudova, F.P. Guengerich, P. Soucek, *The role of oxysterols in human cancer*, Trends in Endocrinology and Metabolism 28 (**2017**) 485-496.
[29] K.E. Bloch, *Sterol structure and membrane function*, Critical Reivews in Biochemistry 14 (**1983**) 47-92.
[30] I. Elina, *Cellular cholesterol trafficking and compartmentalization*, Nature Reviews Molecular Cell Biology 9 (**2008**) 125.
[31] H.J. Armbrecht, K. Okuda, N. Wongsurawat, R.K. Nemani, M.L. Chen, M.A. Boltz, *Characterization and regulation of the vitamin D hydroxylases*, Journal of Steroid Biochemistry and Molecular Biology 43 (**1992**) 1073-1081.
[32] I. Hanukoglu, *Steroidogenic enzymes: Structure, function, and role in regulation of steroid hormone biosynthesis*, Journal of Steroid Biochemistry and Molecular Biology 43 (**1992**) 779-804.
[33] P.E. Verkade, *IUPAC-IUB revised tentative rules for nomenclature of steroids*, Journal of Biochemistry 8 (**1969**) 2227-2242.
[34] M.S. Brown, J.L. Goldstein, M.S. Brown, *A receptor-mediated pathway for cholesterol homeostasis*, Science 232 (**1986**) 34-47.
[35] L.J. Goldstein, S.M. Brown, *The LDL Receptor*, Arteriosclerosis, Thrombosis, and Vascular Biology 29 (**2009**) 431-438.
[36] V. Chajès, M. Mahon, G.M. Kostner, *Influence of LDL oxidation on the proliferation of human breast cancer cells*, Free Radical Biology and Medicine 20 (**1996**) 113-120.
[37] M. Rotheneder, G.M. Kostner, *Effects of low and high density lipoproteins on the proliferation of human breast cancer cells in vitro: differences between hormone dependent and hormone independent cell lines*, International Journal of Cancer 43 (**1989**) 875-879.
[38] A.M. Javier, L. Ruth, *Fatty acid synthase and the lipogenic phenotype in cancer pathogenesis*, Nature Reviews Cancer 7 (**2007**) 763.
[39] M.M. Hussain, *A proposed model for the assembly of chylomicrons*, Atherosclerosis 148 (**2000**) 1-15.
[40] I. Björkhem, U. Diczfalusy, *Oxysterols: friends, foes, or just fellow passengers?*, Arteriosclerosis, Thrombosis, and Vascular Biology 22 (**2002**) 734-742.
[41] C. Helmschrodt, S. Becker, J. Schröter, M. Hecht, G. Aust, J. Thiery, U. Ceglarek, *Fast LC–MS/MS analysis of free oxysterols derived from reactive oxygen species in human plasma and carotid plaque*, Clinica Chimica Acta 425 (**2013**) 3-8.
[42] A.J. Brown, W. Jessup, *Oxysterols and atherosclerosis*, Atherosclerosis 142 (**1999**) 1-28.
[43] V.M. Olkkonen, R. Hynynen, *Interactions of oxysterols with membranes and proteins*, Molecular Aspects of Medicine 30 (**2009**) 123-133.

[44] W. Kulig, H. Mikkolainen, A. Olżyńska, P. Jurkiewicz, L. Cwiklik, M. Hof, I. Vattulainen, P. Jungwirth, T. Rog, W. Kulig, *Bobbing of Oxysterols: Molecular Mechanism for Translocation of Tail-Oxidized Sterols through Biological Membranes*, The Journal of Physical Chemistry Letters 9 (**2018**) 1118-1123.
[45] S. Bergström, O. Wintersteiner, *Autoxidation of sterols in colloidal aqueous solution. The nature of the products formed from cholesterol*, Journal of Biological Chemistry 141 (**1941**) 597-610.
[46] L. Iuliano, *Pathways of cholesterol oxidation via non-enzymatic mechanisms*, Chemistry and Physics of Lipids 164 (**2011**) 457-468.
[47] R.C. Murphy, K.M. Johnson, *Cholesterol, reactive oxygen species, and the formation of biologically active mediators*, The Journal of Biological Chemistry 283 (**2008**) 15521-15525.
[48] J. Li, E. Daly, E. Campioli, M. Wabitsch, V. Papadopoulos, *De novo synthesis of steroids and oxysterols in adipocytes*, Journal of Biological Chemistry 289 (**2014**) 747-764.
[49] A.V. Yantsevich, Y.V. Dichenko, F. MacKenzie, D.V. Mukha, A.V. Baranovsky, A.A. Gilep, S.A. Usanov, N.V. Strushkevich, *Human steroid and oxysterol 7α-hydroxylase CYP7B1: substrate specificity, azole binding and misfolding of clinically relevant mutants*, The FEBS Journal 281(6) (**2014**) 1700-1713.
[50] W.J. Griffiths, J. Abdel-Khalik, P.J. Crick, E. Yutuc, Y. Wang, *New methods for analysis of oxysterols and related compounds by LC–MS*, Journal of Steroid Biochemistry and Molecular Biology 162 (**2016**) 4-26.
[51] N.B. Javitt, *25R,26-Hydroxycholesterol revisited: synthesis, metabolism, and biologic roles*, Journal of Lipid Research 43 (**2002**) 665-670.
[52] K. Karu, J. Turton, Y. Wang, W.J. Griffiths, *Nano-liquid chromatography–tandem mass spectrometry analysis of oxysterols in brain: monitoring of cholesterol autoxidation*, Chemistry and Physics of Lipids 164 (**2011**) 411-424.
[53] D.W. Russell, *Oxysterol biosynthetic enzymes*, Biochimica et Biophysica Acta 1529 (**2000**) 126-135.
[54] F. Guardiola, R. Codony, P.B. Addis, M. Rafecas, J. Boatella, *Biological effects of oxysterols: Current status*, Food and Chemical Toxicology 34 (**1996**) 193-211.
[55] D.Q.H. Wang, N.H. Afdhal, *Good cholesterol, bad cholesterol: Role of oxysterols in biliary tract diseases*, Gastroenterology 121 (**2001**) 216-218.
[56] W. Kulig, L. Cwiklik, P. Jurkiewicz, T. Rog, I. Vattulainen, *Cholesterol oxidation products and their biological importance*, Chemistry and Physics of Lipids 199 (**2016**) 144-160.
[57] G.J. Schroepfer, *Oxysterols: modulators of cholesterol metabolism and other processes*, Physiological reviews 80 (**2000**) 361-554.
[58] N. Sigrid, K.M. Laurel, K. Kathiresan, R. Jayan, H.S. Paul, F.C. Douglas, R. Rajat, *Oxysterols are allosteric activators of the oncoprotein Smoothened*, Nature Chemical Biology 8 (**2012**) 211.
[59] A.J. Bethany, J.W. Patricia, D. Thota Rama, J.R. Falck, J.M. David, *An oxysterol signalling pathway mediated by the nuclear receptor LXRα*, Nature 383 (**1996**) 728.
[60] U. Michihisa, D. Hideharu, K.G. Andrew, S.Y. Ivan, L.C. Carolyn, B.J. Norman, S.K. Kenneth, W.S. Philip, J.M. David, *27-Hydroxycholesterol is an endogenous SERM that inhibits the cardiovascular effects of estrogen*, Nature Medicine 13 (**2007**) 1185.
[61] C.D. Dusell, M. Umetani, P.W. Shaul, D.J. Mangelsdorf, D.P. McDonnell, *27-Hydroxycholesterol Is an Endogenous Selective Estrogen Receptor Modulator*, Molecular Endocrinology 22 (**2008**) 65-77.
[62] M.W. Rooney, S. Yachnin, O. Kucuk, L.J. Lis, J.W. Kauffman, *Oxygenated cholesterols synergistically immobilize acyl chains and enhance protein helical structure in human erythrocyte membranes*, Biochimica et Biophysica Acta 820 (**1985**) 33-39.

[63] O. Kucuk, J. Stoner-Picking, S. Yachnin, L.I. Gordon, R.M. Williams, L.J. Lis, M.P. Westerman, *Inhibition of NK cell-mediated cytotoxicity by oxysterols*, Cellular Immunology 139 (**1992**) 541-549.
[64] C. Moog, J.C. Deloulme, J. Baudier, M.O. Revel, P. Bischoff, H. Hietter, B. Luu, *Membrane-related oxysterol function: preliminary results on the modification of protein kinase C activity and substrate phosphorylation by 7ß,25-dihydroxycholesterol*, Biochimie 73 (**1991**) 1321-1326.
[65] M.J. Duran, S.V. Pierre, P. Lesnik, G. Pieroni, M. Bourdeaux, F. Dignat-Georges, J. Sampol, J.M. Maixent, *7-ketocholesterol inhibits Na,K-ATPase activity by decreasing expression of its α1-subunit and membrane fluidity in human endothelial cells*, Cellular and Molecular Biology 56 (**2010**) 1434.
[66] E.R. Nelson, S.E. Wardell, J.S. Jasper, S. Park, S. Suchindran, M.K. Howe, N.J. Carver, R.V. Pillai, P.M. Sullivan, V. Sondhi, M. Umetani, J. Geradts, D.P. McDonnell, *27-Hydroxycholesterol links hypercholesterolemia and breast cancer pathophysiology*, Science 342 (**2013**) 1094.
[67] Q. Wu, T. Ishikawa, R. Sirianni, H. Tang, J.G. McDonald, I.S. Yuhanna, B. Thompson, L. Girard, C. Mineo, R.A. Brekken, M. Umetani, D.M. Euhus, Y. Xie, P.W. Shaul, *27-Hydroxycholesterol Promotes Cell-Autonomous, ER-Positive Breast Cancer Growth*, Cell Reports 5 (**2013**) 637-645.
[68] N.B. Javitt, *Breast cancer and (25R)-26-hydroxycholesterol*, Steroids 104 (**2015**) 61-64.
[69] C.E. Connor, J.D. Norris, G. Broadwater, T.M. Willson, M.M. Gottardis, M.W. Dewhirst, D.P. McDonnell, C.E. Connor, *Circumventing tamoxifen resistance in breast cancers using antiestrogens that induce unique conformational changes in the estrogen receptor*, Cancer Research 61 (**2001**) 2917-2922.
[70] H. De Boussac, A. Alioui, E. Viennois, J. Dufour, A. Trousson, A. Vega, L. Guy, D.H. Volle, J.-M.A. Lobaccaro, S. Baron, *Oxysterol receptors and their therapeutic applications in cancer conditions*, Expert Opinion on Therapeutic Targets 17 (**2013**) 1029-1038.
[71] F. Bovenga, C. Sabbà, A. Moschetta, *Uncoupling nuclear receptor LXR and cholesterol metabolism in cancer*, Cell Metabolism 21 (**2015**) 517-526.
[72] B. Janowski, P. Willy, T. Devi, J. Falck, D. Mangelsdorf, *An oxysterol signalling pathway mediated by the nuclear receptor LXR alpha*, Nature 383 (**1996**) 728-31.
[73] J.M. Lehmann, S.A. Kliewer, L.B. Moore, T.A. Smith-Oliver, B.B. Oliver, J.L. Su, S.S. Sundseth, D.A. Winegar, D.E. Blanchard, T.A. Spencer, T.M. Willson, *Activation of the nuclear receptor LXR by oxysterols defines a new hormone response pathway*, The Journal of Biological Chemistry 272 (**1997**) 3137-3140.
[74] N. Zelcer, C. Hong, R. Boyadjian, P. Tontonoz, *LXR regulates cholesterol uptake through idol-dependent ubiquitination of the LDL receptor*, Science 325 (**2009**) 100.
[75] L. Raccosta, R. Fontana, G. Corna, D. Maggioni, M. Moresco, V. Russo, *Cholesterol metabolites and tumor microenvironment: the road towards clinical translation*, Cancer Immunology, Immunotherapy 65 (**2016**) 111-117.
[76] N. Rohini, I. Vignesh, K. Prachi, B. Mary Lou, B. Darlene, Z. Robert, W.-G. Bianca, C.R. Todd, R. Murali, W.B. Richard, *Simultaneous determination of oxysterols, cholesterol and 25-hydroxy-vitamin D3 in human plasma by LC-UV-MS*, PLoS ONE 10 (**2015**) 0123771.
[77] S. Dzeletovic, O. Breuer, E. Lund, U. Diczfalusy, *Determination of cholesterol oxidation products in human plasma by isotope dilution-mass spectrometry*, Analytical Biochemistry 225 (**1995**) 73-80.
[78] W.J. Griffiths, P.J. Crick, Y. Wang, *Methods for oxysterol analysis: past, present and future*, Biochemical Pharmacology 86 (**2013**) 3-14.

[79] B. Janoszka, K. Tyrpien, T. Wielkoszynski, C. Dobosz, D. Bodzek, P. Bodzek, A. Olejek, *Determination of selected oxycholesterols in human blood plasma by means of thin-layer chromatography with densitometry*, Chemical Analysis 46 (**2001**) 11-21.
[80] I. Burkard, K.M. Rentsch, A. Von Eckardstein, *Determination of 24S- and 27-hydroxycholesterol in plasma by high-performance liquid chromatography-mass spectrometry*, Journal of Lipid Research 45 (**2004**) 776.
[81] A.E. Debarber, D. Lütjohann, L. Merkens, R.D. Steiner, Liquid chromatography-tandem mass spectrometry determination of plasma 24S-hydroxycholesterol with chromatographic separation of 25-hydroxycholesterol, Analytical biochemistry 381(1) (**2008**) 151.
[82] J.G. McDonald, B.M. Thompson, E.C. McCrum, D.W. Russell, *Extraction and analysis of sterols in biological matrices by high performance liquid chromatography electrospray ionization mass spectrometry*, Methods in Enzymology 432 (**2007**) 145-170.
[83] A. Lövgren-Sandblom, M. Heverin, H. Larsson, E. Lundström, J. Wahren, U. Diczfalusy, I. Björkhem, *Novel LC–MS/MS method for assay of 7α-hydroxy-4-cholesten-3-one in human plasma: Evidence for a significant extrahepatic metabolism*, Journal of Chromatography B 856 (**2007**) 15-19.
[84] M. Axelson, B. Mörk, J. Sjövall, *Occurrence of 3 beta-hydroxy-5-cholestenoic acid, 3 beta,7 alpha-dihydroxy-5-cholestenoic acid, and 7 alpha-hydroxy-3-oxo-4-cholestenoic acid as normal constituents in human blood*, Journal of Lipid Research 29 (**1988**) 629-641.
[85] V. Leoni, D. Lutjohann, T. Masterman, *Levels of 7-oxocholesterol in cerebrospinal fluid are more than one thousand times lower than reported in multiple sclerosis*, Journal of Lipid Research 46 (**2005**) 191-195.
[86] A. Szterk, L. Pakuła, *New method to determine free sterols/oxysterols in food matrices using gas chromatography and ion trap mass spectrometry (GC–IT-MS)*, Talanta 152 (**2016**) 54-75.
[87] R. Soules, E. Noguer, L. Iuliano, C. Zerbinati, J. Leignadier, A. Rives, P. de Medina, S. Silvente-Poirot, M. Poirot, *Improvement of 5,6α-epoxycholesterol, 5,6β-epoxycholesterol, cholestane-3β,5α,6β-triol and 6-oxo-cholestan-3β,5α-diol recovery for quantification by GC/MS*, Chemistry and Physics of Lipids 207 (**2017**) 92.
[88] W.J. Griffiths, Y. Wang, *Analysis of oxysterol metabolomes*, Biochimica et Biophysica Acta 1811 (**2011**) 784-799.
[89] J.G. McDonald, D.D. Smith, A.R. Stiles, D.W. Russell, *A comprehensive method for extraction and quantitative analysis of sterols and secosteroids from human plasma*, Journal of Lipid Research 53 (**2012**) 1399-1409.
[90] O. Quehenberger, A.M. Armando, A.H. Brown, S.B. Milne, D.S. Myers, A.H. Merrill, S. Bandyopadhyay, K.N. Jones, S. Kelly, R.L. Shaner, C.M. Sullards, E. Wang, R.C. Murphy, R.M. Barkley, T.J. Leiker, C.R.H. Raetz, Z. Guan, G.M. Laird, D.A. Six, D.W. Russell, J.G. McDonald, S. Subramaniam, E. Fahy, E.A. Dennis, *Lipidomics reveals a remarkable diversity of lipids in human plasma*, Journal of Lipid Research 51 (**2010**) 3299-3305.
[91] D. Lütjohann, O. Breuer, G. Ahlborg, I. Nennesmo, A. Sidén, U. Diczfalusy, I. Björkhem, *Cholesterol homeostasis in human brain: evidence for an age-dependent flux of 24S-hydroxycholesterol from the brain into the circulation*, Proceedings of the National Academy of Sciences of the United States of America 93 (**1996**) 9799-9804.
[92] H. Sugimoto, M. Kakehi, F. Jinno, Y. Satomi, H. Kamiguchi, *Method development for the determination of 24S-hydroxycholesterol in human plasma without derivatization by high-performance liquid chromatography with tandem mass spectrometry in atmospheric pressure chemical ionization mode*, Journal of Separation Science 38 (**2015**) 3516-3524.
[93] P.W. Park, F. Guardiola, S.H. Park, P.B. Addis, *Kinetic evaluation of 3β-hydroxycholest-5-en-7-one (7-ketocholesterol) stability during saponification*, Journal of the American Oil Chemists' Society 73 (**1996**) 623-629.

[94] T.P. Busch, A.J. King, *Artifact generation and monitoring in analysis of cholesterol oxide products*, Analytical Biochemistry 388 (**2009**) 1-14.
[95] N.C. van de Merbel, K.J. Bronsema, M.W.J. van Hout, R. Nilsson, H. Sillén, *A validated liquid chromatography–tandem mass spectrometry method for the quantitative determination of 4β-hydroxycholesterol in human plasma*, Journal of Pharmaceutical and Biomedical Analysis 55 (**2011**) 1089-1095.
[96] I. Mendiara, C. Domeño, C. Nerín, A.M. Geurts, J. Osada, R. Martínez-Beamonte, *Determination of total plasma oxysterols by enzymatic hydrolysis, solid phase extraction and liquid chromatography coupled to mass-spectrometry*, Journal of Pharmaceutical and Biomedical Analysis 150 (**2018**) 396-405.
[97] M. Cygler, J.D. Schrag, J.L. Sussman, M. Harel, I. Silman, M.K. Gentry, B.P. Doctor, *Relationship between sequence conservation and three-dimensional structure in a large family of esterases, lipases, and related proteins*, Protein Science 2 (**1993**) 366-382.
[98] D.Y. Hui, *Molecular biology of enzymes involved with cholesterol ester hydrolysis in mammalian tissues*, Biochimica et Biophysica Acta 1303 (**1996**) 1-14.
[99] C.-S. Wang, J.A. Hartsuck, *Bile salt-activated lipase. A multiple function lipolytic enzyme*, Biochimica et Biophysica Acta 1166 (**1993**) 1-19.
[100] O. Hernell, T. Olivecrona, *Human milk lipases. I. Serum-stimulated lipase*, Journal of Lipid Research 15 (**1974**) 367-374.
[101] F. Winkler, A. d'Arcy, W. Hunziker, *Structure of human pancreatic lipase*, Nature 343 (**1990**) 771.
[102] L. Brady, A.M. Brzozowski, Z.S. Derewenda, E. Dodson, G. Dodson, S. Tolley, J.P. Turkenburg, L. Christiansen, B. Huge-Jensen, L. Norskov, *A serine protease triad forms the catalytic centre of a triacylglycerol lipase*, Nature 343 (**1990**) 767.
[103] X. Wang, C.-S. Wang, J. Tang, F. Dyda, X.C. Zhang, *The crystal structure of bovine bile salt activated lipase: insights into the bile salt activation mechanism*, Structure (London, England : 1993) 5 (**1997**) 1209-1218.
[104] W.L. DeLano, *Pymol: An open-source molecular graphics tool*, Newsletter On Protein Crystallography 40 (**2002**) 82-92.
[105] M.J. Rosen, J.T. Kunjappu, *Surfactants and Interfacial Phenomena*, John Wiley & Sons, Hoboken, New Jersey, USA, **2012**.
[106] R.M. Garavito, S. Ferguson-Miller, R.M. Garavito, *Detergents as tools in membrane biochemistry*, The Journal of Biological Chemistry 276 (**2001**) 32403-32406.
[107] D. Lichtenberg, R.J. Robson, E.A. Dennis, *Solubilization of phospholipids by detergents structural and kinetic aspects*, Biochimica et Biophysica Acta 737 (**1983**) 285-304.
[108] K. Edwards, M. Almgren, *Solubilization of unilamellar phospholipid bilayers by nonionic surfactants*, Colloid and Polymer Science 272 (**1994**) 721-730.
[109] H. Roberg-Larsen, C. Vesterdal, S.R. Wilson, E. Lundanes, *Underivatized oxysterols and nanoLC–ESI-MS: A mismatch*, Steroids 99 (**2015**) 125-130.
[110] H. Roberg-Larsen, K. Lund, T. Vehus, N. Solberg, C. Vesterdal, D. Misaghian, P.A. Olsen, S. Krauss, S.R. Wilson, E. Lundanes, *Highly automated nano-LC/MS-based approach for thousand cell-scale quantification of side chain-hydroxylated oxysterols*, Journal of Lipid Research 55 (**2014**) 1531-1536.
[111] A.E. DeBarber, Y. Sandlers, A.S. Pappu, L.S. Merkens, P.B. Duell, S.R. Lear, S.K. Erickson, R.D. Steiner, *Profiling sterols in cerebrotendinous xanthomatosis: Utility of Girard derivatization and high resolution exact mass LC–ESI-MSn analysis*, Journal of Chromatography B 879 (**2011**) 1384-1392.
[112] O. Lavrynenko, R. Nedielkov, H.M. Möller, A. Shevchenko, *Girard derivatization for LC-MS/MS profiling of endogenous ecdysteroids in Drosophila*, Journal of Lipid Research 54 (**2013**) 2265-2272.

[113] A. Meljon, S. Theofilopoulos, C.H. Shackleton, G.L. Watson, N.B. Javitt, H.-J. Knölker, R. Saini, E. Arenas, Y. Wang, W.J. Griffiths, *Analysis of bioactive oxysterols in newborn mouse brain by LC/MS*, Journal of Lipid Research 53 (**2012**) 2469-2483.
[114] J.A.T.L. MacLachlan, A.T.L. Wotherspoon, R.O. Ansell, C.J.W. Brooks, *Cholesterol oxidase: sources, physical properties and analytical applications*, Journal of Steroid Biochemistry and Molecular Biology 72 (**2000**) 169-195.
[115] M. Gregus, H. Roberg-Larsen, E. Lundanes, F. Foret, P. Kuban, S.R. Wilson, *Non-aqueous capillary electrophoretic separation of cholesterol and 25-hydroxycholesterol after derivatization with Girard P reagent*, Chemistry and Physics of Lipids 207 (**2017**) 87-91.
[116] A. Honda, T. Miyazaki, K. Yamashita, M. Numazawa, T. Hara, M. Shirai, T. Ikegami, Y. Matsuzaki, G. Xu, *Highly sensitive quantification of key regulatory oxysterols in biological samples by LC-ESI-MS/MS*, Journal of Lipid Research 50 (**2009**) 350-357.
[117] J. Marcos, O.J. Pozo, J. Marcos, *Derivatization of steroids in biological samples for GC-MS and LC-MS analyses*, Bioanalysis 7 (**2015**) 2515-2536.
[118] A. Honda, K. Yamashita, M. Numazawa, H. Miyazaki, M. Shirai, T. Hara, T. Ikegami, Y. Matsuzaki, G. Xu, *Highly sensitive analysis of sterol profiles in human serum by LC-ESI-MS/MS*, Journal of Lipid Research 49 (**2008**) 2063-2073.
[119] A. Honda, T. Miyazaki, T. Ikegami, J. Iwamoto, K. Yamashita, M. Numazawa, Y. Matsuzaki, *Highly sensitive and specific analysis of sterol profiles in biological samples by HPLC–ESI–MS/MS*, Journal of Steroid Biochemistry and Molecular Biology 121 (**2010**) 556-564.
[120] S. Adhikari, Y. Xia, *Thiyl Radical-Based Charge Tagging Enables Sterol Quantitation via Mass Spectrometry*, Analytical Chemistry 89 (**2017**) 12631-12635.
[121] H.C. Kolb, M.G. Finn, K.B. Sharpless, *Click Chemistry: Diverse Chemical Function from a Few Good Reactions*, Angewandte Chemie 40 (**2001**) 2004-2021.
[122] M.H. Amad, N.B. Cech, G.S. Jackson, C.G. Enke, *Importance of gas-phase proton affinities in determining the electrospray ionization response for analytes and solvents*, Journal of Mass Spectrometry 35 (**2000**) 784-789.
[123] K.L. Vikse, J. Scott McIndoe, *Ionization methods for the mass spectrometry of organometallic compounds*, Journal of Mass Spectrometry 53 (**2018**) 1026-1034.
[124] E. Lundanes, L. Reubsaet, T. Greibrokk, *Chromatography: basic principles, sample preparations and related methods*, Wiley-VCH, Weinheim, Germany, **2014**.
[125] A.P. Bruins, *Mechanistic aspects of electrospray ionization*, Journal of Chromatography A 794 (**1998**) 345-357.
[126] G. Taylor, *Disintegration of Water Drops in an Electric Field*, Proceedings of the Royal Society of London 280 (**1964**) 383-397.
[127] P. Kebarle, L. Tang, *From ions in solution to ions in the gas phase: the mechanism of electrospray mass spectrometry*, Analytical Chemistry 65 (**1993**) 972A.
[128] C. Dass, *Fundamentals of contemporary mass spectrometry*, Wiley Interscience, Hoboken, New Jersey, USA, **2007**.
[129] J. Greaves, J. Roboz, *Mass spectrometry for the novice*, CRC Press, Boca Raton, Florida, USA, **2014**.
[130] D. Argoti, *Liquid chromatography-mass spectrometry for detection and characterization of DNA biomarkers and reactive metabolites*, Northeastern University, Boston, USA, **2008**.
[131] K.K. Murray, *The term "multiple reaction monitoring" is recommended*, Rapid Communications in Mass Spectrometry 29 (**2015**) 1926-1928.
[132] R.A. Yost, C.G. Enke, R.A. Yost, *Triple quadrupole mass spectrometry for direct mixture analysis and structure elucidation*, Analytical Chemistry 51 (**1979**) 1251-1264.

[133] L. Anderson, C.L. Hunter, L. Anderson, *Quantitative mass spectrometric multiple reaction monitoring assays for major plasma proteins*, Molecular and Cellular Proteomics 5 (**2006**) 573-588.
[134] M. Martin, G.A. Guiochon, *Effects of high pressure in liquid chromatography*, Journal of Chromatography A 1090 (**2005**) 16-38.
[135] Y. Xiang, Y. Liu, M.L. Lee, *Ultrahigh pressure liquid chromatography using elevated temperature*, Journal of Chromatography A 1104 (**2006**) 198-202.
[136] G.A. Guiochon, F. Gritti, *Shell particles, trials, tribulations and triumphs*, Journal of Chromatography A 1218 (**2011**) 1915-1938.
[137] N. Wu, A.M. Clausen, *Fundamental and practical aspects of ultrahigh pressure liquid chromatography for fast separations*, Journal of Separation Science 30 (**2007**) 1167-1182.
[138] J.J. van Deemter, F.J. Zuiderweg, A. Klinkenberg, *Longitudinal diffusion and resistance to mass transfer as causes of nonideality in chromatography*, Chemical Engineering Science 50 (**1995**) 3867-3867.
[139] R. Hayes, A. Ahmed, T. Edge, H. Zhang, *Core-shell particles: preparation, fundamentals and applications in HPLC*, Journal of Chromatography A 1357 (**2014**) 36-52.
[140] A.E. Ibrahim, H. Hashem, M. Elhenawee, H. Saleh, *Comparison between core–shell and totally porous particle stationary phases for fast and green LC determination of five hepatitis-C antiviral drugs*, Journal of Separation Science 41 (**2018**) 1734-1742.
[141] F. Gritti, A. Cavazzini, N. Marchetti, G. Guiochon, *Comparison between the efficiencies of columns packed with fully and partially porous C 18-bonded silica materials*, Journal of Chromatography A 1157 (**2007**) 289-303.
[142] J.J. Destefano, S.A. Schuster, J.M. Lawhorn, J.J. Kirkland, *Performance characteristics of new superficially porous particles*, Journal of Chromatography A 1258 (**2012**) 76-83.
[143] G.A. Howard, A.J. Martin, *The separation of the C12-C18 fatty acids by reversed-phase partition*, The Biochemical Journal 46 (**1950**) 532-538.
[144] A. Tchapla, S. Héron, E. Lesellier, H. Colin, *General view of molecular interaction mechanisms in reversed-phase liquid chromatography*, Journal of Chromatography A 656 (**1993**) 81-112.
[145] R.E. Majors, *High-performance liquid chromatography on small particle silica gel*, Analytical Chemistry 44 (**1972**) 1722-1726.
[146] S.C. Moldoveanu, V. David, *Essentials in Modern HPLC Separations*, Elsevier Science, Oxford, United Kingdom, **2012**.
[147] Á. Bartha, J. Ståhlberg, *Electrostatic retention model of reversed-phase ion-pair chromatography*, Journal of Chromatography A 668 (**1994**) 255-284.
[148] T. Saldanha, A.C.H.F. Sawaya, M.N. Eberlin, N. Bragagnolo, T. Saldanha, *HPLC separation and determination of 12 cholesterol oxidation products in fish: comparative study of RI, UV, and APCI-MS detectors*, Journal of Agricultural and Food chemistry 54 (**2006**) 4107-4113.
[149] P. Kebarle, *A brief overview of the present status of the mechanisms involved in electrospray mass spectrometry*, Journal of Mass Spectrometry 35 (**2000**) 804-817.
[150] A.E. Debarber, D. Lütjohann, L. Merkens, R.D. Steiner, *Liquid chromatography-tandem mass spectrometry determination of plasma 24S-hydroxycholesterol with chromatographic separation of 25-hydroxycholesterol*, Analytical Biochemistry 381 (**2008**) 151.
[151] H. Roberg-Larsen, K. Lund, K.E. Seterdal, S. Solheim, T. Vehus, N. Solberg, S. Krauss, E. Lundanes, S.R. Wilson, *Mass spectrometric detection of 27-hydroxycholesterol in breast cancer exosomes*, Journal of Steroid Biochemistry and Molecular Biology 169 (**2017**) 22-28.
[152] W. Griffiths, Y. Wang, G. Alvelius, S. Liu, K. Bodin, J. Sjövall, *Analysis of oxysterols by electrospray tandem mass spectrometry*, The Official Journal of The American Society for Mass Spectrometry 17 (**2006**) 341-362.

[153] S.K. Solheim, *Exploring selectivity and sensitivity for oxysterol measurements using liquid chromatography-mass spectrometry (LC-MS)* (Unpublished Master's thesis), Department of Chemistry, University of Oslo, Oslo, Norway, **2018**.
[154] Z. Pataj, G. Liebisch, G. Schmitz, S. Matysik, *Quantification of oxysterols in human plasma and red blood cells by liquid chromatography high-resolution tandem mass spectrometry*, Journal of Chromatography A 1439 (**2016**) 82-88.
[155] D.V. McCalley, *Overload for ionized solutes in reversed-phase high-performance liquid chromatography*, Analytical chemistry 78 (**2006**) 2532-2538.
[156] J.-T. Wu, H. Zeng, M. Qian, B.L. Brogdon, S.E. Unger, *Direct plasma sample injection in multiple-component LC-MS-MS assays for high-throughput pharmacokinetic screening*, Analytical Chemistry 72 (**2000**) 61.
[157] K.O. Svendsen, H. Roeberg-Larsen, S.A. Pedersen, I. Brenna, E. Lundanes, S.R. Wilson, *Automatic filtration and filter flush for robust online solid-phase extraction liquid chromatography*, Journal of Separation Science 34 (**2011**) 3020-3022.
[158] H. Roberg-Larsen, M.F. Strand, A. Grimsmo, P.A. Olsen, J.L. Dembinski, F. Rise, E. Lundanes, T. Greibrokk, S. Krauss, S.R. Wilson, *High sensitivity measurements of active oxysterols with automated filtration/filter backflush-solid phase extraction-liquid chromatography–mass spectrometry*, Journal of Chromatography A 1255 (**2012**) 291-297.
[159] O.K. Brandtzaeg, E. Johnsen, H. Roberg-Larsen, K.F. Seip, E.L. Maclean, L.R. Gesquiere, S. Leknes, E. Lundanes, S.R. Wilson, *Proteomics tools reveal startlingly high amounts of oxytocin in plasma and serum*, Scientific Reports 6 (**2016**).
[160] K. Yamashita, S. Kobayashi, S. Tsukamoto, M. Numazawa, *Synthesis of pyridine-carboxylate derivatives of hydroxysteroids for liquid chromatography–electrospray ionization-mass spectrometry*, Steroids 72 (2007) 50-59.
[161] D.C. Harris, C.A. Lucy, *Quantitative Chemical Analysis*, 9th ed., Freeman, New York, USA, **2016**.
[162] M. Schüller, *Evaluating and optimizing picolinylester derivatization of sterols for liquid chromatography-tandem mass spectroscopy* (Unpublished Bachelor thesis), Department of Chemistry, University of Oslo, Oslo, Norway, **2018**.
[163] I. Shiina, M. Kubota, H. Oshiumi, M. Hashizume, *An effective use of benzoic anhydride and its derivatives for the synthesis of carboxylic esters and lactones: A powerful and convenient mixed anhydride method promoted by basic catalysts*, Journal of Organic Chemistry 69 (**2004**) 1822-1830.
[164] S. Xu, I. Held, B. Kempf, H. Mayr, W. Steglich, H. Zipse, *The DMAP-Catalyzed Acetylation of Alcohols - A Mechanistic Study (DMAP=4-(Dimethylamino)pyridine)*, Chemistry – A European Journal 11 (**2005**) 4751-4757.
[165] Y. Su, N.J.W. Straathof, V. Hessel, T. Noël, *Photochemical Transformations Accelerated in Continuous-Flow Reactors: Basic Concepts and Applications*, Chemistry 20 (**2014**) 10562-10589.
[166] M. He, S. Jiang, R. Xu, J. Yang, Z. Zeng, G. Chen, *Facile functionalization of soybean oil by thiol-ene photo-click reaction for the synthesis of polyfunctional acrylate*, Progress in Organic Coatings 77 (**2014**) 868-871.
[167] M. Arca, S. Natoli, F. Micheletta, S. Riggi, E. Di Angelantonio, A. Montali, T.M. Antonini, R. Antonini, U. Diczfalusy, L. Iuliano, *Increased plasma levels of oxysterols, in vivo markers of oxidative stress, in patients with familial combined hyperlipidemia: Reduction during atorvastatin and fenofibrate therapy*, Free Radical Biology and Medicine 42 (**2007**) 698-705.
[168] W.J. Griffiths, M. Hornshaw, G. Woffendin, S.F. Baker, A. Lockhart, S. Heidelberger, M. Gustafsson, J. Sjövall, Y. Wang, W.J. Griffiths, *Discovering oxysterols in plasma: a window on the metabolome*, Journal of Proteome Research 7 (**2008**) 3602-3612.

[169] H. Fuda, N.B. Javitt, K. Mitamura, S. Ikegawa, C.A. Strott, *Oxysterols are substrates for cholesterol sulfotransferase*, Journal of Lipid Research 48 (**2007**) 1343.
[170] I. Björkhem, *Are side-chain oxidized oxysterols regulators also in vivo?*, Journal of Lipid Research 50 (**2009**) 213-218.
[171] A.R. Johnson, M.F. Vitha, *Chromatographic selectivity triangles*, Journal of Chromatography A 1218 (**2011**) 556-586.
[172] I.D. Watson, M.J. Stewart, Y.Y.Z. Farid, *The effect of surfactants on the high-performance liquid chromatography of anthracyclines*, Journal of Pharmaceutical and Biomedical Analysis 3 (**1985**) 555-563.
[173] W.J. Griffiths, P.J. Crick, Y. Wang, M. Ogundare, K. Tuschl, A.A. Morris, B.W. Bigger, P.T. Clayton, Y. Wang, *Analytical strategies for characterization of oxysterol lipidomes: Liver X receptor ligands in plasma*, Free Radical Biology and Medicine 59 (**2013**) 69-84.
[174] J. Vial, A. Jardy, *Experimental comparison fo the different approaches to estimate LOD and LOQ of an HPLC method*, Analytical Chemistry 71 (**1999**) 2672.
[175] K. Karu, M. Hornshaw, G. Woffendin, K. Bodin, M. Hamberg, G. Alvelius, J. Sjövall, J. Turton, Y. Wang, W.J. Griffiths, *Liquid chromatography-mass spectrometry utilizing multi-stage fragmentation for the identification of oxysterols*, Journal of Lipid Research 48(4) (**2007**) 976-987.
[176] J.N. Miller, J.C. Miller, *Statistics and chemometrics for analytical chemistry*, 6th ed., Pearson Prentice Hall, Harlow, Essex, England, **2010**.

7 Appendix

7.1 Experimental details: derivatization of cholesterol and selected oxysterols

7.1.1 Chemicals

Cholesterol (≥ 99 %), TGA (≥ 99 %), DMPA (99 %), MNBA (97 %), 2-picolinic acid (99%), pyridine (99.8 %), Hünig's base (≥ 99 %), DMAP (≥ 99 %), THF (≥ 99.9 %) and triethylamine (≥ 99.5 %) were purchased from Sigma Aldrich. DMF (99.9 %) was purchased from Merck. Ethyl acetate (99.8 %) was purchased from Labscan Ltd. (Dublin, Ireland).

7.1.2 Equipment

Quartz cuvettes for storage of samples during UV irradiation and two of the UV lamps were provided by Marita Clausen, and had unknown suppliers. The deuterium UV lamp was disassembled from a SpectraSystem UV2000 detector from Thermo Scientific.

7.1.3 Charge tagging with picolinic acid

The parameters tested are shown in **Table 12**.

Table 12. The parameters tested in the derivatization with picolinic acid.

Date (dd/mm-2018)	**23/01**	**31/01**	**01/02**	**13/02**	**14/02**		**30/4**	
Derivatization mixture	**Amount (mg)**							
Chemicals								
MNBA	100				50	25	100	
Picolinic acid	80				40	20	60	
DMAP	30				15	-	40	-
Base + solvents	**Amount (µL)**							
Triethylamine	200			-				
Hünig's base	-			200	100	50	200	
Tetrahydrofuran	1500		-	-		450	-	
Pyridine	-		1500	1500	750	-	1800	
Solvent of stock solution								
Cholesterol	Acetonitrile	Isopropanol		Methanol			-	
25-OHC(-d_6)	-						Methanol	
Solvent of sample								
Cholesterol	Acetonitrile	Isopropanol		Methanol			-	
25-OHC(-d_6)	-						Methanol	
Analyte cons. (µg/mL)	10						0.01	
Instrument injection	Direct injection						LC-MS	

7.1.4 Liquid chromatography-mass spectrometry system

The LC system is the same as shown in **Figure 17** in **Introduction 2.6**. However, injection was performed with an autosampler. The MP was ACN/H_2O/FA (70/30/0.1, v/v/v), the flow rate was 800 µL/min, and the analytical column was an ACE Excel 1.7 CN-ES 50 x 2.1 mm ID from VWR (**Table 13**).

Table 13. The column used for separation of 25-OHC and 25-OHC-d6 with serial number, batch number and suggested interactions.

Column	Serial number	Batch number	Suggested interactions
ACE Excel 1.7 CN-ES	A192268	V17-1145	Hydrophobic interactions, $\pi - \pi$ and dipole-dipole interactions.

The MS used is the same as described in **Experimental 3.6** and was operated in MRM. The initial MS tune settings are shown in **Table 14**, and is based on the settings recommended from Thermo Scientific (**Table 15** in **Appendix 7.2.1**).

Table 14. Tune settings for the TSQ Vantage MS, based on recommendations from Thermo Scientific.

Spray voltage (V)	3000
Capillary temperature (°C)	380
Vaporizer temperature (°C)	300
Sheath gas (psi)	50
Auxiliary gas flow	10
Collision gas pressure (mTorr)	1

7.2 Hydrolysis of oxysterols in human plasma

7.2.1 Tune settings for the TSQ Vantage mass spectrometer

The settings described in **Experimental 3.6.1** are based on the recommended settings from Thermo Scientific, shown in **Table 15**.

Table 15. The recommended tune settings for the MS: capillary temperature, vaporizer temperature, sheath gas pressure, auxiliary gas flow and spray voltage for different flow rates recommended from Thermo Scientific.

Liquid flow rate (µL/min)	Capillary temperature (°C)	Vaporizer temperature (°C)	Sheath gas pressure (psi)	Auxiliary gas flow (arbitrary units)	Spray voltage (V)
5	240	Off to 50	5	0	3000
200	350	250 – 350	35	10	3000
500	380	300 – 500	60	20	3000
1000	400	500	75	20	3000

7.2.2 Fragmentation patterns of the oxysterols

The fragmentation patterns for the Girard T derivatives of 24S-, 25-, and 27-OHC are illustrated with 25-OHC in **Figure 59**, and the monitored *m/z* transitions are shown in **Table 16**, together

with the *m/z* transitions for 25- and 27-OHC-d_6. Girard T derivatives provide fragments of -59 Dalton (Da) and -87 Da. The suggested fragmentation patterns have been reported in previous works [52, 78, 175].

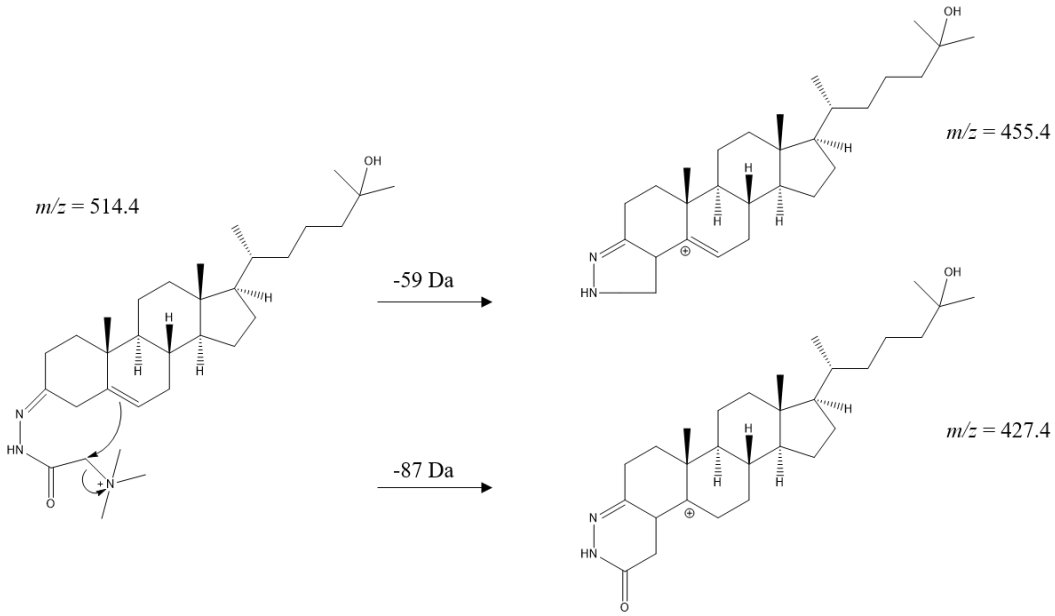

Figure 59. Suggested fragmentation patterns for the Girard T derivatives of the oxysterols in MS/MS, illustrated with 25-OHC.

Table 16. The monitored m/z transitions for 24S-, 25-, and 27-OHC and 25- and 27-OHC-d_6.

Analyte	*m/z*	Monitored *m/z* transitions
24S-OHC	514.4	514.4 → 455.4 514.4 → 427.4
25-OHC	514.4	514.4 → 455.4 514.4 → 427.4
27-OHC	514.4	514.4 → 455.4 514.4 → 427.4
25-OHC-d_6	520.4	520.4 → 461.4 520.4 → 433.4
27-OHC-d_6	520.4	520.4 → 461.4 520.4 → 433.4

7.2.3 Reported concentrations of oxysterols in plasma

Table 17 shows the free and total oxysterol concentration of 25-, 24S-, and 27-OHC in plasma, reported by McDonald [89] and Griffiths [173].

Table 17. Concentrations (ng/mL and nM) in plasma of free and total 25-, 24S-, and 27-OHC reported by McDonald [89] and Griffiths [173].

	Free oxysterol concentration [173]		**Total oxysterol concentration [89]**	
	ng/mL	**nM**	**ng/mL**	**nM**
25-OHC	4.06	10.1	11.8	29.3
24S-OHC	6.86	17.0	56.1	139
27-OHC	19.1	47.5	151	376

7.3 Comparison of two experimental means: t-test

The two-tailed t-test was performed by using the standard deviations from **Table 22** in **Appendix 7.6**. The pooled standard deviation (s) was calculated with **Equation 2**, while the experimental t-value (t_{exp}) was calculated with **Equation 3** [176 (p. 40)]. The critical t-values (t_{crit}, P = 0.01 and P = 0.02) are from [176 (p. 266)]. The results from the t-test are shown in **Table 18**.

Equation 2.

$$s^2 = \frac{(n_1 - 1)s_1^2 + (n_2 - 1)s_2^2}{(n_1 + n_2 - 2)}$$

Equation 3.

$$t = \frac{\bar{x}_1 - \bar{x}_2}{s\sqrt{\frac{1}{n_1} + \frac{1}{n_2}}}$$

Table 18. Sample means, pooled standard deviations (s), t_{exp}, degrees of freedom (d.o.f), critical t-value (t_{crit}) and sample replicates (n) for 25-, 24S-, and 27-OHC for the two-tailed t-test.

	25-OHC		**24S-OHC**		**27-OHC**	
n	**Enzymatic**	**Alkaline**	**Enzymatic**	**Alkaline**	**Enzymatic**	**Alkaline**
1	1.10203994	0.699217	4.74866774	1.926988	13.0224935	7.435446
2	0.86459595	0.607309	3.44508944	1.702655	11.3448051	6.893169
3	0.82267653	0.618523	4.16769632	1.761179	12.0310269	6.673965
4	0.80794268	0.485974	3.10541311	1.535982	10.1573619	6.062475
s	**0.115280177**		**0.532906275**		**0.941389874**	
t_exp	**3.638060337**		**5.665852463**		**7.32000578**	
d.o.f	6		6		6	
t_crit (P = 0.01)	3.71					
t_crit (P = 0.02)	3.14					
n	4		4		4	

7.4 Evaluation of enzymatic hydrolysis

The chromatograms of 5 µL plasma spiked with 0 – 75 nM 22R-, 25-, 24S-, and 27-OHC after enzymatic hydrolysis without and with TX-100, and after no hydrolysis are shown in **Figure 60**, **Figure 61**, and **Figure 62**, respectively.

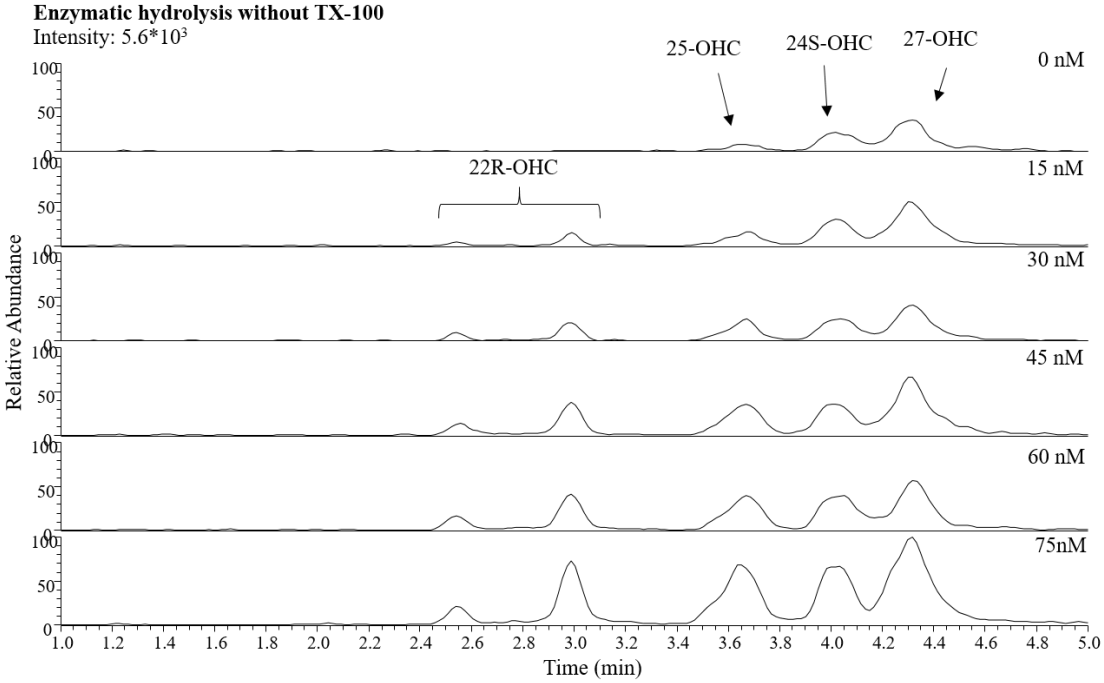

Figure 60. TIC chromatograms (7 points smoothing) of m/z 514 -> 433, 461 of 5 µL plasma spiked with 0 – 75 nM 22R-, 24S-, 25-, and 27-OHC after enzymatic hydrolysis **without TX-100**. Separation was done with the ACE UltraCore SPH (150 x 2.1 mm ID, 2.5 µm core-shell particles) column B with a C18 SPE column, by using the AFFL-SPE system described in **Section 3.6.3**. The MP was 56/11/33/0.1 (H_2O/MeOH/ACN/FA, v/v/v/v), the flow rate was 650 µL/min at 55 °C, and the injection volume was 60 µL.

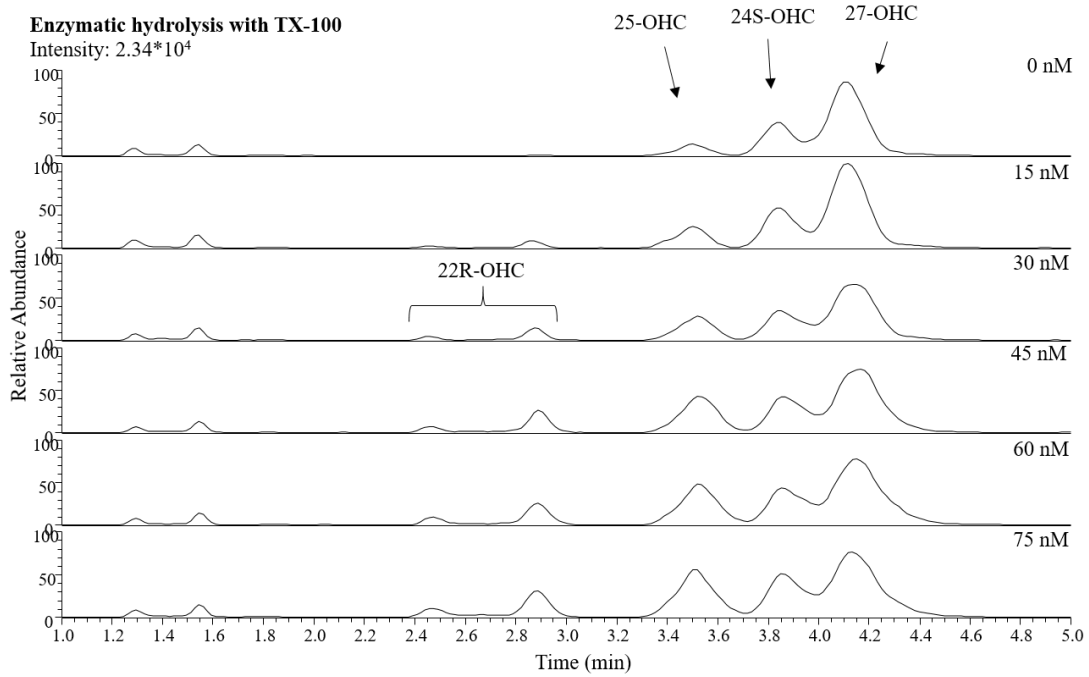

Figure 61. TIC chromatograms (7 points smoothing) of m/z 514 -> 433, 461 of 5 µL plasma spiked with 0 – 75 nM 22R-, 24S-, 25-, and 27-OHC after enzymatic hydrolysis **with TX-100**. Separation was done with the ACE UltraCore SPH (150 x 2.1 mm ID, 2.5 µm core-shell particles) column B with a C18 SPE column, by using the AFFL-SPE system described in **Section 3.6.3**. The MP was 56/11/33/0.1 (H_2O/MeOH/ACN/FA, v/v/v/v), the flow rate was 650 µL/min at 55 °C, and the injection volume was 60 µL.

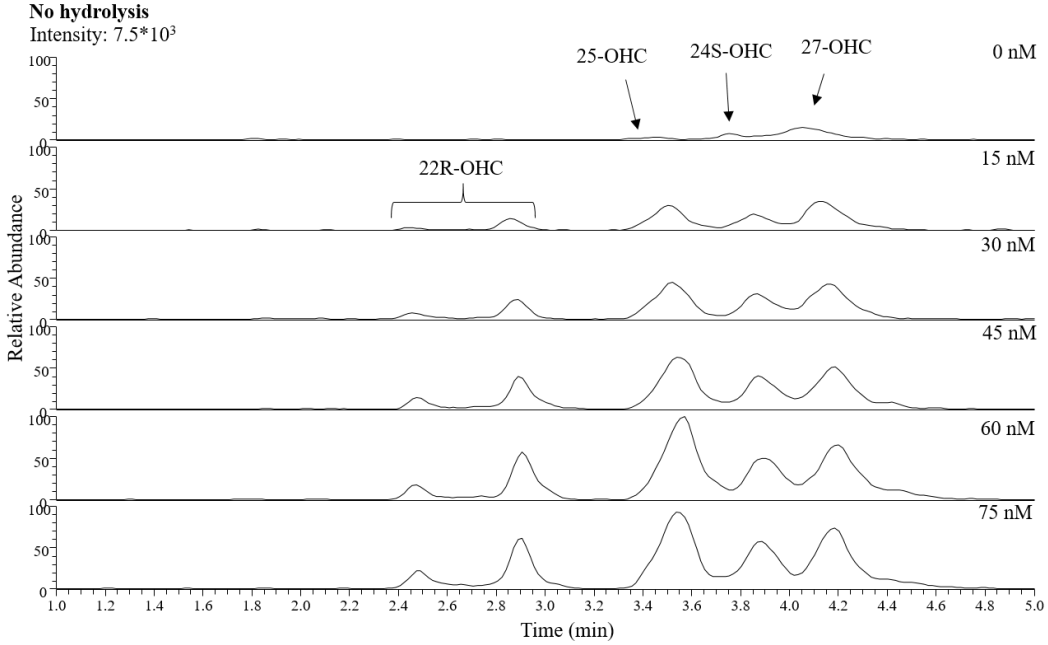

Figure 62. TIC chromatograms (7 points smoothing) of m/z 514 -> 433, 461 of 5 µL plasma spiked with 0 – 75 nM 22R-, 24S-, 25-, and 27-OHC after no hydrolysis. Separation was done with the ACE UltraCore SPH (150 x 2.1 mm ID, 2.5 µm core-shell particles) column B with a C18 SPE column, by using the AFFL-SPE system described in **Section 3.6.3**. The MP was 56/11/33/0.1 (H_2O/MeOH/ACN/FA, v/v/v/v), the flow rate was 650 µL/min at 55 °C, and the injection volume was 60 µL.

7.5 Supplementary figures

The different scan modes in the TQ is illustrated in **Figure 63.** The UV lamps used for the thiyl radical-based charge tagging is shown in **Figure 64**.

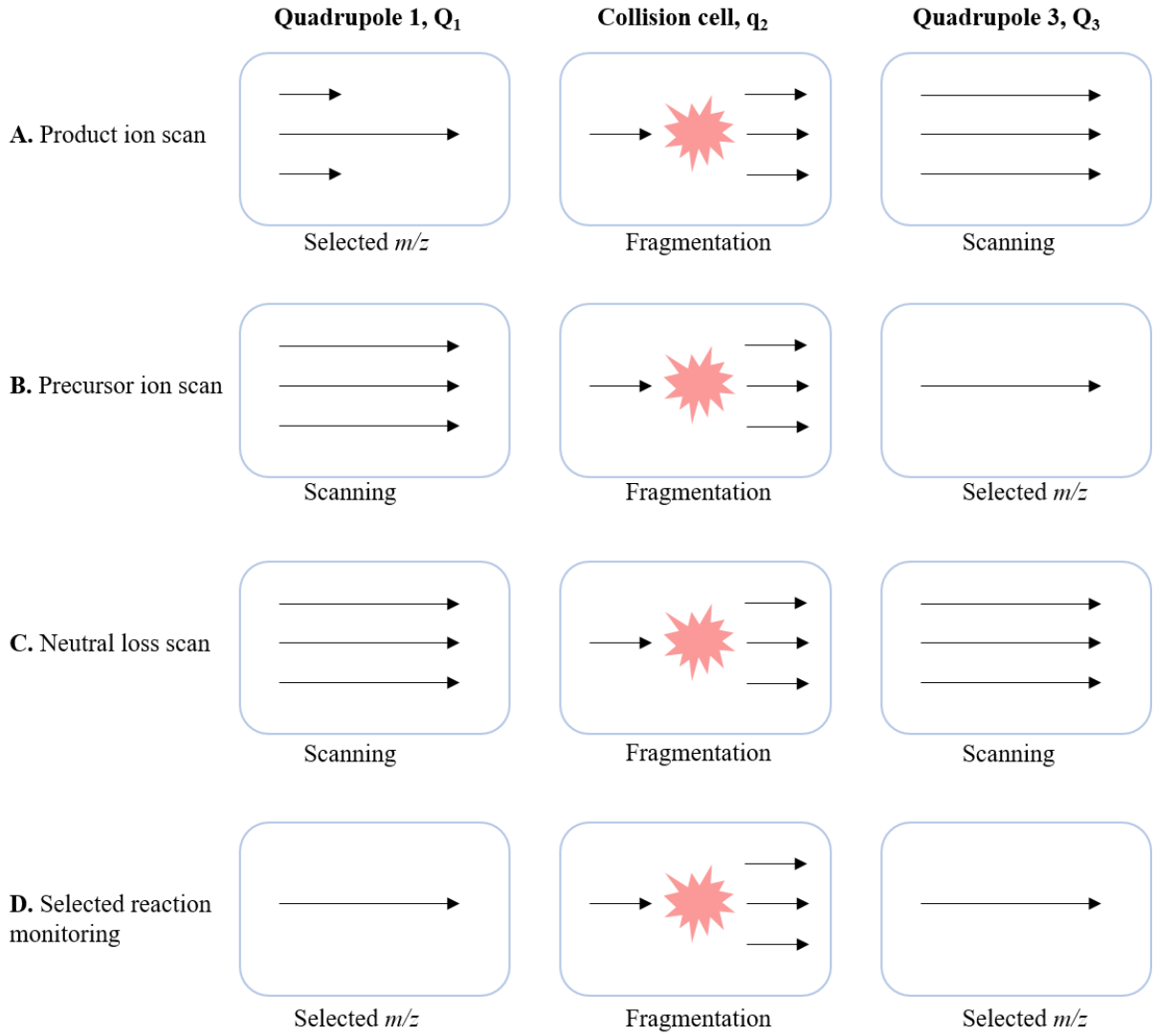

Figure 63. Schematic illustration of the different operational modes for the triple quadrupole. **A**. Product ion scan. Ions with a specific m/z is selected in Q_1 followed by transfer to q_2, where they undergo fragmentation. The product ions (fragments) formed in q_2 are analyzed according to their m/z in Q_3. **B**. Precursor ion scan. Q_1 scans ions to identify the precursor ion for the product ion (fragment) given in Q_3, by fragmentation in q_2. **C**. Neutral loss scan. Q_1 and Q_3 are scanned simultaneously with a constant mass difference, which corresponds to a selected component that is lost as a neutral species upon fragmentation in q_2. **D**. Selected reaction monitoring. Ions with a specific m/z is selected in Q_1, and the product ion (fragment) formed in q_2 is selected in Q_3.

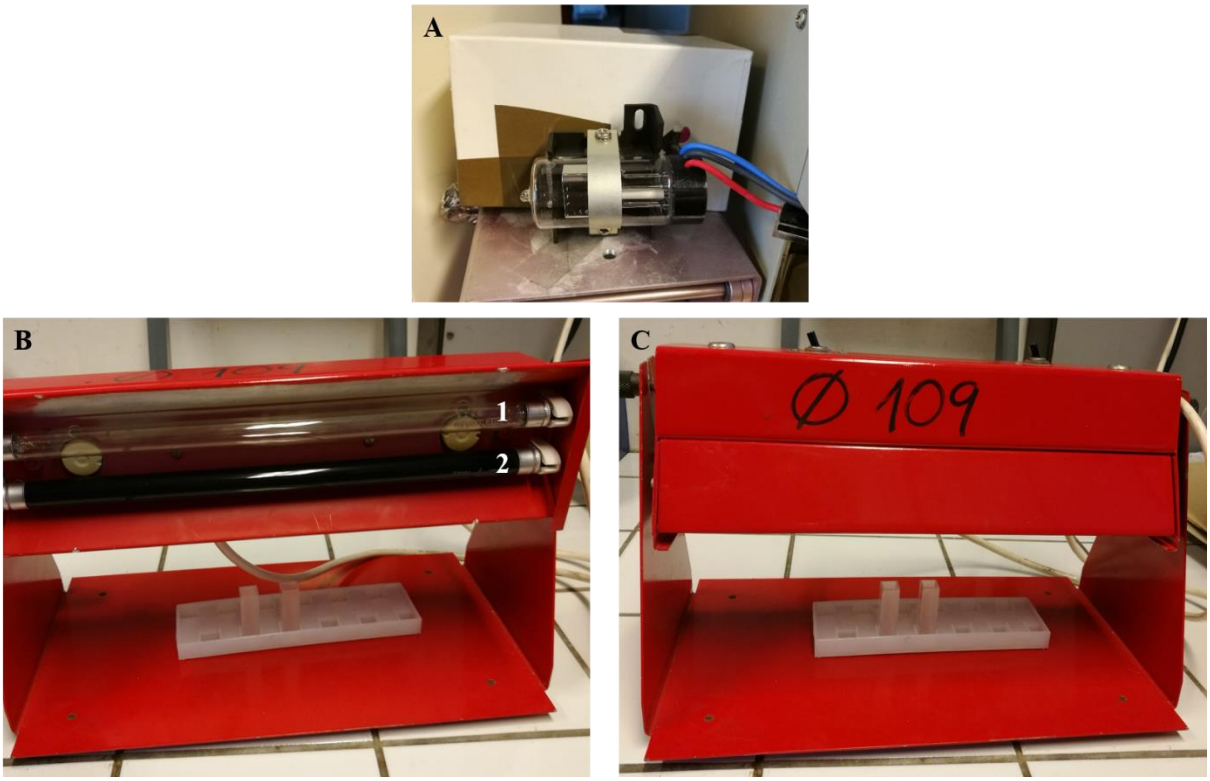

Figure 64. The UV lamps used for the thiyl radical-based charge tagging. **Figure A** shows a deuterium lamp. The sample was covered with the cardboard box observed in the back during irradiation. **Figure B** shows UV lamp 1 and 2 with unidentifiable wavelengths. **Figure C** shows the system set up during irradiation. The sample was covered with a cardboard box.

7.6 Raw data

The raw data is presented in **Table 19 - Table 28**.

Table 19. Retention times (t_R), peak width at half height (0.5w) and resolution (Rs) with means, standard deviations and %RSD for 6 replicates of 25-, 24S-, and 27-OHC after alkaline hydrolysis of 5 µL plasma**.**

Alkaline hydrolysis

Day 1	**tR**			**0.5w**			**Rs**	
Replicate	**25**	**24S**	**27**	**25**	**24S**	**27**	**25/24S**	**24S/27**
1	3.07	3.36	3.58	0.13	0.13	0.25	1.313923	0.682
2	3.08	3.32	3.58	0.18	0.17	0.22	0.807771	0.785333
3	3.03	3.3	3.56	0.11	0.16	0.24	1.178	0.7657
4	3.07	3.33	3.56	0.16	0.15	0.22	0.988	0.73227
5	3.05	3.3	3.56	0.18	0.17	0.25	0.841429	0.729238
6	3.08	3.32	3.58	0.2	0.14	0.24	0.831529	0.806
Mean	3.063333	3.321667	3.57	0.16	0.153333	0.236667	0.993442	0.75009
STD	0.019664	0.022286	0.010954	0.034059	0.01633	0.013663	0.210046	0.044722
RSD (%)	0.64191	0.670929	0.306847	21.28673	10.64996	5.77293	21.14326	5.962215
Day 2								
1	2.98	3.25	3.48	0.14	0.13	0.22	1.178	0.774114
2	2.98	3.25	3.5	0.15	0.13	0.2	1.135929	0.892424
3	3.02	3.26	3.51	0.16	0.15	0.22	0.912	0.795946
4	2.98	3.26	3.51	0.14	0.12	0.21	1.268615	0.892424
5	2.98	3.27	3.5	0.16	0.15	0.21	1.102	0.752611
6	3	3.25	3.5	0.13	0.15	0.2	1.051786	0.841429
Mean	2.99	3.256667	3.5	0.146667	0.138333	0.21	1.108055	0.824825
STD	0.016733	0.008165	0.010954	0.012111	0.013292	0.008944	0.120904	0.060059
RSD (%)	0.559639	0.250715	0.312984	8.257228	9.608387	4.259177	10.91141	7.281425

Table 20. Area, t_R, peak width at half height (0.5w) and Rs with means, standard deviations and %RSD for 6 replicates of 25-, 24S-, and 27-OHC after enzymatic hydrolysis with different concentrations of ChE of 5 µL plasma.

Injection number	Enzyme conc. (UN	Area			tR			0.5w			Rs	
		25	24S	27	25	24S	27	25	24S	27	25/24S	24S/27
1	0.03	3707	12466	22171	2.87	3.12	3.33	0.14	0.13	0.19	1.09	0.77
2	0.03	3688	13430	20148	2.90	3.18	3.43	0.18	0.15	0.20	1.00	0.84
3	0.03	4304	13643	19615	2.89	3.18	3.42	0.16	0.18	0.20	1.00	0.74
4	0.03	4843	13503	22429	2.89	3.15	3.37	0.12	0.13	0.16	1.23	0.89
5	0.03	4563	15531	24029	2.90	3.15	3.38	0.11	0.11	0.20	1.34	0.87
6	0.03	4059	15511	19497	2.90	3.17	3.40	0.11	0.14	0.18	1.27	0.85
Mean		4194	14014	21314.83	2.89	3.16	3.39				1.16	0.83
STD		464.9499	1239.227	1838.289	0.01	0.02	0.04				0.14	0.06
RSD (%)		**11.0861**	**8.84278**	**8.62446**	**0.40**	**0.73**	**1.08**				**12.44**	**7.04**
1	0.05	2278	7300	11746	2.90	3.14	3.35	0.10	0.13	0.15	1.23	0.88
2	0.05	3003	9219	11243	2.92	3.22	3.47	0.12	0.15	0.17	1.31	0.92
3	0.05	2885	8639	11997	2.97	3.22	3.45	0.12	0.12	0.17	1.23	0.93
4	0.05	3040	9117	13064	2.85	3.15	3.35	0.10	0.12	0.20	1.61	0.74
5	0.05	3708	10469	13109	2.89	3.15	3.37	0.12	0.16	0.18	1.09	0.76
6	0.05	2777	9299	12849	2.87	3.15	3.38	0.11	0.14	0.18	1.32	0.85
Mean		2948.5	9007.167	12334.67	2.90	3.171667	3.395				1.30	0.85
STD		462.8601	1032.378	780.8126	0.041952	0.037639	0.052058				0.17	0.08
RSD (%)		**15.6982**	**11.4617**	**6.33023**	**1.44663**	**1.18671**	**1.53336**				**13.22**	**9.70**
1	0.08	3061	7582	12694	2.95	3.18	3.43	0.13	0.13	0.15	1.04	1.05
2	0.08	2468	9551	13529	2.99	3.20	3.47	0.14	0.14	0.10	0.88	1.33
3	0.08	3380	9018	12297	2.94	3.22	3.43	0.11	0.12	0.13	1.43	0.99
4	0.08	2238	10547	14104	2.89	3.12	3.37	0.12	0.13	0.15	1.08	1.05
5	0.08	2910	8088	11766	2.90	3.15	3.38	0.12	0.12	0.16	1.23	0.97
6	0.08	2162	7517	12418	2.89	3.17	3.37	0.10	0.14	0.19	1.37	0.71
Mean		2703.167	8717.167	12801.33	2.926667	3.173333	3.408333				1.17	1.02
STD		488.5638	1204.9	861.5302	0.040332	0.03559	0.041191				0.21	0.20
RSD (%)		**18.0738**	**13.8222**	**6.73**	**1.37809**	**1.12154**	**1.20853**				**17.89**	**19.30**

Table 21. Area, t_R, peak width at half height (0.5w) and Rs of spiked (400 pM) 25-, 24S-, and 27-OHC after enzymatic hydrolysis of 5 µL plasma with 0.034 UN ChE.

MP comp.	Enzyme conc. (UN)	Spike conc. (pM)	Area			tR			0.5w			Rs	
			25	24S	27	25	24S	27	25	24S	27	25/24S	24S/27
10% MeOH	0.034	400	14628	15851	28218	4.43	4.86	5.16	0.17	0.16	0.08	1.53	1.47
11% MeOH	0.034	400	18680	22703	27669	3.87	4.26	4.56	0.16	0.16	0.15	1.44	1.14
12% MeOH	0.034	400	18395	20693	26907	3.63	3.98	4.28	0.15	0.14	0.18	1.42	1.10

Table 22. Area with means, standard deviations and %RSD for 4 replicates of 25-, 24S-, and 27-OHC, and 25- and 27-OHC-d_6 after enzymatic hydrolysis with TX-100 and alkaline hydrolysis of 5 µL plasma.

	Enzymatic hydrolysis with TX-100			Alkaline hydrolysis		
25-OHC	**A**	**A_IS**	**A/A_IS**	**A**	**A_IS**	**A/A_IS**
1	25607	23236	1.102039938	15445	22089	0.699217
2	19986	23116	0.864595951	15688	25832	0.607309
3	19235	23381	0.822676532	14719	23797	0.618523
4	16011	19817	0.807942675	12647	26024	0.485974
Mean	20209.75	22387.5	0.899313774	14624.75	24435.5	0.602756
SD	3989.988	1717.088	0.137265156	1381.266	1860.761	0.087962
%RSD	19.74289	7.669853	15.26332189	9.444717	7.614988	14.59331
24S-OHC	**A**	**A_IS**	**A/A_IS**	**A**	**A_IS**	**A/A_IS**
1	76634	16138	4.748667741	41806	21695	1.926988
2	58160	16882	3.445089444	42076	24712	1.702655
3	60715	14568	4.167696321	43679	24801	1.761179
4	51230	16497	3.105413105	41599	27083	1.535982
Mean	61684.75	16021.25	3.866716653	42290	24572.75	1.731701
SD	10741.6	1015.348	0.736156477	946.371	2210.15	0.161406
%RSD	17.41371	6.337508	19.03828346	2.237813	8.994313	9.320652
27-OHC	**A**	**A_IS**	**A/A_IS**	**A**	**A_IS**	**A/A_IS**
1	210157	16138	13.02249349	161312	21695	7.435446
2	191523	16882	11.34480512	170344	24712	6.893169
3	175268	14568	12.03102691	165521	24801	6.673965
4	167566	16497	10.15736194	164190	27083	6.062475
Mean	186128.5	16021.25	11.63892187	165341.8	24572.75	6.766264
SD	18876.67	1015.348	1.204095965	3769.175	2210.15	0.567964
%RSD	10.14174	6.337508	10.34542528	2.279627	8.994313	8.394051

Table 23. The SNRs with means, standard deviations and %RSD for 25- and 27-OHC-d_6 for concentrations 150 – 4500 pM after enzymatic hydrolysis of 5 µL plasma.

25-OHC-d6						
Replicate	**150**	**450**	**750**	**1500**	**3000**	**4500**
1	1	1	1	11	13	22
2	1	1	11	16	19	24
3	1	1	9	8	20	24
4	-	-	2	12	12	15
5	-	-	2	1	16	24
6	-	-	1	2	17	25
7	-	-	-	-	-	18
8	-	-	-	-	-	19
9	-	-	-	-	-	16
10	-	-	-	-	-	18
Mean	1	1	4.333333	8.333333	16.16667	20.5
SD	0	0	4.457204	5.887841	3.188521	3.719319
%RSD	0	0	102.8586	70.65409	19.72281	18.14302

27-OHC-d6						
Replicate	**150**	**450**	**750**	**1500**	**3000**	**4500**
1	1	1	1	1	1	1
2	1	1	1	1	10	9
3	1	1	1	1	1	9
4	-	-	1	1	2	10
5	-	-	1	2	1	1
6	-	-	1	1	1	2
7	-	-	-	-	-	1
8	-	-	-	-	-	1
9	-	-	-	-	-	13
10	-	-	-	-	-	2
Mean	1	1	1	1.166667	2.666667	4.9
SD	0	0	0	0.408248	3.614784	4.748099
%RSD	0	0	0	34.99271	135.5544	96.89998

Table 24. The areas of spiked concentrations of 25-, 24S-, and 27-OHC and 25- and 27-OHC-d_6 after enzymatic hydrolysis of 5 µL plasma **with TX-100**.

	0 nM			15 nM			30 nM			45 nM			60 nM			75 nM		
25-OHC	**A**	**A_IS**	**A/A_IS**	**A**	**A_IS**	**A/A_IS**	**A**	**A_IS**	**A/A_IS**	**A**	**A_IS**	**A/A_IS**	**A**	**A_IS**	**A/A_IS**	**A**	**A_IS**	**A/A_IS**
1	25607	23236	1.10204	52500	22847	2.297895	61971	24291	2.551192	100867	31866	3.165349	115300	25497	4.522101	135496	27213	4.979091
2	19986	23116	0.864596	45235	24288	1.862442	51027	24494	2.083245	95615	30624	3.122224	104130	23603	4.411727	123249	23926	5.151258
3	19235	23381	0.822677	40129	22717	1.766474	50636	19359	2.615631	82089	25603	3.206226	88448	20126	4.394713	105967	22778	4.652164
4	16011	19817	0.807943	36104	22500	1.604622	49650	20434	2.429774	86832	26310	3.300342	93841	22243	4.2189	113520	21138	5.370423
Mean	20209.75	22387.5	0.899314	43492	23088	1.882858	53321	22144.5	2.41996	91350.75	28600.75	3.198535	100429.8	22867.25	4.38686	119558	23763.75	5.038234
SD	3989.988	1717.088	0.137265	7072.822	812.7045	0.296441	5795.7	2633.909	0.237334	8464.474	3108.56	0.076045	11857.35	2262.819	0.125407	12764.74	2568.392	0.303135
%RSD	19.74289	7.669853	15.26332	16.26235	3.52003	15.74422	10.86945	11.89419	9.807351	9.265905	10.86881	2.377491	11.80661	9.895459	2.85869	10.67661	10.80803	6.016682

	0 nM			15 nM			30 nM			45 nM			60 nM			75 nM		
24S-OHC	**A**	**A_IS**	**A/A_IS**	**A**	**A_IS**	**A/A_IS**	**A**	**A_IS**	**A/A_IS**	**A**	**A_IS**	**A/A_IS**	**A**	**A_IS**	**A/A_IS**	**A**	**A_IS**	**A/A_IS**
1	76634	16138	4.748668	99875	21591	4.62577	76666	15998	4.792224	97886	21773	4.495752	103237	16396	6.296475	112981	18216	6.202295
2	58160	16882	3.445089	70701	18668	3.787283	51696	19012	2.719125	80794	20560	3.929669	86790	16094	5.392693	98408	16960	5.802358
3	60715	14568	4.167696	74198	16971	4.372046	61095	14908	4.098135	79744	20599	3.871256	83460	17044	4.896738	95242	16298	5.843785
4	51230	16497	3.105413	68408	17931	3.815069	64054	13740	4.661863	72272	18661	3.87289	90991	14668	6.203368	97128	17317	5.608824
Mean	61684.75	16021.25	3.866717	78295.5	18790.25	4.150042	63377.75	15914.5	4.067837	82674	20398.25	4.042392	91119.5	16050.5	5.697318	100939.8	17197.75	5.864315
SD	10741.6	1015.348	0.736156	14581.99	1992.246	0.416095	10307.1	2261.487	0.948252	10827.83	1287.69	0.303458	8646.056	1003.263	0.670522	8132.143	799.4016	0.247498
%RSD	17.41371	6.337508	19.03828	18.6243	10.60255	10.02627	16.26297	14.21023	23.31097	13.09702	6.312749	7.506887	9.488699	6.250666	11.76909	8.056433	4.648292	4.220412

	0 nM			15 nM			30 nM			45 nM			60 nM			75 nM		
27-OHC	**A**	**A_IS**	**A/A_IS**	**A**	**A_IS**	**A/A_IS**	**A**	**A_IS**	**A/A_IS**	**A**	**A_IS**	**A/A_IS**	**A**	**A_IS**	**A/A_IS**	**A**	**A_IS**	**A/A_IS**
1	210157	16138	13.02249	249898	21591	11.57417	185593	15998	11.60101	216482	21773	9.942681	231198	16396	14.10088	224997	18216	12.35161
2	191523	16882	11.34481	216413	18668	11.59273	166345	19012	8.749474	191860	20560	9.331712	202020	16094	12.5525	212674	16960	12.53974
3	175268	14568	12.03103	196761	16971	11.59395	151209	14908	10.14281	173725	20599	8.433662	188980	17044	11.08777	196688	16298	12.06823
4	167566	16497	10.15736	186925	17931	10.42468	146049	13740	10.62948	179639	18661	9.62644	189057	14668	12.88908	182231	17317	10.52324
Mean	186128.5	16021.25	11.63892	212499.3	18790.25	11.29638	162299	15914.5	10.28069	190426.5	20398.25	9.333624	202813.8	16050.5	12.65756	204147.5	17197.75	11.87071
SD	18876.67	1015.348	1.204096	27783.2	1992.246	0.581204	17757.92	2261.487	1.187229	18940.73	1287.69	0.649776	19890.67	1003.263	1.239897	18649.22	799.4016	0.918976
%RSD	10.14174	6.337508	10.34543	13.07449	10.60255	5.145048	10.94148	14.21023	11.54814	9.94648	6.312749	6.961672	9.807359	6.250666	9.795708	9.135168	4.648292	7.741545

Table 25. The areas of spiked concentrations of 25-, 24S-, and 27-OHC and 25- and 27-OHC-d_6 after enzymatic hydrolysis of 5 µL plasma **without TX-100**.

	0 nM			15 nM			30 nM			45 nM			60 nM			75 nM		
25-OHC	**A**	**A_IS**	**A/A_IS**	**A**	**A_IS**	**A/A_IS**	**A**	**A_IS**	**A/A_IS**	**A**	**A_IS**	**A/A_IS**	**A**	**A_IS**	**A/A_IS**	**A**	**A_IS**	**A/A_IS**
1	3558	8926	0.398611	6801	9627	0.706451	10698	7755	1.379497	18034	10563	1.70728	20369	10118	2.013145	34562	13955	2.476675
2	2463	10308	0.238941	9349	10599	0.882064	12577	8442	1.489813	21589	12913	1.671881	21470	10352	2.073995	34794	13755	2.529553
3	2546	10987	0.231728	8466	11077	0.764286	9991	8454	1.181807	19709	10403	1.89455	22206	8552	2.596586	35220	14475	2.433161
Mean	2855.667	10073.67	0.28976	8205.333	10434.33	0.784267	11088.67	8217	1.350372	19777.33	11293	1.757904	21348.33	9674	2.227909	34858.67	14061.67	2.479796
SD	609.6526	1050.292	0.094337	1293.846	738.892	0.089496	1336.531	400.1487	0.156055	1778.485	1405.24	0.119655	924.5238	978.6991	0.32073	333.7324	371.6629	0.048272
%RSD	21.34887	10.42612	32.5568	15.76835	7.081353	11.41137	12.05312	4.869767	11.55641	8.992541	12.44346	6.806701	4.330661	10.1168	14.39601	0.957387	2.643093	1.946606

	0 nM			15 nM			30 nM			45 nM			60 nM			75 nM		
24S-OHC	**A**	**A_IS**	**A/A_IS**	**A**	**A_IS**	**A/A_IS**	**A**	**A_IS**	**A/A_IS**	**A**	**A_IS**	**A/A_IS**	**A**	**A_IS**	**A/A_IS**	**A**	**A_IS**	**A/A_IS**
1	10994	5784	1.900761	13728	6348	2.162571	13278	1787	7.43033	17374	7283	2.385555	21885	2736	7.998904	30563	6342	4.819142
2	9075	5169	1.755659	14156	5626	2.516175	14595	1935	7.542636	21029	5922	3.550996	21753	2256	9.642287	29397	5714	5.144732
3	11086	4994	2.219864	11421	5129	2.22675	13567	2388	5.681323	15833	5642	2.806274	22131	3408	6.493838	30115	5818	5.176177
Mean	10385	5315.667	1.958761	13101.67	5701	2.301832	13813.33	2036.667	6.884763	18078.67	6282.333	2.914275	21923	2800	8.04501	30025	5958	5.046684
SD	1135.425	414.9197	0.237476	1471.148	612.9511	0.18838	692.1939	313.1331	1.043721	2668.711	877.8384	0.590179	191.8437	578.6605	1.574731	588.187	336.5947	0.197683
%RSD	10.93332	7.8056	12.12376	11.22871	10.75164	8.183906	5.011056	15.37478	15.15987	14.76166	13.97313	20.25131	0.87508	20.66645	19.57401	1.958991	5.649458	3.91709

	0 nM			15 nM			30 nM			45 nM			60 nM			75 nM		
27-OHC	**A**	**A_IS**	**A/A_IS**	**A**	**A_IS**	**A/A_IS**	**A**	**A_IS**	**A/A_IS**	**A**	**A_IS**	**A/A_IS**	**A**	**A_IS**	**A/A_IS**	**A**	**A_IS**	**A/A_IS**
1	19492	5784	3.369986	28278	6348	4.454631	21801	1787	12.19978	37043	7283	5.086228	31192	2736	11.40058	55429	6342	8.739987
2	24851	5169	4.8077	30270	5626	5.380377	25710	1935	13.28682	43313	5922	7.313914	31625	2256	14.01817	63691	5714	11.14648
3	21895	4994	4.384261	30585	5129	5.963151	20784	2388	8.703518	39299	5642	6.965438	32854	3408	9.640258	59953	5818	10.30474
Mean	22079.33	5315.667	4.187316	29711	5701	5.266053	22765	2036.667	11.39671	39885	6282.333	6.455193	31890.33	2800	11.68634	59691	5958	10.06374
SD	2684.251	414.9197	0.738814	1250.969	612.9511	0.76073	2600.642	313.1331	2.394861	3175.81	877.8384	1.198294	862.1846	578.6605	2.202902	4137.227	336.5947	1.221216
%RSD	12.1573	7.8056	17.64409	4.210457	10.75164	14.44592	11.42386	15.37478	21.01363	7.962418	13.97313	18.56325	2.703592	20.66645	18.85023	6.931073	5.649458	12.13481

Table 26. The areas of spiked concentrations of 25-, 24S-, and 27-OHC and 25- and 27-OHC-d_6 after **no hydrolysis** of 5 µL plasma.

	0 nM			15 nM			30 nM			45 nM			60 nM			75 nM		
25-OHC	**A**	**A_IS**	**A/A_IS**	**A**	**A_IS**	**A/A_IS**	**A**	**A_IS**	**A/A_IS**	**A**	**A_IS**	**A/A_IS**	**A**	**A_IS**	**A/A_IS**	**A**	**A_IS**	**A/A_IS**
1	1620	11135	0.145487	21236	16511	1.286173	34396	15755	2.18318	50990	13253	3.847431	79667	16229	4.908928	71975	15019	4.792263
2	2847	11659	0.244189	16961	15217	1.114609	31647	14031	2.255506	41133	13215	3.112599	70032	15978	4.383027	70227	14345	4.895573
3	1824	10252	0.177917	16132	14019	1.150724	30062	15839	1.897973	40039	13068	3.063897	60499	14553	4.15715	66158	12166	5.437942
Mean	2097	11015.33	0.189198	18109.67	15249	1.183835	32035	15208.33	2.11222	44054	13178.67	3.341309	70066	15586.67	4.483035	69453.33	13843.33	5.041926
SD	657.4793	711.0924	0.050309	2739.029	1246.308	0.090448	2192.897	1020.465	0.189034	6031.607	97.70534	0.43899	9584.045	903.936	0.385738	2984.676	1491.192	0.346828
%RSD	31.35333	6.455477	26.59053	15.12468	8.173048	7.640248	6.845316	6.709909	8.949544	13.69139	0.74139	13.13827	13.6786	5.799418	8.604402	4.297384	10.77192	6.878877

	0 nM			15 nM			30 nM			45 nM			60 nM			75 nM		
24S-OHC	**A**	**A_IS**	**A/A_IS**	**A**	**A_IS**	**A/A_IS**	**A**	**A_IS**	**A/A_IS**	**A**	**A_IS**	**A/A_IS**	**A**	**A_IS**	**A/A_IS**	**A**	**A_IS**	**A/A_IS**
1	3311	11838	0.279693	12662	16688	0.758749	22329	17713	1.2606	28423	14456	1.966173	37850	18797	2.013619	44099	13471	3.273625
2	4629	12370	0.374212	15301	16344	0.936185	21743	16762	1.29716	24359	13919	1.750054	38613	16529	2.336076	38528	15324	2.514226
3	4105	11452	0.358453	12904	15804	0.816502	16257	15875	1.024063	24143	11498	2.099756	36868	15288	2.411565	39420	16875	2.336
Mean	4015	11886.67	0.337452	13622.33	16278.67	0.837145	20109.67	16783.33	1.193941	25641.67	13291	1.938661	37777	16871.33	2.253753	40682.33	15223.33	2.70795
SD	663.5932	460.9309	0.050638	1458.795	445.6067	0.090501	3349.348	919.1857	0.14825	2411.125	1575.826	0.176467	874.7874	1779.372	0.21136	2992.344	1704.231	0.497928
%RSD	16.52785	3.877714	15.00605	10.70885	2.737366	10.81069	16.65541	5.476777	12.41686	9.403154	11.85634	9.102527	2.315661	10.54672	9.37812	7.35539	11.19486	18.38762

	0 nM			15 nM			30 nM			45 nM			60 nM			75 nM		
27-OHC	**A**	**A_IS**	**A/A_IS**	**A**	**A_IS**	**A/A_IS**	**A**	**A_IS**	**A/A_IS**	**A**	**A_IS**	**A/A_IS**	**A**	**A_IS**	**A/A_IS**	**A**	**A_IS**	**A/A_IS**
1	16396	11838	1.385031	28971	16688	1.736038	35810	17713	2.021679	43135	14456	2.983882	60766	18797	3.23275	62290	13471	4.624007
2	16413	12370	1.326839	26158	16344	1.600465	35426	16762	2.113471	36149	13919	2.597097	58720	16529	3.552544	53091	15324	3.464565
3	12817	11452	1.119193	19991	15804	1.264933	31068	15875	1.957039	33194	11498	2.886937	48632	15288	3.181057	48715	16875	2.886815
Mean	15208.67	11886.67	1.277021	25040	16278.67	1.533812	34101.33	16783.33	2.03073	37492.67	13291	2.822639	56039.33	16871.33	3.322117	54698.67	15223.33	3.658462
SD	2071.262	460.9309	0.139746	4593.206	445.6067	0.242522	2633.951	919.1857	0.078608	5104.895	1575.826	0.201249	6495.996	1779.372	0.201223	6928.824	1704.231	0.884679
%RSD	13.61896	3.877714	10.9431	18.34348	2.737366	15.81172	7.723894	5.476777	3.870902	13.61572	11.85634	7.129827	11.59185	10.54672	6.057057	12.66726	11.19486	24.18171

Table 27. The areas of spiked concentrations of 25-, 24S-, and 27-OHC and 25- and 27-OHC-d_6 after enzymatic hydrolysis of 5 µL plasma **with TX-100**.

	0 µM			15 µM			30 µM			45 µM			60 µM			75 µM		
25-OHC	**A**	**A_IS**	**A/A_IS**	**A**	**A_IS**	**A/A_IS**	**A**	**A_IS**	**A/A_IS**	**A**	**A_IS**	**A/A_IS**	**A**	**A_IS**	**A/A_IS**	**A**	**A_IS**	**A/A_IS**
1	39162	17907	2.186966	8716080	18854	462.2934	15001436	18979	790.4229	20276933	18313	1107.243	25481416	14946	1704.899	33440285	14263	2344.548
2	24109	15051	1.60182	6883705	15538	443.0239	11699744	14506	806.5452	15797866	14965	1055.654	21898433	15116	1448.692	26622518	12557	2120.134
3	15606	15749	0.99092	6614339	17204	384.4652	10149051	13459	754.0717	14560838	15972	911.6478	20368710	13641	1493.198	22666755	12580	1801.809
Mean	26292.33	16235.67	1.593236	7404708	17198.67	429.9275	12283410	15648	783.6799	16878546	16416.67	1024.848	22582853	14567.67	1548.93	27576519	13133.33	2088.83
SD	11928.81	1488.898	0.598069	1143640	1658.006	40.53326	2478288	2931.846	26.87874	3007380	1717.723	101.3711	2624169	807.0058	136.894	5449755	978.3876	272.7202
%RSD	45.36992	9.170538	37.53803	15.44477	9.64032	9.427928	20.17589	18.73624	3.429811	17.81777	10.46329	9.891325	11.62018	5.539705	8.837972	19.7623	7.449652	13.05612

	0 µM			15 µM			30 µM			45 µM			60 µM			75 µM		
24S-OHC	**A**	**A_IS**	**A/A_IS**	**A**	**A_IS**	**A/A_IS**	**A**	**A_IS**	**A/A_IS**	**A**	**A_IS**	**A/A_IS**	**A**	**A_IS**	**A/A_IS**	**A**	**A_IS**	**A/A_IS**
1	60936	14538	4.191498	5905948	13701	431.0596	10011529	12929	774.3467	13621779	13838	984.3748	17134114	11101	1543.475	22876736	11390	2008.493
2	41402	15055	2.75005	4527764	12743	355.3138	7770469	11149	696.9656	10730158	10220	1049.918	14505155	9281	1562.887	18910934	9215	2052.19
3	36787	11733	3.135345	4510921	14023	321.6802	6574937	10773	610.3163	9732521	10406	935.2797	14118061	9340	1511.57	15519307	9152	1695.728
Mean	46375	13775.33	3.358964	4981544	13489	369.3512	8118978	11617	693.8762	11361486	11488	989.8574	15252443	9907.333	1539.311	19102326	9919	1918.804
SD	12819.58	1787.503	0.746289	800601.4	665.8138	56.02457	1744602	1151.674	82.05887	2020028	2037.283	57.51525	1641028	1034.166	25.91089	3682447	1274.313	194.4206
%RSD	27.6433	12.97611	22.21784	16.07135	4.935976	15.16837	21.48795	9.913692	11.82615	17.77961	17.73401	5.810458	10.75912	10.43839	1.683279	19.27748	12.84719	10.13238

	0 µM			15 µM			30 µM			45 µM			60 µM			75 µM		
27-OHC	**A**	**A_IS**	**A/A_IS**	**A**	**A_IS**	**A/A_IS**	**A**	**A_IS**	**A/A_IS**	**A**	**A_IS**	**A/A_IS**	**A**	**A_IS**	**A/A_IS**	**A**	**A_IS**	**A/A_IS**
1	181896	14538	12.51176	8363589	13701	610.4364	14791760	19292	766.7303	20289146	13838	1466.191	24950324	11101	2247.574	32785815	11390	2878.474
2	180665	15055	12.00033	7090672	12743	556.4366	11581650	11149	1038.806	16217740	10220	1586.863	23193014	9281	2498.978	27909424	9215	3028.695
3	147601	11733	12.57999	6969239	14023	496.9863	9949671	10773	923.5748	14594998	10406	1402.556	21992075	9340	2354.612	23895128	9152	2610.919
Mean	170054	13775.33	12.36403	7474500	13489	554.6198	12107694	13738	909.7037	17033961	11488	1485.203	23378471	9907.333	2367.055	28196789	9919	2839.362
SD	19454.61	1787.503	0.316811	772363.9	665.8138	56.74686	2463534	4813.578	136.5673	2933512	2037.283	93.6129	1487819	1034.166	126.1628	4452304	1274.313	211.6164
%RSD	11.44025	12.97611	2.562364	10.33332	4.935976	10.23167	20.34684	35.03842	15.01228	17.22155	17.73401	6.303037	6.364056	10.43839	5.329947	15.79011	12.84719	7.452956

Table 28. The areas of spiked concentrations of 25-, 24S-, and 27-OHC and 25- and 27-OHC-d_6 after enzymatic hydrolysis of 5 µL plasma **without TX-100**.

	0 µM			15 µM			30 µM			45 µM			60 µM			75 µM		
25-OHC	**A**	**A_IS**	**A/A_IS**	**A**	**A_IS**	**A/A_IS**	**A**	**A_IS**	**A/A_IS**	**A**	**A_IS**	**A/A_IS**	**A**	**A_IS**	**A/A_IS**	**A**	**A_IS**	**A/A_IS**
1	12361	7303	1.692592	9878529	14308	690.42	17458572	12196	1431.5	11338692	8534	1328.649	21532569	11205	1921.693	25245281	13192	1913.681
2	11369	9875	1.151291	10204036	10178	1002.558	19652201	14253	1378.812	10007770	8055	1242.43	18273418	11486	1590.93	22242798	10619	2094.623
3	11066	10708	1.033433	9862673	12588	783.498	19631675	16222	1210.188	8726990	6854	1273.27	16489739	9785	1685.206	20068097	11343	1769.205
Mean	11598.67	9295.333	1.292439	9981746	12358	825.492	18914149	14223.67	1340.167	10024484	7814.333	1281.449	18765242	10825.33	1732.609	22518725	11718	1925.836
SD	677.3598	1774.969	0.351518	192672	2074.584	160.2503	1260609	2013.16	115.6061	1305931	865.4712	43.68796	2557137	911.8445	170.4007	2599598	1326.858	163.0488
%RSD	5.83998	19.09527	27.19801	1.930243	16.78738	19.41271	6.664898	14.1536	8.626249	13.02742	11.07543	3.409261	13.62699	8.423246	9.834919	11.54416	11.32324	8.466389

	0 µM			15 µM			30 µM			45 µM			60 µM			75 µM		
24S-OHC	**A**	**A_IS**	**A/A_IS**	**A**	**A_IS**	**A/A_IS**	**A**	**A_IS**	**A/A_IS**	**A**	**A_IS**	**A/A_IS**	**A**	**A_IS**	**A/A_IS**	**A**	**A_IS**	**A/A_IS**
1	20244	7303	2.772012	7010658	14308	489.9817	11135044	12196	913.0079	7940739	8534	930.4827	14753388	11205	1316.679	17200400	13192	1303.851
2	17107	9875	1.732354	6916369	10178	679.5411	12421331	14253	871.4889	6660973	8055	826.9364	12261911	11486	1067.553	15134128	10619	1425.193
3	24737	10708	2.310142	6492554	12588	515.7733	12452213	16222	767.6127	5785968	6854	844.1739	10674125	9785	1090.866	13618194	11343	1200.581
Mean	20696	9295.333	2.271503	6806527	12358	561.7653	12002863	14223.67	850.7031	6795893	7814.333	867.1977	12563141	10825.33	1158.366	15317574	11718	1309.875
SD	3835.03	1774.969	0.520904	275965.4	2074.584	102.8088	751711.6	2013.16	74.89309	1083703	865.4712	55.47995	2056247	911.8445	137.5977	1798135	1326.858	112.4271
%RSD	18.53029	19.09527	22.93215	4.054423	16.78738	18.30102	6.262769	14.1536	8.803669	15.94644	11.07543	6.397613	16.3673	8.423246	11.87861	11.73903	11.32324	8.583041

	0 µM			15 µM			30 µM			45 µM			60 µM			75 µM		
27-OHC	**A**	**A_IS**	**A/A_IS**	**A**	**A_IS**	**A/A_IS**	**A**	**A_IS**	**A/A_IS**	**A**	**A_IS**	**A/A_IS**	**A**	**A_IS**	**A/A_IS**	**A**	**A_IS**	**A/A_IS**
1	47704	7303	6.53211	6833222	14308	477.5805	12075089	12196	990.086	8023284	8534	940.1551	14158432	11205	1263.582	18998925	13192	1440.185
2	45045	9875	4.561519	7128493	10178	700.3825	13727695	14253	963.1443	7529570	8055	934.7697	12666473	11486	1102.775	16893234	10619	1590.85
3	47998	10708	4.482443	6414429	12588	509.567	13763501	16222	848.4466	6343249	6854	925.4813	11383021	9785	1163.313	15738866	11343	1387.54
Mean	46915.67	9295.333	5.192024	6792048	12358	562.51	13188762	14223.67	933.8923	7298701	7814.333	933.4687	12735975	10825.33	1176.557	17210342	11718	1472.858
SD	1626.7	1774.969	1.161222	358808.2	2074.584	120.4674	964635	2013.16	75.21428	863484.1	865.4712	7.422915	1389010	911.8445	81.21721	1653002	1326.858	105.5195
%RSD	3.467286	19.09527	22.36549	5.282769	16.78738	21.41605	7.314068	14.1536	8.053849	11.83065	11.07543	0.795197	10.90619	8.423246	6.902958	9.604699	11.32324	7.164267